Acute effects of LGI1 on network excitability

Eleonora Lugarà

A thesis submitted to University College London for the degree of

Doctor of Philosophy

University College London

Department of Clinical and Experimental Epilepsy

UCL Queen Square Institute of Neurology

Queen Square

London

WC1N 3BG

March 2019

Declaration

I, Eleonora Lugarà, confirm that the work presented in this thesis is my own. When information has been derived from other sources or are from the contribution of others, I confirm that this has been clearly indicated in the thesis.

Abstract

LGI1 (leucine rich glioma inactivated1) is a secreted trans-synaptic protein and is part of the brain extracellular matrix. LGI1 interacts presynaptically with Kv1.1 potassium channels and ADAM23, a structural transmembrane protein. Postsynaptically, LGI1 also influences AMPA and NMDA receptors via the ADAM22 adhesion protein. Mutations in the gene encoding LGI1 lead to temporal lobe epilepsy in humans and animal models. Autoantibodies against LGI1 have been detected in the serum of adult patients with limbic encephalitis and seizures.

Although LGI1 is strongly implicated in the generation and spread of seizures in genetic and developmental forms of epilepsy, the mechanisms by which LGI1 affects neuronal networks are still debated. This thesis aimed to determine whether an acute reduction of LGI1 in the brain leads to network hyperactivity and epilepsy in rodent animals and the mechanisms behind it.

Initially, *in vivo* experiments on rats demonstrated that LGI1 concentrations in the brain are reduced after generation of chronic seizures using the perforant path stimulation model. I then chose and validated a silencing RNA (shRNA) against LGI1 which reduced endogenous LGI1 levels in primary cultures. In the transduced neurons, spontaneous calcium activity was significantly higher, without affecting the viability of the cells. Also the MBR (mean bursting rate) of transduced neuronal cultures measured with a MEA (multielectrode arrays) system was increased.

In *ex vivo* granule cells, shRNA-LGI1 increased neuronal firing. Local field potential (LFP) of *ex vivo* slices after injection of shRNA-LGI1 in the hippocampus, revealed an increase in the short-term facilitation of mossy fibers to CA3 pyramidal cell synapses. Application of Kv1 family blocker, αDendrotoxin, occluded the increased facilitation in shRNA-LGI1 injected mice.

My results indicate that an acute reduction of LGI1 is sufficient to increase neuronal network excitability in *in vitro* and *ex vivo* systems and that LGI1 concentrations are reduced in the brains of animals during the development of epilepsy.

Impact Statement

Epilepsy is a major health burden, affecting about 1% of the worldwide population. Although many are treated effectively by antiseizure drugs, approximately 30% have drug-resistant, refractory epilepsy. For these people, epilepsy can be a devastating condition with major consequences including unemployment, injuries, depression and increased mortality. The epilepsies have a multitude of causes from acquired brain lesions, developmental disorders and genetic mutations.

My thesis focuses on LGI1 (leucine rich glioma inactivated protein 1) a brain protein which is part of a matrix which surrounds neurons. LGI1 has many interactions with pre and post synaptic ion channels and several trans-synaptic partners, important for brain and circuit development and neuronal transmission. Importantly, mutations in the gene encoding LGI1 lead to familial temporal lobe epilepsy with audiogenic features (ADTLE, autosomal dominant lateral temporal epilepsy). In recent years, specific auto antibodies against LGI1 have also been shown to be a cause of epilepsy, characterised by focal dystonic seizures and cognitive impairment. However, it is not clear whether it is the targeting of LGI1 by antibodies or the consequent inflammation that is the cause of the condition.

The aim of my work was to identify the acute role of LGI1 in brain circuits and epilepsy.

In particular, in this thesis I show that LGI1 is downregulated after acquired chronic epilepsy and this is associated with changes in network excitability associated with LGI1 partners. This indicates that loss of LGI1 may play a broader role in the epilepsies, and may be common feature amongst a number of aetiologies. I then validated a method to downregulate LGI1 in neuronal circuits and demonstrated that local alterations of LGI1 levels in specific brain circuits, affect network excitability.

These novel findings confirm that reduction of LGI1 alone affects brain circuits and neuronal behaviour, suggesting a pathophysiological role in acquired epilepsy, a genetic epilepsy and acute limbic encephalitis due to IgG-LGI1. This work opens up promising prospects to develop protective strategies for epilepsy by redressing the loss of LGI1

through small molecule and gene delivery approaches. The insights from this thesis will, therefore, hopefully lead to improved therapies for those people with drug-resistant epilepsies.

Acknowledgements

This work would not have been possible without the input, help and supervision of many people. I dedicate this thesis to all of you, who enlightened these years in London and my daily life.

First and foremost, I am very grateful to Professor Matthew Walker for giving me the chance to work in his lab, for teaching me so much about epilepsy and the brain, and for being such a positive and supportive supervisor. Thank you for having always patience with me for all the failed experiments and for all the right advices during these years. You are a role model by whom I will always be inspired.

A sincere and invaluable thanks to Dr. Gabriele Lignani, my secondary supervisor, mentor and friend. Gabriele hugely contributed to shape this project and get me through tough times, helping me with every aspect of the project and encouraging me to think critically. Thank you for involving me in many collaborative works and for all the coffees we shared. Any student who has and will have the chance to be guided by you is a lucky student.

Thanks to all the Epilepsy Department (DCEE), it has been a great family with which I spent a lot of time during these three and half years. A special mention to Professor Dimitri Kullmann for *adopting* me in his weekly lab meetings and supporting part of the *in vivo* works. A warm acknowledgement to Dr. Gareth Morris, for all the coffees and help with electrophysiology, English and broccoli, but especially for the latter ones. Thanks to Dr. Erica Tagliatti, for her advices on molecular biology, immunohistochemistry, imaging and uncountable other topics. Good luck for your promising future career. Thanks to Jenna Carpenter, for the precious help with virus design, cell cultures and long talks during weekends and nights at work. Thanks to Dr. Tawfeeq Shekh-Ahmad, for his great help in calcium imaging, *in vivo* works, ugly molarity calculations and the delicious baklava. Thanks to (Dr.) Sylvain Rama, Marion Mercier, Vincent Magloire, Tom Jensen, Edward Maguire for all the patch clamp and LFP tips. Thanks to my previous colleagues

in Walker's lab: (Dr.) Amy Nick, Pi-Shan Chang, Ramona Eckel and Sophie Williams for being so nice to me. Thanks to Dr. Elodie Chabrol, for teaching me the value of communicating science in an accessible and creative way. Thanks to Dr. Nicol Birsa, Dr. Carmelo Milioto and Dr. Nancy Malintan for their insights into western blot. Thanks to Dr. Sarah Crisp and Dr. Michael Chou for their help with the autoantibody work. Thanks to Dr. Jonathan Cornford, Yichen Qiu, Dr. Christine Dixon, Dr. Andreas Lieb, Dr. Albert Snowball, Dr. Elizabeth Nicholson, Dr. Bao-Luen Chang, Dr. Mikail Weston, Steffan Jones, Olga Tiurikova, Dr. Janosch Heller and many many many other colleagues in the Department and in the Institute of Neurology.

I am very grateful for having had the chance to contribute to a fantastic PhD program founded by the Marie Skłodowska-Curie Actions (ECMED project). I had the pleasure to know irreplaceable fellows with which I have built a relationship that goes well beyond collaborations, borders and research projects. Thanks to Antonia, Mehwish, Eduardo, Sandra, Shaobo, Anatoly, Danylo, Alessandra R., Marion, Alessandra P., Armand, Anvesh and Greg. I look forward to see you all again.

Thanks to my brilliant students, Elizabeth Brockman and Liam Colclough. These teaching experiences have been a journey from which I have learnt a lot as well.

Thanks to my lifetime friends: Sara, Francesca, Valentina, Guendalina, Cristina, Emily, Valentina (Valigia), Roberta (Sbomb), Francesca (Pepper), Chiaretta & Mattia. I cannot wait to buy a teleportation machine to be closer to all of you. Thanks to newer friends which make my life in London rich and vibrant: Carolina, Ilaria & Michele, Karine and Xun.

Thanks to Dr. Marco Leite, for all the discussions about statistics, for the Python scripts, for your endless curiosity and your kindness: you are a wonderful human being. A heartfelt thanks to my beloved family: Silvia, Leonardo, Beatrice, Nonna Mary, Elena, Adriano and Claudia. I bring you always in my heart and despite the distance you always found creative ways to support me and send me your love.

Table of Content

Abbreviations

4-AP	4-Aminopyridine
AAV	Adeno-Associated Viral
Abs	Auto-Antibodies
aCSF	Artificial Cerebrospinal Fluid
ADAM	A Disintegrin And Metalloprotease
ADH	Antidiuretic Hormone
ADLTE	Autosomal Dominant Lateral Temporal Lobe Epilepsy
ADPEAF	Autosomal Dominant Partial Epilepsy With Auditory Features
AED	Anti-Epileptic Drugs
AM	acetoxymethyl
AMPA	A-Amino-3-Hydroxy-5-Methylisoxazole-4-Propionate
ANOVA	Analysis Of The Variance
AP	Action Potential
AR	Access Resistance
ATP	Adenosine Triphosphate
BrdU	5-Bromo-2-Deoxyuridine
BSA	Bovine Serum Albumine
bp	Base Pair
c57bl	C57 Black/C
CA1	*Cornu Ammonis*
CAMK II	Ca^{2+}/Calmodulin-Dependent Protein Kinase *II*
CASPR2	Contactin-Associated-Protein-Like-2
CC	Current Clamp
CCD	Charge-Coupled Device
CHO	Chinese Hamster Ovary,
cKO	Conditional Knocked Out
CNS	Central Nervous System
CRISPR	Clustered Regularly Interspaced Short Palindromic Repeats
D-current	Delayed
DG	Dentate Gyrus
DGC-IV	(2S,2'R,3'R)-2-(2',3'-Dicarboxycyclopropyl Glycine
dH_2O	Distilled Water
DIV	Days *In vitro*
DMEM	Dulbecco's Modified Eagle Medium

DNA	Deoxyribonucleic Acid
DTX	Dendrotoxin
E18	Embryonic Day 18
EAR	Epilepsy Associated Repeat
ECL	Enhanced Chemiluminescence
ECM	Extracellular Matrix
EDTA	Ethylenediaminetetraacetic Acid
EEG	Electroencephalogram
EF1α	Elongation Factor 1-*Alpha* 1
EGFP	Enhanced Green Fluorescent Protein
EMX	Empty Spiracles Homeobox 1
EPTP	Epitemptin
ER	Endoplasmic Reticulum
ETX	Ethanol Withdrawal
Fab	Antigen Binding Fragment
FBS	Fetal Bovine Serum
Fc-region	Fragment Crystallisable
FDA	Food Drug Administration
FDG-PET imaging	18F-Fluoro-2-Deoxy-D-Glucose Positron Emission Tomography
fEPSP	Field Excitatory Postsynaptic Potential
GABA-A, GABA-B	Gamma-Aminobutyric Acid Receptor A Or B
GAG,	(HIV-1) Group-Specific Antigen Polyprotein
GFAP	Glial Fibrillary Acid Protein
GFP	Green Fluorescent Protein
GluA1	AMPA Receptor, Glutamate A1
GΩ	Giga Seal
HBSS	Hank's Balanced Salt Solution
HEK293	Human Embryonic Kidney
HEPES	4-(2-Hydroxyethyl)-1-Piperazineethanesulfonic Acid
HF	High Fidelity Enzyme.
HLA	Human Leukocyte Antigen
HRP	Horseradish Peroxidase
IgGs	Immunoglobulins,
ILAE	International League Against Epilepsy
IP	Intraperitoneally
IQR	Inter Quartile Range
IR	Input Resistance

ITR	Inverted Terminal Repeat
KA	Kainic Acid
KD	Knock Down
KDa	Kilo Dalton
KO	Knocked Out
Kv	Voltage-gated potassium channel
Kv1.1	Voltage-gated potassium channel subfamily A member 1
LB	Luria Broth
LE	Limbic Encephalitis
LFP	Local Field Potential
LGI1	Leucine Rich Glioma Inactivated1
LRR	Leucine Rich Repeats
LTP	Long Term Potentiation
LV	Lenti Virus
MASS1	Monogenic Audiogenic Seizure-Susceptible
MBD	Mean Burst Duration
MBR	Mean Bursting Rate
MCS	Internal Multiple Cloning Site
MEA	Microelectrode Arrays or Multielectrode Arrays System
mEPSC	Miniature Excitatory Post Synaptic Currents
MF	Mossy Fibers
MFIB	Mean Frequency Intra-Burst
MFR	Mean Firing Rate
mGluR1	Metabotropic Glutamate Receptor1,
microRNA	MicroRNA
MMP/ ERK	Matrix Metalloproteinases /Extracellular Signal
MMP-9	Metalloproteinase 9
MO	Morpholino
MOI	Multiplicity Of Infection
MPP	Perforant Path
MRI	Magnetic Resonance Imaging
mU6	Murine U6 Small-Non-Coding-RNA
NBQX	2,3-Dioxo-6-Nitro-1,2,3,4-Tetrahydrobenzo [F] Quinoxaline-7-Sulfonamide Disodium Sal
NeoR/KanR	Neomycin/Kanamycin Resistance Gene
NgR1	Nogo Receptor1
NMDA	N-Methyl-D-Aspartate
NR2B/NR2A	Glutamate NMDA Receptor Subunit Epsilon-2 Or -1

o/n	Over Night
Pax6	Paired-Box Homeodomain Transcription Factor Markers.
PBS	Phosphate Buffer Saline
PC12	Rat Adrenal Pheochromocytoma
PDS	Paroxysmal Depolarising Shift
PFA	Paraformaldehyde
PGK	Phosphoglycerate Kinase Mammalian Promoter
PI	Propidium Iodide
PLL	Poly-L-Lysine Hydrobromide,
PNN	Perineuronal Net
PNS	Peripheral Nervous System
POL	(HIV-1) Polymerase Polyprotein
Poly A	Polyadenylation
PP	Perforant Path
PPR	Paired Pulse Ratio
PPS	Perforant Path Stimulation
PSD-95	Post Synaptic Density-95
PTX	Picrotoxin
QPCR	Quantitative Polymerase Chain Reaction
REV	(HIV-1) Regulator Of Expression Of Virion Proteins
RIPA	Radioimmunoprecipitation Assay Buffer
RNA	Ribonucleic Acid
Robo	Roundabout
ROI	Region Of Interests
RPK	RNA-Protein Kinase Dependent
RT	Room Temperature
SC	Schaffer Collaterals
SD	Sprague Dawley
SDS	Sodium Dodecyl Sulphate
SDS PAGE	Sodium Dodecyl Sulphate - Polyacrylamide Gel Electrophoresis
SE	Status Epilepticus
SEM	Standard Error of The Mean
shRNA	Silencing RNA or Short Hairpin RNA
SSSE	Self-Sustained Status Epilepticus
TAE	Tris-Acetate-EDTA Buffer
TE buffer	Tris-EDTA
TiN	Titanium Nitride

TLE	Temporal Lobe Epilepsy
TM	Transmembrane
TNEP1	Thrombospondin-Type Laminin G Domain
TROY	Tumour Necrosis Factor Receptor Orphan Y,
TTX	Tetrodotoxin
uPAR complex	Urokinase-Type Plasminogen Activator Receptor
UPR-ER	Unfolded Protein Response/ Endoplasmic Reticulum
VC	Voltage Clamp
VGKC	Voltage-Gated Kv1 Potassium Channel-Complex
VGKG	*Voltage*-Gated Potassium Channel
vGLUT1	Vesicular Glutamate Transporter 1
VLGR1	Very Large G Protein Coupled Receptor1
VSV	Vesicular Stomatitis Virus
VSVG	VSV Glycoprotein G
Wt	Wild Type
γ-DGG	γ -D-Glutamylglycine

Table of Figures

List of Tables

Chapter 1

1 Introduction

1.1 Epilepsy

1.1.1 General definition and epidemiology

Epilepsy is a chronic and debilitating neurological disease affecting 65 million people worldwide (Devinsky *et al.*, 2018). Epilepsy can be defined as a chronic disease characterised by a propensity to have non-physiological, excessive and synchronised brain neuronal firing, leading to clinically discernible events able to affect the patient's cognition, health and social status (Devinsky *et al.*, 2018). However, the complexity of defining "a propensity" is illustrated by the most recent ILAE (International League Against Epilepsy) definition of epilepsy, which uses three different descriptions to adequately identify a person as "affected by epilepsy" (Fisher *et al.*, 2014). In high-income economies, the estimated new cases per year are of the order of 50 every 100 000 people (1 person out every 2000). This incidence is even higher in emergent and underdeveloped nations, making epilepsy one of the commonest serious neurological condition. Epilepsy is more common in the young and elderly, and those of poor social status who have poor access to treatments (Shorvon, 1990; Abramovici and Bagić, 2016).

1.1.2 Socio-economic consequences

Epilepsy is often an underestimated condition, which highly affects not only patients' lives, but also the lives of the patients' friends, and family. People with epilepsy are often socially stigmatised and discriminated against. Mood disorders and mental health issues are frequent co-morbidities associated with this disorder, alongside sexual dysfunction,

sleep problems and higher levels of stress, which, in itself, can increase the probability of having a seizure (Devinsky *et al.*, 2018). People with active epilepsy need constant medication and supervision; European healthcare costs for epilepsy care were 15 billions in 2004, comprising direct (diagnosis and medical devices, drugs, healthcare and social services) and indirect (unemployment, sick leave, early retirement and sudden death) costs (Pugliatti *et al.*, 2007).

1.1.3 Classification and aetiology of epilepsy

Epilepsy is not a single disease, but a collection of different disorders with different aetiologies, which can be classified in many ways. The latest ILAE classification subdivides epilepsy according to three distinct aspects: the location of the seizures, the EEG (electroencephalogram) pattern and the aetiology, i.e. the original cause of the abnormal activity. The localisation of seizures can be classified as focal, generalised, focal & generalised or unknown. A focal seizure arises from the synchronous activity of neurons in a specific brain area, and the manifestation depends on the areas of the brain involved. A focal seizure can generalise when aberrant activity spreads from the focus to the whole cortex resulting in loss of consciousness, vocalisation and tonic-clonic movements. Focal seizures are frequently preceded by a distinct experience termed an *aura*, which often identifies the brain area where the seizure begins (Bromfield, Cavazos and Sirven, 2006).

The ILAE includes in the aetiology of epilepsy genetic, structural, metabolic, immune, infectious and/or unknown causes (Scheffer *et al.*, 2017). These causes are not mutually exclusive and, in fact, the resulting epilepsy can result from a combination of two or more aetiologies. Historically epilepsies have been divided into monogenic, polygenic and acquired forms (Shorvon, 2011). Monogenic epilepsies arise from a defect in the structure and function of a protein. These can be inherited or *de novo* mutations of a single gene. In contrast, a polygenic epilepsy involves multiple genes which together contribute to lower the seizure threshold. Epilepsy can also occur as a consequence of

an acquired disorder such as cerebral tumour, traumatic brain injury, stroke, a neurodegenerative disease, infection or an autoimmune disease (Scheffer *et al.*, 2017).

1.1.4 The process and metabolic changes during epileptogenesis

Generally, epilepsy has been considered to arise from an imbalance between excitation and inhibition in neuronal networks which gives rise to uncontrollable over-activity (Devinsky *et al.*, 2018). The series of events by which a regulated physiological brain state becomes epileptic is termed epileptogenesis. Epileptogenesis is characterised by the development and expansion of a cerebral area able to generate synchronised neuronal activity that leads to spontaneous seizures; it involves multiple processes including: damage to neurons, glial cells and blood brain barrier; inflammation, and changes in gene expression. Other changes include dendritic and axonal sprouting or death, plus modifications of the extracellular space (Pitkänen and Lukasiuk, 2009).

Nevertheless, many factors contribute to differing degrees to the final outcome. In the physiological state, the neuronal resting membrane potential in the central nervous system (CNS) varies from -60 mV to -70 mV due to an ionic imbalance between the inner and the outer part of the cellular membrane. When neurotransmitters arrive to the post synapse, they can elicit fast and finely tuned changes to their transmembrane receptors that lead to a change of the electrical properties of the lipid bilayer. The initial phase of depolarisation is mainly mediated by the recruitment of excitatory receptors such as AMPA (α-amino-3-hydroxy-5-methylisoxazole-4-propionate), and NMDA (N-methyl-D-aspartate) receptors, and voltage-gated calcium channels, and this is offset by feedback and feedforward inhibition predominantly mediated by GABA-A and GABA-B (Gamma-Aminobutyric Acid Receptor type A and type B) receptors. Once the membrane of neurons reaches a certain threshold, sodium channels open in the initial segment of the axon and the electrochemical signal progresses along the axon by the opening of sodium (Na^+), potassium (K^+) and calcium channels (Ca^{2+}) that mediate the generation and termination of the action potential (AP). Lastly, the redistribution of ions, to return the cell

to its resting state, is established through specific ionic pumps (Kandel, Schwartz and Jessell, 2000). Alterations occurring at any level of this process can lead to impairments of normal neuronal function and, consequently to increases in cellular excitability, networks alterations, seizures and to a diagnosis of epilepsy.

In epilepsy, neurons within the focus exhibit a stereotypical behaviour, named the paroxysmal depolarising shift (PDS). Experiments in brain slices showed that neurons display an initial and enduring state of hyperexcitability (epileptic bursts for a few hundreds of milliseconds) (Wong, Miles and Traub, 1984). Then, a long hyperpolarisation phase occurs followed by a repolarisation phase and the cycle starts again. This pattern is believed to be reflected in local field potential (LFP) and EEG recordings.

The extracellular space and the glial cells also play a pivotal role in maintaining a healthy neuronal state. For example, the astroglial cells regulate the recycling and uptake of neurotransmitters (Kandel, Schwartz and Jessell, 2000). It has also been suggested that astrocytes can directly be involved in the generation and spread of seizure activity through the generation and spreading of astrocytic calcium waves. This can in turn, promote neuronal synchronisation and activity through release of glial chemical signals (Carmignoto and Haydon, 2012). Astrocytes participate in another important safeguarding mechanism which is the potassium buffering in the synaptic and extrasynaptic space. Potassium is directly taken up via a sodium-potassium pump or indirectly via Kir4.1 potassium channels which are predominantly expressed on perivascular astrocytes. Impairment of potassium clearance and the subsequent increase of membrane excitation, leading to epileptiform activity, has been observed in mice KO for connexin proteins and in hippocampal sclerotic tissue from patients (de Curtis et al., 2018).

Another important mechanism is the change of GABA(A) receptor transmission from hyperpolarising to excitatory. This phenomenon, which is physiological during the first two weeks of postnatal life in rodents and in the late prenatal/early postnatal period in humans, is caused by the change in expression of the chloride transporters KCC2 (K+,

Cl- transporter) and NKCC1 (Na+, K+, Cl- cotransporter) on the neuronal membrane. NKCC1 moves sodium, potassium and chloride into neurons. In this situation, upon GABA-A binding to its receptor, the chloride moves out of cells, depolarising the cellular membrane. KCC2 instead extrudes chloride and potassium, increasing the concentrations of this ion outside the cells together with potassium ions. The K+/Na+ ATPase pump helps maintaining the high potassium concentration inside the cell and expels sodium ions too (Ben-Ari, 2002; Mathews, 2007; Schulte, Wierenga and Bruining, 2018). Studies from KCC2 KO mice, indicate that these animals have a lower threshold for epileptic attacks. In pathological situations, such as status epilepticus and following traumatic brain injury, KCC2 mRNA concentrations greatly decrease while NKCC1 increase, leading to an early development-like situation (van den Pol, Obrietan and Chen, 1996; Cohen et al., 2002). Recently, the first monogenic epilepsy due to mutations in the gene encoding for KCC2, SLC12A5, revealed that patients display lower activity and expression of the transporter which contributes to altered inhibitory function (Stödberg et al., 2015). During prolonged seizure activity, chloride loading through GABA(A) receptor activity reverse its physiological driving force and promote an excitatory GABA action and its contribution to ictogenesis. In other situations, such as focal cortical dysplasia, which cause aberrant cortical layers and abnormal neuronal morphology, an underexpression of KCC2, leads to intracellular chloride loading, so that GABA-A receptors paradoxically promote seizure-like activity. In addition, inhibitory interneurons can coordinate and enhance excitatory neuronal network activity through synchronising principal cell activity. Upregulation of KCC2 in cortical pyramidal neurons via gene therapy approach, it has been shown to be able to prevent this hyperexcitation up to a certain extent (Magloire et al., 2019).

During epileptogenesis, other metabolic changes inside and outside the brain, appear to contribute to the process. Over production of proinflammatory cytokines released from activated microglia in the acute phase of the epileptogenic process contribute to inflammation, to aberrant synaptic plasticity and to neurodegeneration. During an epileptic attack, the damage is often extended to the mitochondria present in the neurons

and glia. Mitochondrial failure leads to depletion of ATP resources and alterations of many cofactors in the Krebs cycle, leading to the production of aberrant metabolites such as lactate and malate, increasing levels of reactive oxygen and nitrogen species (hydroxyl, superoxide) plus nitric oxide. These agents, which are produced in the cell in physiological conditions for mechanisms such as cell differentiation and vasodilatation, when produced uncontrolled and in excess lead to protein damage, neuronal degeneration and disruption of the blood brain barrier. In addition, gross alteration of mitochondrial activity leads to lipid peroxidation, damage to mitochondrial DNA, depolarisation of the mitochondrial membrane potential and opening of the mitochondrial transition pore, resulting in apoptosis. Consequent lack of ATP results in the failure of sodium-potassium ATPase, breakdown of ion gradients and necrotic cell death (Kovac et al., 2017).

Blood brain barrier disruption with consequent infiltration of serum albumins, IgGs and leukocytes has been proposed also to be a critical element for the triggering and worsening of epileptogenesis (Marchi et al., 2012; Hiragi, Ikegaya and Koyama, 2018).

1.1.5 Temporal Lobe Epilepsy (TLE)

Among the focal epilepsies, TLE is the commonest (comprising about 60% of all focal epilepsies) and consequently the best characterised. TLE can arise from neocortical areas (in the lateral temporal lobe) or archicortical areas (the hippocampal formation in mesial temporal lobe). The hippocampal formation, formed by hippocampus and para-hippocampal structures, is one of the brain regions most commonly affected by epilepsy and also one of the area most commonly resected in epilepsy surgery. Typical histopathological hallmarks of mesial TLE are hippocampal sclerosis and hyper activation of glial cells, both astrocytes and glia, probably due to release of pro-inflammatory molecules such as ATP (Adenosine Triphosphate) and cytokines (Jimenez-pacheco *et al.*, 2016) (**Figure 1.1B**). The areas most affected within the hippocampal sub field are the CA1 (*Cornu Ammonis*) and the CA3 regions, meanwhile

the dentate gyrus (DG) is mainly preserved, but characterised by a widening of the cell granule layer (also called “dispersion”) due to aberrant formation of new-born neurons with altered physiological characteristics. Selectively abolishing adult neurogenesis in the hilus and DG in animals injected with pilocarpine, by a genetic approach, led to a prolonged reduction of the frequency of seizures and ameliorated the cognitive decline (Cho *et al.*, 2015). It has been hypothesised that the DG might be a major site of seizure onset (Ladino, Moien-Afshari and Tellez-Zenteno, 2014). This apparent incongruence could be explained by the duality of granule cells, serving both excitatory and inhibitory roles. Despite uncertainty of the underlying mechanisms, physiologically granule cells express many traits of inhibitory cells. While maintaining a strong excitatory profile, it has been shown that granule cells release GABA and are positive for the GABA-synthesizing enzyme (GAD67). In addition, granule cells express both zinc and dynorphin, neuropeptides with a complex modulatory role. Interestingly, during epilepsy and hyperexcitation, the mRNA of GAD67, GAD65 and GABA itself increase, indicating that a shift in the inhibitory direction might occur during this time. This phenomenon may reflect and try to compensate for mossy fiber sprouting and the loss in lateral inhibition due to the cellular death in this subfield of the hippocampus. These changes added to the pathophysiological excitatory shift of GABA, might help explaining why the DG is a highly epileptogenic zone, despite the granule cells’ hyperpolarised membrane potential (Sloviter, 1992, 2003; Walker, Ruiz and Kullmann, 2002).

The aetiology of TLE can be genetic, but it can also derive from tumours, vascular pathologies, immune problems, and brain injury. One of the commonest associations in people with TLE is a history of febrile seizures or convulsions during childhood (Pitkänen and Lukasiuk, 2009). Temporal lobe seizures often begin with an experiential aura, followed by loss of awareness during which the person may respond, and automatisms (eg fiddling with the hands) occur. After the seizure, the person is confused, and may have difficulty speaking, if the seizure began in the dominant temporal lobe, for several minutes. Generalisation to bilateral tonic-clonic seizures is rare in TLE. Sleep deprivation

and stress increase the chances of a seizures (Diehl and Duncan, 2017; Jan, Sadler and Rahey, 2018).

Patients with mesial temporal lobe epilepsy often show decreased volume of the hippocampus when visualised by magnetic resonance imaging (MRI), sometimes accompanied by a lesion, such as tumour or brain malformations. The ictal scalp-EEG pattern depends upon the underlying pathology and where in the temporal lobe the seizure begins (lateral neocortex versus mesial temporal onset) (Pelliccia *et al.*, 2013; Diehl and Duncan, 2017). Scalp EEG is a non-invasive technique, but is prone to many artefacts from patient's mastication and muscle twitches, and will not pick up abnormal activity generated in the mesial temporal lobe until it has spread to lateral neocortex. For better spatial and temporal resolution (sometimes necessary prior to surgery resection), intracranial EEG and sphenoidal electrodes (electrodes implanted under the zygomatic bone) are normally used alongside MRI scans. The higher temporal-spatial resolution helps to recognise the low amplitude-high frequency (>20Hz) trace, typical of the first part of the seizure.

Medical treatments of TLE alone have generally a low success rate, especially in patients with severe hippocampal sclerosis. Medical treatments of TLE alone have generally a low success rate, especially in patients with severe hippocampal sclerosis. The strategy most commonly followed for the prescription of anti-epileptic drugs (AEDs) is monotherapy, followed by combination therapy with two or more drugs. It has been observed that the more AEDs that fail, the lower is the probability of effectively controlling the epileptic seizures with subsequent drugs, and it has been argued that failure of two or more AEDs at adequate does should be used as the definition of drug-resistance. Approximately 60-70% become seizure free with AED therapy (Kwan and Brodie, 2000). However, the response to treatment is dependent upon the cause of the epilepsy Carbamazepine, valproate and clobazam have been reported to have the highest retention rates in mesial temporal epilepsy; however, one year seizure free rates, even with the most effective drug carbamazepine, were low (11%). Moreover, adverse

reactions are frequent, with dizziness, anxiety, memory loss, nausea, ataxia and vision disturbances as commonest symptoms (Androsova et al., 2017).

In fact, hippocampal sclerosis is the commonest cause of drug resistant epilepsy and just 25-40% of the patients are successfully managed with AEDs (Ladino, Moien-Afshari and Tellez-Zenteno, 2014; Blumcke et al., 2017). In contrast, surgical resection in hippocampal sclerosis can be very successful with over 70% becoming seizure free, and so the early use of surgical resection for hippocampal sclerosis is encouraged. Unfortunately, surgical resection is suitable for fewer than 10% of all people with drug resistant epilepsies (López González *et al.*, 2015; Androsova *et al.*, 2017).

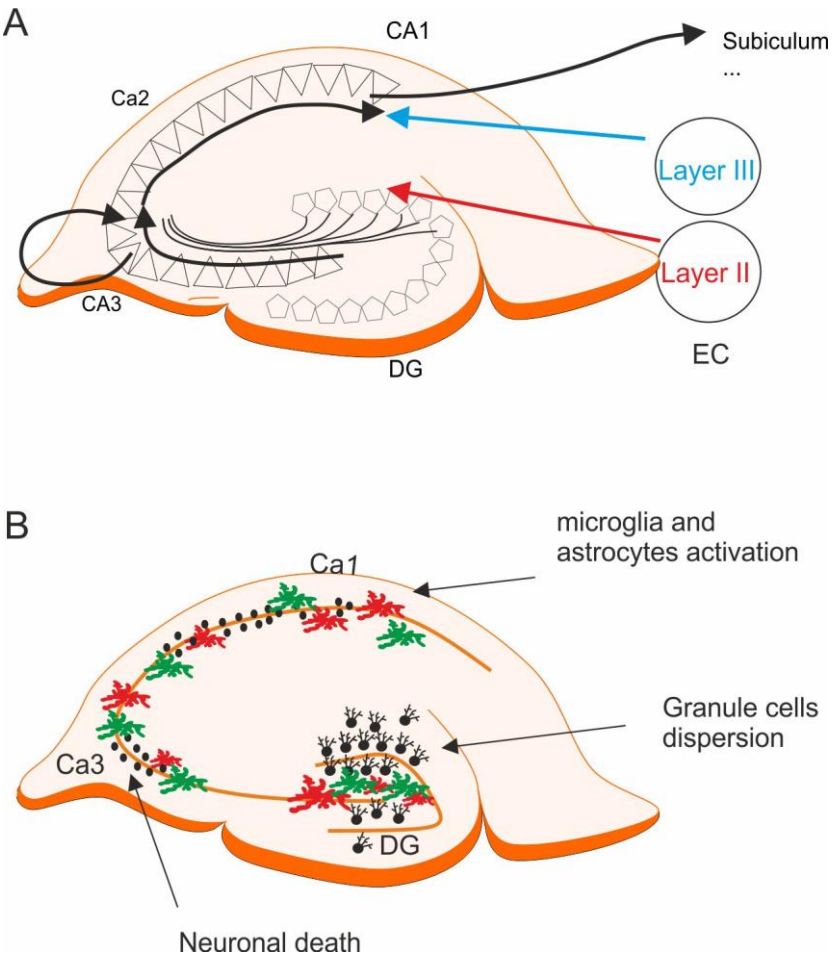

Figure 1.1: Schematic representation of hippocampal circuits and hippocampal sclerosis. ***A)*** *Simplified hippocampal circuits.* ***B)*** *Typical consequences of an epileptic insult in the hippocampus;*

1.1.6 The hippocampus and its circuits

As mentioned above, the hippocampus, an oblong structure (**Figure 1A**), is part of the temporal lobe, and is located on the medial aspect of the temporal lobe. It is extensively connected with other areas of the brain. Longitudinally, the hippocampal formation is divided in three main subsections: the CA1, CA3 (also called *hippocampus proper*) and the dentate gyrus. The layer II and III of the entorhinal cortex (EC) are two of the main sources of hippocampal inputs and reach the hippocampus through the perforant path fibres. One pathway comprises projections from layer II to the DG, (which then projects to CA3, and CA3 projects to CA1 as the "*trisynaptic circuit"*), while an alternative pathways originates in layer III which projects to primarily CA1 and the subiculum (Andersen *et al.*, 2007a). Within the hippocampus, the DG projects to the CA3 through the mossy fibres; similarly, the axons from CA3 pyramidal cells, beyond forming many recurrent excitatory connections, synapse onto CA1 neurons passing through the small CA2 area as the "Schaffer collaterals". The CA1 is classically recognised as the main output of the hippocampus and is connected to the entorhinal cortex and subiculum, and in turn the EC projects to the prefrontal cortex and other part of the neocortex (Witter *et al.*, 2014). Although the hippocampus exhibits several inter species differences, the overall structure and principal connections are well conserved between rodents, primates and humans (Andersen *et al.*, 2007a).

The hippocampus is organised as a five-layer structure – alveus, stratum moleculare, stratum pyramidale, stratum radiatum and stratum oriens-lacunosum. Stratum pyramidale is organised as a linear collection of heavily packed pyramidal neurons, studded by fewer GABAergic inhibitory neurons strategically located to control excitation. The rhythmic activity of the interneurons suppresses pyramidal neuronal firing, synchronising them and giving rise to oscillations at different bands frequency bands. Distinct frequencies have different biological functions. For instance, gamma oscillations (30-130 Hz) have been connected to memory formation, one of the hippocampus' main

roles. Memory is initially consolidated and reinforced in these circuits and subsequently is stored for long term retrieval in other parts of the cortex (Bragin *et al.*, 1995). Human studies revealed that damage or removal of one or both hippocampi, severely impairs the possibility to store new event-related memories (Neves, Cooke and Bliss, 2008). Dorsal and ventral hippocampus are attributed to different type of memories: the ventral part is believed to be concerned with emotional memory, while the dorsal part more with spatial memory (Knierim, 2015).

Other types of frequencies typical of the hippocampus are the theta oscillations (4-8 Hz). Theta oscillations have been found to be involved in the initial phase of learning, sleep phases and exploratory behaviour (Bragin *et al.*, 1995). The hippocampus has also special cells called *place cells,* the activity of which is correlated with the animal's speed and location. These cells fire bursts of action potentials when the animal passes through specific locations (Witter *et al.*, 2014; Knierim, 2015).

Other frequencies detected in the hippocampus are the fast ripples (140-200 Hz) which are believed to encode the reinforcement of prior acquired notions after an initial theta phase and be responsible for the transfer of information to higher cortical structure (Knierim, 2015).

The hippocampus exhibits both structural and functional plasticity in an activity dependent way. This activity can be physiological such as hormones, stress and learning, but also pathological such as a trauma, stroke or epilepsy. Experimentally, triggering of similar mechanisms underlying memory formation and synaptic plasticity is achieved through paradigms such as long term potentiation (LTP) in slices. The protocol consists of repeated and long term stimulations that cause a potentiation of neuronal activity. In turn, spines increase in number and enlarge in shape (Andersen *et al.*, 2007b). The opening and recruitment of NMDA receptors at the synapse is believed to represent one of the fundamental mechanisms for the occurrence of the LTP. Pharmacological prevention of LTP using blockings agents of NMDA receptors markedly decreased LTP induction. Similar results were obtained when AMPA receptor mobility was prevented

with specific antibodies against AMPA subunits (Neves, Cooke and Bliss, 2008; Penn *et al.*, 2017).

In the recent years, it has been found that the hippocampus, and especially the DG, is part of those adult niches able to produce new-born neurons. The function of these neurons is still under debate and it has been proposed having a role in learning and neuroendocrine activity. Adult neurogenesis has also been described occurring after a damage from seizures and it might be directly involved in seizures generations (Andersen *et al.*, 2007b; Sakai *et al.*, 2018).

The DG to CA3 connection is the second synapse in the classic view of the trisynaptic circuit. The DG has a distinctive shape of an acute angle, which smooths from dorsal to the ventral part of the hippocampus. The cells comprising the DG, called granule cells, due to their characteristic small granular shape, are densely packed together, and give rise to the central granule cell layers. Granule cells dendrites project into the molecular layer where they receive inputs from the medial and lateral perforant path fibres, interneurons and other afferent fibres. Below the granule cells the polymorphic layer is composed of the mossy cells, which form the commissural fibres and receive inputs from mossy fibres (MF). MF are the large unmyelinated axons coming from granule cells. They release glutamate from large boutons from their multiple release sites and they facilitate greatly upon an increase in the frequency of stimulation (Gunn and Baram, 2017). They have multiple sites of termination in stratum lucidum in CA3 area, which is rich in dendrites from excitatory neurons and to a less extent, inhibitory neurons (Amaral, Scharfman and Lavenex, 2007). The DG is believed to filter and limit the excitation and information arriving from afferent fibres such as the EC, in fact the granule cells are not spontaneously very active cells, with relatively negative resting membrane potential (Ruiz and Kullmann, 2013). Impairment of this filtering function due to damage, can result in loss of this gating function (Gunn and Baram, 2017). Glutamate is not the only

neurotransmitter released at MF. GABA, opioids, zinc and other peptides are also released at these synapses and are believed to have important neuromodulatory functions (Walker, Ruiz and Kullmann, 2002; Grauert, Engel and Ruiz, 2014). Presynaptic GABA, NMDA and kainate receptors have been described on mossy fibre boutons and are believed to regulate the potentially large excitatory input from MF (Ruiz and Kullmann, 2013).

1.1.7 Animal models of mesial TLE

Due to lack of easy access and availability of human brain samples from surgical resections, researchers have long tried to model TLE in other animals. Classic models are generated by the use of chemoconvulsants, locally or systemically, or application of electric stimuli, either subthreshold or suprathreshold in rodents. The most widely used drugs are kainic acid (KA) and pilocarpine. Kainic acid is an agonist of kainate receptors and AMPA receptors. When injected, either through local stereotaxic injection or intraperitoneally (IP), it causes marked neuronal depolarisation and consequent hyperactivation of hippocampal circuitry that lead to neurotoxicity and cell death in CA1 and CA3 areas, with mossy fibre sprouting. KA injection also mimics a chronic acquired model of epilepsy since the animal undergoes a latent interictal period after which TLE becomes established. The major drawback is the high variability of the number and type of seizures developed by these animals accompanied by a high mortality rate (Shekh-Ahmad *et al.*, 2018).

Another widely-used chemoconvulsant is the M1 muscarinic agonist pilocarpine. Pilocarpine administration leads to the occurrence of status epilepticus in the limbic system due to an excessive release of glutamate and recurrent activation of NMDA receptors (Curia *et al.*, 2008). Pilocarpine can be also used together with lithium, which activates the inflammatory response and damages the blood brain barrier. Similar to the kainic acid model, there is a high variability and mortality. Other molecules employed for modelling TLE are pesticides and flurothyl (Nirwan, Vyas and Vohora, 2018).

Chemical models have the disadvantage that any acute effects observed may not be a direct consequence of the epilepsy but rather a side effect of the chemoconvulsant (Sloviter, 1983). Hence, the use of electrical stimulation models has been important to shed light onto molecular and pathophysiological mechanisms of TLE. Electrical stimulation is generally applied to ventral hippocampal, peri-hippocampal areas (perforant path) or amygdala. Electrical stimulation models can be divided into kindling models or post-status epilepticus models. Briefly, the kindling model is a two-steps electrical stimulation in which the first day is used to determine an afterdischarge threshold and accommodate the rat to the procedure, whilst the second day is used for repeated subthreshold electrical stimulation until the animal reaches Racine score 5 several times (see Table 2) (Kelly and McIntyre, 1994). This model has been reported to reproduce the pathophysiology observed in TLE and is comparable with other chemoconvulsant agents (McNamara *et al.*, 1980); however, spontaneous seizures do not always occur and the extent of damage is less than is generally observed in the human condition and in other TLE models.

The perforant path model of acquired chronic epilepsy is another well-known model of TLE consisting of a one-step procedure in which repeated electrical stimulations (over 2-3 hours) results in self-sustained status epilepticus (SSSE). The mechanisms behind it have been described as hyper-activation of granule cells leading to damage of principal neurons in different hippocampal regions (CA3 and CA1), glial swelling and neuronal loss of hilar interneurons that impacts on feedback inhibition. Perforant path treated rats also display marked memory decline when tested with a T maze behavioural test. The PP stimulation model results in a refractory TLE which is particularly useful for testing of anti-epileptic drugs (Mazarati *et al.*, 1998; Khalil *et al.*, 2017). The PP stimulation model will be described in greater detail in the general method section and in chapter 4 in the results section.

Lastly, transgenic mice and rats with either *de novo* or targeted genetic mutations display differential susceptibility to seizure generation. A few examples of such a model are the

several rat strains sensitive to audiogenic seizures (ethanol withdrawal) or the stargazin mice in which a strong acoustic stimulus leads to seizures. The hippocampus, in this case, might not be the location of initiation, but represents an important module of seizures generation (Nirwan, Vyas and Vohora, 2018).

1.2 The extracellular matrix in epilepsy and epileptogenesis

The ECM (extracellular matrix) represents the external space between cellular units, and consists of a tangled network of secreted proteins and locally released polysaccharides. The ECM is a highly dynamic structure which plays fundamental roles during early phases of development, especially during synaptogenesis, neurite growth and formation, and gliogenesis, helping to shape the neural architecture and cellular polarity. In the adult brain, the ECM is an active player in the regulation of synaptic transmission, homeostatic plasticity and memory formation and retrieval by influencing excitatory and inhibitory signalling and by promoting tissue reorganisation. ECM proteins have also been reported to be unexpected, but crucial components in the pathophysiological mechanisms of acquired and genetic diseases, such as Alzheimer's disease, schizophrenia and epilepsy (Berretta, 2012; Herring *et al.*, 2012; Dityatev, Wehrle-Haller and Pitkänen, 2014).

Local neurons and glial cells produce the constituents of this neural scaffold. The major components are secreted glycoproteins and polysaccharides, whilst some transmembrane and anchor proteins are also considered integral parts of ECM due to their interactions with other external ligands.

Examples of ECM proteins are the abundant group of chondroitin sulphate lecticans, tenascin proteins and hyaluronic acid, which all together form the perineuronal net (PNN) - a particular subtype of matrix unique to parvalbumin interneurons. The PNN has been associated with neuroprotection and plasticity of parvalbumin interneurons, and KO (KnockOut) animals for Tenascin-R, for example, exhibit decreased inhibitory signalling, increased excitatory population activity in the CA1 area of the hippocampus and marked activation of GFAP (glial fibrillary acid protein), potentially facilitating the epileptic

phenotype. Fragmentation of the PNN by enzymatic digestion of hyaluronic acid, exacerbates burst activity and calcium waves of primary neuronal cultures (Senkov *et al.*, 2014).

Interestingly, just as the different ECM factors influence neuronal behaviour, the ECM itself can change in response to external stimuli, (e.g. trauma) or pathologies, such as tumours or epileptic seizures. For instance, metalloproteinase 9 (MMP-9) has been detected at high concentrations in the serum of patients affected by intractable and recurrent epilepsy as a result of pathologies such as hippocampal sclerosis, focal cortical dysplasia and tuberous sclerosis. These results have been confirmed in animal models of SE and traumatic brain injury in which concentrations of MMP-9 increased in response to seizures. It has been suggested that MMP-9 activity can be linked to granule cell dispersion and anomalous synapse formation, exacerbating the epileptogenic process. On the other hand, inhibition of MMP-9 has been found to be protective for CA1 and CA3 brain regions following pilocarpine injection, with reduced activation of caspase-3, a member of the apoptotic chain. These findings suggest that MMP-9 inhibitors or Tenascin-R mimetics could have antiepileptogenic effects (Pitkänen *et al.*, 2014) .

Another example of a dysregulated ECM molecule in epilepsy and epileptogenesis is the uPAR complex (urokinase-type plasminogen activator receptor). uPAR is a multi-glycoprotein complex anchored over the extracellular membrane of brain cells. uPAR's main role is the remodelling of the ECM during cell migration and adhesion, and it does so by interacting with several extracellular and lateral molecular partners. uPAR is involved in tumour metastasis, but uPAR concentrations have also been found to be abnormally increased in the plasma of patients affected by TLE. Raised uPAR concentrations, together with macrophage and microglia activation, have been detected in the hippocampus of epileptic animals a few days after induction of SE using either a chemical (KA) or an electrical stimulation model (Pitkänen *et al.*, 2014).

ECM remodelling is also one of the features observed after traumatic brain injury. Post-traumatic epilepsy occurs in ~17% of severe traumatic brain injury after a latent period

in which secondary molecular changes, typical of the initial phase of TLE. As already detailed, these include changes in inhibition and excitation, modifications of neuronal and glial morphology and location, infiltration of immune system cells into the brain parenchyma and release of inflammatory mediators (Pitkänen and Bolkvadze, 2012).

Tumour-related epilepsy is a common comorbidity in patients affected by brain tumours. The epileptogenicity can arise either from the tumour mass itself or from the peripheral areas (Stone *et al.*, 2018). This can be due to the high level of glutamate released from the cells in the tumour or around the tumour, blood brain barrier disruption and leakage, and brain inflammation with release of toxic cytokines. In addition to these factors, variation in the ECM proteins that have been reported to be altered in primary tumours are hyaluronan, MMP-9 and tenascin-C; these are all upregulated and implicated in tumour metastasis and growth (Yang, Kwok and Fawcett, 2014). On the contrary, LGI1 (leucine rich glioma inactivated protein 1) has been found reduced in malignant forms of gliobastoma, and it was first proposed to be a tumour suppressor protein. Lately, LGI1 role preponderantly emerged in familial audiogenic epilepsy and acute forms of autoimmune encephalitis (Pitkänen *et al.*, 2014).

1.3 LGI1 protein

The LGI1 protein was initially cloned from the T98G tumour cell line, characterised from the disruption and partial rearrangement of chromosome 10 with chromosome 19. In the breaking point of chromosome 10 (q24) the novel gene identified was named *LGI1*, since T98G is a malignant type of glioblastoma and LGI1 structure is enriched in leucine motifs (Chernova, Somerville and Cowell, 1998). LGI1 protein has been reported to be reduced in the evolution from low to high malignant gliomas, and *in vitro* re-expression experiments of endogenous LGI1 diminished tumour invasion onto the surroundings matrix, through induction of apoptosis by inhibition of MMP/ERK (matrix metalloproteinases /extracellular signal – regulated kinases) pathways (Kunapuli, Chitta and Cowell, 2003). For this reason, *LGI1* was initially proposed to be a "*tumour*

metastasis suppressor" gene (Kunapuli *et al.*, 2004). A few years later, this view was challenged by other studies that suggested the lack of LGI1 in gliomas was ascribed to a developmental neuronal expression pattern, rather than a downregulation in glial cells (Piepoli *et al.*, 2006).

Nevertheless, these preliminary works paved the way for initial studies of LGI1 structure, physiological properties and expression profiles.

1.3.1 LGI1 gene structure and expression

LGI1 is encoded in the long arm of chromosome 10 (10q24) and full length LGI1 protein has 557 aminoacids (Chernova, Somerville and Cowell, 1998). The LGI1 protein is composed of two main domains, the LRR (the leucine rich repeats) and the EPTP (epitemptin) domain. The LRR domain is formed by a horseshoe-shaped α-helix with a recurved β-strand at the end of it. LRR is located at the N-terminal (amino-terminus, NH_2) of the protein and, as the name suggests, it is made of four repeats enriched in leucines, flanked by several cysteines on each side (Kobe and Kajava, 2001). At the C-terminal (carboxy-terminus, COOH) there is the epitemptin domain (also called the EAR, epilepsy associated repeat) that is a beta propeller motif and specifically a 7-fold repeated 44-residue motif. The EAR domain is conserved among other human genes related to epilepsies such as VLGR1 and TNEP1. Mutations in human VLGR1 (very large G protein coupled receptor 1) is associated with febrile seizures and it is homologous to the MASS1 gene (monogenic audiogenic seizure-susceptible) in mice. Mice with mutant MASS1 are affected by audiogenic seizures (Fringe strain). Interestingly, MASS1 is not part of an ion channel, but belongs to a large protein complex involved in transmission via G protein coupled receptors (Owuor et al., 2009; Herranz-Pérez et al., 2010). TNEP1 (Thrombospondin-type laminin G domain and EAR repeat-containing protein) is a candidate mouse gene for neurological disorders and mental retardation (Staub et al., 2002). The C- and N- terminal domains mediate protein-protein interactions and *in silico* predictions revealed that the EPTP domain interacts with ligands, meanwhile LRRs

dimerise with other LGI1 proteins in the synaptic cleft. Additional structural analysis revealed that the mature form of the LGI1 protein does not have any hydrophobic transmembrane stretches that would permit its insertion in the neuronal lipid membrane, identifying LGI1 as a secreted extracellular protein. The secretion takes place after the loss of a signal peptide at the 5' end of the sequence (Scheel, Tomiuk and Hofmann, 2002; Leonardi et al., 2011). Experiments with overexpression of WT (Wild Type)-LGI1 in cell lines, confirmed that LGI1 was detectable in the external media (Senechal, Thaller and Noebels, 2005). Lastly, LGI1 has glycosylations over three N-sites (N192Q, N277Q and N422Q) to ensure correct localisation. In triple mutant animals for these residues, the LGI1 protein is not correctly secreted (Sirerol-Piquer et al., 2006). By immunoprecipitation, cell-ELISA assay and western blot experiments, different groups identified ADAM22 and ADAM23 protein (A Disintegrin And Metalloprotease) as the direct ligands for the EPTP domain of LGI1. These protein are respectively post- and presynaptic transmembrane inactive anchor proteins which are part of a bigger molecular complex (Fukata et al., 2006; Sagane, Ishihama and Sugimoto, 2008; Yamagata et al., 2018) (**Figure 1.2**). LGI1 is, therefore, a secreted extracellular trans-synaptic protein, which is able to interact with proteins on both sides of the synaptic cleft. Protein interactions and LGI1 3D conformation have been confirmed by *in silico* computational analysis, and by a recent crystal analysis (Leonardi et al., 2011; Yamagata et al., 2018).

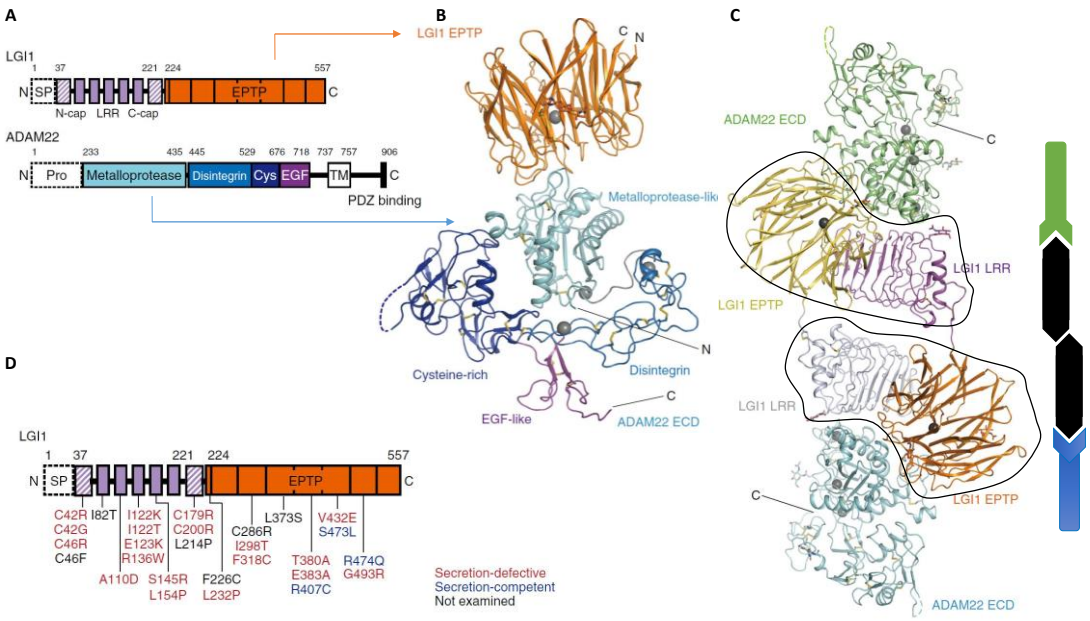

Figure 1.2: LGI1 structure and mutations with predicted 3D interactions between LGI1-EPTP and ADAM22 domains. ***A)*** *schematic structure and amino acidic length of the two main domains at the C- and N- terminus of LGI1 and ADAM22 proteins. The signal peptide (SP) highlighted in dotted line is lost before secretion.* ***B)*** *zoomed 3D conformational prediciton of the link between LGI1 and ADAM22 protein.* ***C)*** *entire 3D structure of the link between LGI1 dimers and ADAMs pre- and post synaptic partners.* ***D)*** *schematic map of the 28 missense mutations reported in ADTLE (images adapted from Yamagata et al., 2018).*

LGI1 concentrations increase from the moment of birth up to the third post-natal week, when it reaches a plateau and then remains stable through the life span (Fukata et al., 2006). LGI1 is majorly expressed in the brain, with lower peripheral expression in the skeletal muscle, liver, pancreas and thymus (Chernova, Somerville and Cowell, 1998; Morante-Redolat et al., 2002). Within the brain, the LGI1 protein is predominantly expressed in the limbic regions such as the hippocampus and the amygdala, in the cerebellum, in the occipital and frontal lobe, in the cortex and in the brain stem. Within the hippocampus, the DG is abundant in LGI1, followed by the neurons of the hilar region, and then the CA3 and CA1 regions. RNA (Ribonucleic acid) *in situ* experiments revealed

that LGI1 antibodies stained excitatory pyramidal neurons with the highest efficiency, whereas little or no expression was detected in glia and interneurons (Kalachikov et al., 2002; Furlan et al., 2006). The difference in LGI1 expression within cells and brain regions suggests that its transcription has a functional importance.

1.3.2 LGI1 in epilepsy

Since 2002, LGI1 emerged as the first gene causative of an idiopathic familial epilepsy that did not encode an ion channel (Gu, Brodtkorb and Steinlein, 2002; Kalachikov et al., 2002; Morante-Redolat et al., 2002). The onset of the ADLTE (autosomal dominant lateral temporal lobe epilepsy), sometimes also called ADPEAF (autosomal dominant partial epilepsy with auditory features, OMIM 600512), typically arises during childhood or adolescence, and the classic symptoms are partial seizures often accompanied with auditory or sensory hallucinations. Curiously, these patients experience seizures either triggered by certain type of noise or they hear acoustic auras with psychic or visual manifestations while having a seizure. The distinct pathological manifestations, confirmed by EEG and SPECT (single-photon emission computed tomography) of several members of distinct families, indicate a temporal lobe epilepsy origin (Winawer et al., 2000). Nevertheless, not all the individuals with LGI1 mutations suffer from ADLTE, meaning that the penetrance is incomplete (~67% of the cases) (Ottman et al., 2004; Ribeiro et al., 2008). Conversely, LGI1 mutations account for 50% of all the ADLTE cases, with about 2% of them occurring *de novo* (without a family history, but with similar clinical semiology) (Michelucci *et al.*, 2007).

LGI1 mutations have been found in several families and 42 mutations have been listed and investigated so far (Yamagata et al., 2018). The mutations are spread all along the LGI1 gene structure, with missense mutations being the most frequent, followed by frameshift, nonsense and point mutations. It has been suggested that alterations in LGI1 cause epilepsy by haploinsufficiency or dominant negative activity depending on the mutation. The haploinsufficiency mechanism describes a reduced (50%) amount of

correct protein available. This can happen either by increased degradation of the mutated copy of the protein, prior to secretion, or the protein is secreted, but has reduced or no physiological activity, leading to a loss of function (Senechal, Thaller and Noebels, 2005; Fukata et al., 2010). Fukata's group showed that a particular secretion defective form of LGI1, the E383A substitution, is incorrectly detected and processed by the UPR-ER (unfolded protein response/ endoplasmic reticulum) quality control machinery, leading to retention in the ER (endoplasmic reticulum) and subsequent degradation. For this reason, ADLTE has been proposed to be a "conformational disease" and the same group was able to restore LGI1 secretion and interaction with its postsynaptic partner ADAM22 using chemical correction of the LGI1 misfolded monomers (Yokoi et al., 2015). Alternatively, some of these mutations act as a dominant negative copy of LGI1, where the mutated protein interferes with the WT copy, altering its function. Experiments with a mouse carrying the 835delC mutation, suggest that dominant negative inhibition interferes with brain development in patients affected by ADLTE leading to a reduction of hippocampal volume and sclerosis (Zhou et al., 2009; Teng et al., 2010; Smith et al., 2012; Boillot et al., 2016).

Alternatively, it has been proposed that inflammation may contribute to epilepsy in animals with LGI1. Chronic inflammation due to the inflammatory enzyme cyclooxygenase-2 (cox2) has been observed in the brains of people with epilepsy and has been proposed to contribute to hyperexcitability (Rojas *et al.*, 2014). Celecoxib, recently approved by FDA (Food Drug Administration) for use in pain and inflammation, was found to restore normal neuronal excitability and to improve the quality and the length of life of animals with a LGI1 mutation (Zhou *et al.*, 2018).

1.3.3 LGI1 *in vitro* and *in vivo* models

In addition to human clinical observations, the functional consequences of LGI1 mutations and deletions were initially tested using simple systems such as CHO (Chinese Hamster Ovary), PC12 (rat adrenal pheochromocytoma) and HEK293 (Human

Embryonic Kidney) biomedical cell lines. With the use of these *in vitro* systems, it was possible to gain the first understanding of LGI1 isoforms, molecular weights and extracellular location (Furlan *et al.*, 2006; Chabrol *et al.*, 2007).

Further insights into LGI1's pathophysiological role in epilepsy came from the creation of animal models, such as *null*, heterozygous and mutant rodents. Human LGI1 and mouse LGI1 share 97% of their amino acid structure, suggesting sufficient homology for animal models to give an insight into the human disease. In the initial transgenic animal work, published in 2010, the elimination of LGI1 was achieved from early embryonic stages, influencing the development of the whole brain and the formation of neuronal circuits. A Japanese group in 2010 was the first to make a complete KO mouse by elimination of exons1-2 with homologous recombination techniques (Fukata *et al.*, 2010). Another French group opted for the disruption of allele 6 and 7, meanwhile an Australian group eliminated that part of *LGI1* gene spanning from the 3rd to the 8th exons using the *Cre/LoxP* system (Chabrol *et al.*, 2010; Yu *et al.*, 2010).

LGI1 *null* mice have spontaneous generalised seizures from P14, with sudden death around the third week of life. The seizures originate in the hippocampus, and then propagate to the cortex. The electrographic signature of the seizures was high frequency and low amplitude (18-47 Hz) spikes, followed by low frequency, high amplitude activity (20-27 Hz), terminating with slower waves (1 Hz). Post mortem analysis confirmed hippocampal pathology and developmental abnormalities of dendritic arborisation in the cerebellum and in layers II-IV of the cortex. Specific neuronal reintroduction of *LGI1*, but not *LGI3*, in KO animals rescued the lethal epileptic phenotype. Heterozygous $^{(+/-)}$ mice were more susceptible to seizure induction, both by injection of the GABA-A receptor antagonist pentylenetetrazol (PTZ) and also after strong auditory stimuli.

Affinity purification assays revealed that LGI1 protein co-precipitate in high copy numbers with distinct proteins, then identified as ADAM22, ADAM23, PSD-95 and KV1.1 channel (Voltage-gated potassium channel sub-family A member 1) by mass spectrometry and western blot techniques. In LGI1 $^{(-/-)}$ all these proteins were present in lower concentration

than normal, suggesting that LGI1 is necessary for correctly positioning these proteins at the synapse. Electrophysiological investigations revealed contrasting findings between animals: Fukata et al. (2010) in transversal hippocampal preparation (300µm) from CA1 of LGI1 KO mice found that the amplitude of mEPSC (Miniature Excitatory Post Synaptic Currents) was significantly decreased in 14-15 days old animals, suggesting a postsynaptic defect in AMPAR function. Yu et al. (2010) also in transversal hippocampal preparation (400µm) from CA1 in slightly older animals (p14-18) did not detect any deficit in the amplitude of mEPSC, but instead reported an increase in mEPSC frequency, attributing these changes to increased glutamate release from the presynaptic terminal. Extracellular recordings of slices in 0-$Mg2^{+}$, low $Ca2^{+}$ and high-K^{+} aCSF (Artificial Cerebrospinal Fluid) revealed that CA1 circuits were more easily excitable than WT controls (Chabrol *et al.*, 2010; Fukata *et al.*, 2010; Yu *et al.*, 2010).

Further insights were gained from decreased LGI1 expression using conditional knockouts, in which the elimination of LGI1 was triggered either during development (Emx1-LGI1 cKO, Empty Spiracles Homeobox 1) or in post-natal excitatory (CAMKIIα-LGI1 cKO, Ca^{2+}/Calmodulin-Dependent Protein Kinase *II*) and inhibitory (parvalbumin interneurons-LGI1 cKO) neurons in the forebrain. LGI1 removal in Emx1 (Empty Spiracles Homeobox 1) neurons during early phases of brain development confirmed the severe epileptic phenotype that results in animals death, while adult removal of LGI1 from CAMKIIα positive neurons resembled the milder heterozygous phenotype. No major problems were found in parvalbumin interneurons-LGI1 cKO during EEG recordings, suggesting that LGI1 expression is particularly important in excitatory pyramidal neurons (Boillot *et al.*, 2014). Complementary experiments were carried out in zebrafish with the use of morpholino knock down (KD) from early stages of development. KD-fish developed physical, cerebral and behavioural abnormalities and they displayed a lower threshold for seizure induction when exposed to PTZ (Teng *et al.*, 2010). Hence, LGI1 is highly conserved across the animal kingdom (92-100% protein structure homology) (Pakozdy *et al.*, 2015) and different animal models can be used to LGI1-related diseases.

1.3.4 LGI1 and the presynapse

Previous work established that LGI1 is part of a multiprotein complex, able to directly bind to the pre-synaptic anchor protein ADAM23 and to indirectly interact with the Kv1.1 shaker potassium channel (**Figure 1.4**).

ADAM23 is part of the metalloprotease and disintegrin family, but, lacking the zinc-finger motif responsible for any catalytic activity, it serves as structural membrane protein (Pakozdy *et al.*, 2015). ADAM23 KO mice display defects in neuronal dendritic maturation and neuronal growth in the hippocampus, and suffer from spontaneous seizures. Despite this, mutations in ADAM23 are not a major cause of ADLTE in patients (Mitchell *et al.*, 2001; Owuor *et al.*, 2009; Rigon *et al.*, 2011). Kv1.1 is a selective potassium ion channel formed by four α subunits, each consisting of six TM (transmembrane) regions, and four β regulatory regions renamed kvβ1. The four α subunits can contain either Kv1.1 homodimers or Kv1.2, Kv1.4 or Kv1.6 heterodimers, depending on brain area (**Figure 1.3A**). Kv1.1 is highly expressed in the mossy fibres of the hippocampus and in the Schaffer collaterals of CA1, together with cortex and auditory brainstem. Kv1.1 staining has been observed in dendritic and somatic locations (Hoffman *et al.*, 1997), but its main expression is in axons and synaptic boutons, where Kv1.1 plays an important role in regulating neuronal excitability and action potential shape and precision. It has been reported that Kv1.1 channel is rapidly activating (less than 1 msec) after the initial depolarisation of the neuronal membrane (A-type), letting potassium ions flowing out of the cytoplasm, while it closes very slowly over several seconds, ~4s, in a time-space dependent way. Re-polarization to negative potential is required for the reopening of Kv1.1 (Bialowas *et al.*, 2015). Mutations in Kv1.1 function and structure have been reported to alter these kinetics, especially increasing the half width of the action potential, broadening the spike shape and, consequently, neuronal excitability. The same changes have been mimicked by use of broad (4-aminopyridine (4-AP)) and specific (α or k-dendrotoxin (α-DTX, k-DTX)) potassium channels antagonists. The Kv1.1

channel is also directly responsible for the length of the D-current (delayed, I_D), that is the inward current before the rise of the action potential (see **Figure 1.3B**). Pharmacological manipulation of Kv1.1 can alter I_D and increase network synchronisation. These findings identify Kv1.1 as able to influence network synchronisation and homeostatic plasticity in an activity dependent way (Geiger and Jonas, 2000; Shu *et al.*, 2007; Cudmore *et al.*, 2010; Rama *et al.*, 2017). In families, mutations in KCNA1 (the gene encoding Kv1.1) cause movement disorders, such as episodic ataxia and, less frequently, epilepsy, while in rodents the epileptic phenotype is more evident and is often accompanied by various type of involuntary movements (Eunson *et al.*, 2000; Robbins and Tempel, 2012).

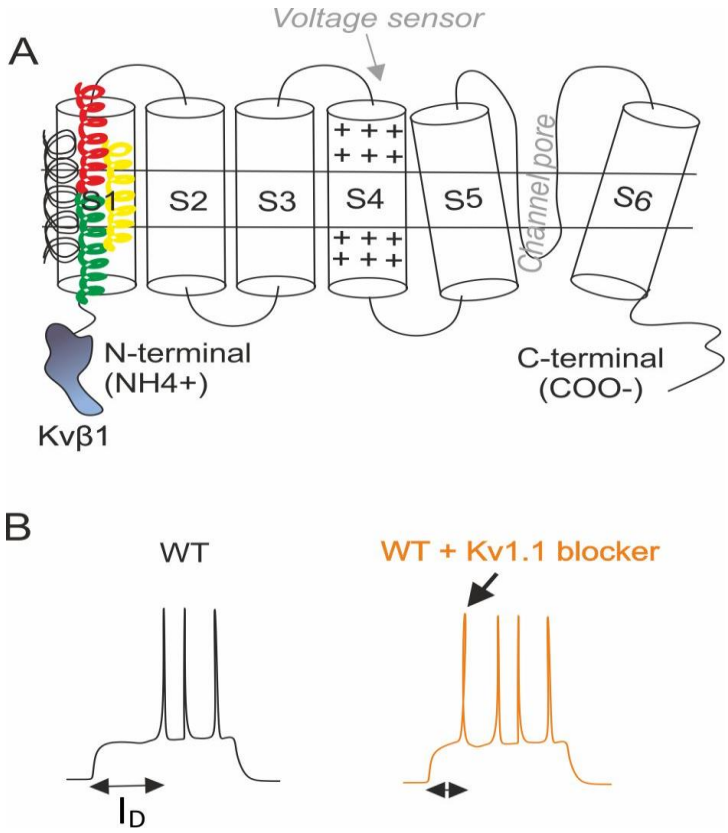

Figure 1.3:Kv1.1 structure and function. A) *Kv1.1 hetero/homomeric subunits which form the transmembrane units of the channel. The kvβ1 subunit is at the N-terminal and is the gate mechanism which cause the channel to inactivate;* ***B)*** *Kv1.1 channel influences neuronal excitation by helping controlling membrane depolarization and I_D current.*

Experiments in *Xenopus* oocytes revealed that LGI1 modulates Kv1.1 channel by interactions with the Kvβ1 regulatory intracellular subunit by preventing early inactivation of Kv1.1 (N-type inactivation). It is still unclear how a secreted protein directly interacts with an intracellular subunit and it has been proposed that this function is either exerted by a (still undetected) intracellular truncated form of LGI1 or via direct interaction with the other presynaptic partner, ADAM23 (Schulte *et al.*, 2006). Seagar et al. (2017) showed that LGI1 is able to control the density of axonal Kv1.1 and Kv1.2 channels, and that LGI1 depletion significantly decreases their concentration, lowering the threshold for neuronal excitability in CA3 organotypic cultures of p9-11 mice and p8-9 rats. As a consequence, the neurons release a greater amount of glutamate which would potentially explain how seizures are generated and/or spread in the hippocampus (Seagar *et al.*, 2017). Interesting insights also suggest a possible activity-dependent release of LGI1. *In vitro* work from Lee et al. (2015) using microarray analysis and QPCR (Quantitative Polymerase Chain Reaction), examined the mRNAs of a plethora of synaptic proteins and ion channels involved in homeostatic plasticity. They found that 48 hours after application of the sodium channel blocker tetrodotoxin (TTX) LGI1 mRNA levels decreased proportionally with those of the subunits of the Kv1.1 potassium channel, in DIV 10-13 of rat neuronal cultures. Interestingly, 48 hours of TTX application, led to paradoxical homeostatic changes that caused increases of neuronal intrinsic excitability. On the other hand, using the GABA-A receptor blocker bicuculline for the same amount of time, LGI1 and Kv1 mRNAs were found to be increased (Lee *et al.*, 2015).

It is not clear whether Kv1.1 is the only presynaptic ion channel which interacts with LGI1: recent work pinpointed the importance of Kv1.2 alone in regulating the intrinsic excitability of neurons in layer 2/3, layer 5 and prefrontal cortex (Zhou *et al.*, 2018).

Curiously, another family of potassium channels, Kv4.2, in the thalamus is similar to Kv1.1. The thalamus is an area of the brain intensely activated during a seizure. Under

physiological conditions, homeostatic events ensure that thalamocortical excitatory neurons decrease their (phasic) activity after intense firing. This is achieved by enhancement of a fast potassium current through addition of surface Kv4.2 channels at the presynaptic terminal. In coronal preparations from 2-6 months old LGI1 dominant negative mutant mice, mutations or ablation of LGI1, prevented these homeostatic processes, impairing the trafficking of Kv4.2 channels to the cellular surface and increasing instead their firing pattern (Smith et al., 2012). Interestingly, LGI1 has also been associated with synaptic proteins such as synaptophysin, synaptotagmin and syntaxin 1A, all part of the presynaptic machinery responsible for the calcium sensor and for neurotransmitter release at the presynaptic site (Kunapuli *et al.*, 2009).

1.3.5 LGI1 and the postsynapse

Postsynaptically, LGI1 interacts with the extracellular domain of the transmembrane protein ADAM22 (Fukata *et al.*, 2006) (**Figure 1.4)**. This cell adhesion molecule, together with ADAM23, might promote the formation of a tight bridge with the presynaptic side. At the post synaptic density, ADAM22 binds to PSD-95 (post synaptic density-95) scaffold protein, that acts via stargazin to control and modulate the number of AMPA receptors at the postsynaptic site. Stargazin itself is part of the molecular machinery of AMPARs (**Figure 1.4**). Mutant mice for stargazin suffer from ataxia and absences, while ADAM22 KO animals are a lethal genotype associated with ataxia and loss of myelination of peripheral nerves (Fukata *et al.*, 2016).

The importance of LGI1 for post-synaptic function was demonstrated in *ex vivo* electrophysiological experiments in young (P8-P18) LGI1 KO animals in which AMPAR-mediated mEPSC amplitudes were reduced in all the three principal subfield of the hippocampus (DG, CA1, CA3) (Fukata *et al.*, 2010, 2016; Boillot *et al.*, 2016). This was confirmed by use of auto-antibodies for LGI1 against the EPTP domain, which selectively inhibited the link between LGI1 and ADAM22/ADAM23, causing a decrease of AMPAR in dendritic spines. Additionally, $LGI1^{(-/-)}$ showed a significant decrease of GluA1 (AMPAR

subunits) in the molecular layer of the DG, the area where the majority of fibres from the perforant path and interneurons arrive (Amaral, Scharfman and Lavenex, 2007). Conversely vGLUT marker for excitatory synapses, was unaffected, suggesting that one possible mechanism of action by which LGI1 reduction causes epilepsy is the internalisation of synaptic AMPAR. How does the reduction of excitatory signalling cause epilepsy? This has been strongly debated in the field, and it is possible that the reduction of AMPAR would be restricted to inhibitory neurons, altering the physiological excitatory/inhibitory balance. Indeed INs express ADAM 22 and ADAM23 (Ohkawa *et al.*, 2013; Fukata *et al.*, 2016), but the presence and action of LGI1 on INs is contradictory.

Another protein, which is part of the postsynaptic macromolecular structure and which was co-purified with LGI1, is the cellular receptor NgR1 (Nogo receptor1) (Thomas *et al.*, 2010). This interaction is particularly important during early neuronal development and it will be discussed in further detail in the next section.

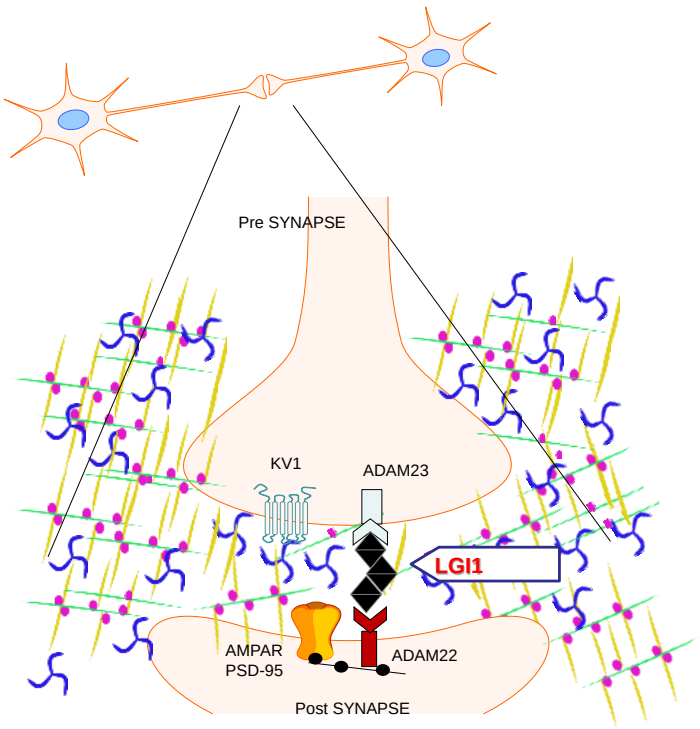

Figure 1.4:Schematic representation of LGI1 and its pre and post synaptic partners. *LGI1 acts as a bridge between the two sides of the synaptic cleft, helping*

shaping the correct cellular cytoarchitecture and maintaining a balanced synaptic transmission.

1.3.6 LGI1 during development

It is clear that LGI1 has critical roles during development, since mouse and rat models lacking LGI1 from early stages of embryonic life, develop a strong and lethal epileptic phenotype (Chabrol *et al.*, 2010; Fukata *et al.*, 2010; Yu *et al.*, 2010). Physiological and immunohistochemical analysis revealed that LGI1 performs this important function by influencing axonal and dendritic maturation, especially at excitatory synapses. Slices experiments in perforant path-DG circuits of p13-19 mice carrying a dominant negative mutation (835delC), revealed that, during development, the NR2B/NR2A (Glutamate (NMDA) receptor subunit epsilon-2 or -1) ratio is higher than normal, and as a consequence, the excitatory synapses have arrested development. In physiological conditions, during the first three postnatal weeks, excitatory synapses undergo a process of outgrowth and pruning. This process is strongly influenced by the postsynaptic NMDA receptor: NMDARs go through modifications of their subunit compositions, changing from a high expression of NR2B in immature neurons, to a higher expression of NR2A in mature ones. Hence, under physiological conditions, the NR2B/NR2A ratio decreases as LGI1 concentrations increase. Lack of LGI1 prevents subunit switching, freezing the neurons in an undeveloped state. LGI1, through the Kv1.1 channel, also helps tune presynaptic function in adult neurons by lowering presynaptic glutamate release. *Ex vivo* experiments in LGI1^{835delC} adult hippocampal slices showed that paired-pulse facilitation remains similar to the levels of WT immature brain, whereas mice over expressing LGI1 display reduced amplitude of paired responses, lowering the overall excitability in perforant path-DG circuits. Hence, in mutant LGI1 mouse, developmental dendritic pruning decreases, but the spine density rises together with network excitability and seizure probability (Zhou et al., 2009).

Further experimental observations from ADAM23$^{(-/-)}$ highlighted how also the presynaptic link with ADAM23 is essential for the formation of neuronal circuits. *In vitro* hippocampal and cortical primary cultures from embryonic KO animals for ADAM23, exhibit neurite outgrowth and abnormalities of the dendritic tree (Owuor *et al.*, 2009).

LGI1 is structurally similar to SLIT1, another extracellular molecule which has a role in guiding cellular migration and axons through the neural tube. During early development, SLIT1 has a crucial role to stop the consolidation of the growth cone thorough an interaction with Robo receptor (roundabout). LGI1, on the contrary, has been reported to indirectly antagonise neurite collapse induced by contact with myelin associated factors and to promote synapse formation. This mechanism is mediated by direct contact with the postsynaptic Nogo Receptor 1, which simultaneously complexes with ADAM22 to promote links with LGI1 (Thomas et al., 2010). A recent study showed that the binding between LGI1 and NgR1 is important for sending a repression signal to TROY (Tumour necrosis factor Receptor Orphan Y), hence antagonising RhoA activity. The RhoA signal is responsible for obstructing the polymerisation of actin of the cytoskeleton, hence inhibiting synapse growth. These authors attribute to this phenomenon the reason for a lower number and smaller size of mushroom synapses in adult LGI1 KO mice, while the total number of synapses was generally preserved. Finally, electrophysiological experiments from CA1 neuron in P10 LGI1$^{(-/-)}$ mice, demonstrated that the amplitude of mEPSC was decreased, but inter event interval increased, indicating the presence of weaker synapses. Therefore, LGI1 promotes the correct synapse number, shape and strength (Thomas *et al.*, 2018).

Anatomical abnormalities have been also detected in the cerebellum of LGI1(-/-) mice. The irregular migration of granule cells in the cerebellum was investigated by biochemical and immunohistochemical experiments with BrdU (5-bromo-2-deoxyuridine) and Pax6 (paired-box homeodomain transcription factor) markers. Pax6, is an important protein for early neuronal migration and axonal growth, while BrdU is a marker of DNA (Deoxyribonucleic Acid) synthesis in dividing cells. Assays for these markers showed

decreased levels of Pax6 and BrdU in granule cells layers in LGI1 KO embryos and in new-borns, suggesting a lower number of granule cells precursors overall. Also, the maturation of radial cells in the cerebellum, which is essential for the correct positioning of granule cells, is impaired and immature (Xie et al., 2015). Curiously, biochemical studies showed a tendency of LGI1 to be preferentially expressed in one side of the globus pallidus compared to the other, raising the possibility that LGI1 is involved in cerebral lateralisation (Jang et al., 2018).

1.3.7 LGI1 superfamily

The LGI1 gene has been identified in all vertebrates since the amphioxus. The N- and C- terminal is a characteristic of this family, together with being secreted proteins. All the LGI members have similar molecular weights and promote protein-protein interaction. Besides LGI1, this family is composed of three more isoforms: LGI2, LGI3 and LGI4.

LGI2, similar to LGI1, is an epilepsy-associated gene and mutations have been reported in benign forms of epilepsy in young dogs. It has an earlier expression than does LGI1 during development and this might explain why genetic epilepsies caused by mutations of the LGI2 gene have been described to resolve with age. LGI2 has the highest expression profile in the neurons of the ventral thalamus and the pyriform cortex (Senechal, Thaller and Noebels, 2005). LGI3 has been found expressed mainly in astrocytes, neurons and myelinated nerves fibres in the CNS. Similar to LGI1, its concentration increases after birth, but still there is no clear evidence that mutations in this gene are causative of any specific pathology. LGI3 is highly expressed in the facial nerve. LGI4 is specifically involved in peripheral nervous system (PNS) myelination. It is initially expressed in stem cells from the neural crest, and later confined to glial cells such as Schwann cells, some particular glial cells in the gastro-enteric apparatus and peripheral satellite glial cells. LGI4, like LGI1 and LGI2, binds ADAM22 and ADAM23, and this seems to be required for the correct myelination process, maybe through interactions with other structural protein such as neuregulin or integrins. LGI4 can also

bind to ADAM11 (Kegel et al., 2013). The level of interplay between these isoforms is not clear and further experiments to define temporal and neuronal expression with correlated function will be required to have a better idea of the specific roles of LGI proteins in the brain. So far, acute reintroduction of LGI3 in LGI KO mice was not sufficient to prevent the epileptic phenotype (Fukata *et al.*, 2010). Of note, LGI2, LG3 and LGI4 are poorly expressed in the hippocampus (Herranz-Pérez *et al.*, 2010)

1.3.8 LGI1 and Limbic Encephalitis: an acute hypothesis

An autoimmune disorder is characterised by the presence of IgGs (immunoglobulins), auto-antibodies (abs), against an antigen from the same host which is producing them (also called “self-antigen”). IgGs are proteins produced and released by the B-cells of the immune system, and, in physiological conditions, they have the role of tagging cells infected by a pathogen and triggering cellular death either by the release of the extracellular complement system or by promotion of auto-proteolysis. Their structure is composed of a heavy chain “perch” which is the Fc-region (fragment crystallisable) connected to two light arms responsible for antigen recognition (Fab). Sometimes the occurrence of IgGs is an indication of ongoing inflammation that can be just a secondary effect of an underlying pathology (e.g. infection by herpes virus). Alternatively, the IgGs are the primary cause of autoimmune diseases, but the chain of events leading to the production of auto-antibodies is still poorly understood. It is generally believed that production of auto-antibodies is triggered by multifactorial elements such as the genetic background of the patients (depending on the type of HLA (Human Leukocyte Antigen)), the environment around him/her (pollution, drug abuse, viral infection, tumours), abnormal interference of small-non coding RNA important for the regulation of protein translation (microRNA, miRNA) and sex hormones that can influence the physiological function of the thymus.

Limbic encephalitis (LE) is an inflammation of the limbic regions of the brain, which includes the hypothalamus, the hippocampus, the amygdala and some areas of the cortex. The invasion of the brain by auto-antibodies is also debated. It is likely that production of antibodies starts in the periphery and then enters the brain after damage of the blood brain barrier, where the production is auto-sustained by local immune cells. The auto-antibodies are not just detected in the CNS, but also in the serum. LE symptoms vary among patients, and depend upon the target of the underlying autoantibody. Autoantibodies to LGI1 usually result in unilateral dystonic seizures affecting arm and face (often termed faciobrachial dystonic seizures), confusion and cognitive impairments (Irani *et al.*, 2010; Plantone *et al.*, 2013). LGI1 patients often suffer from hyponatraemia, which is a reduced concentration of sodium in the serum (< than 135 mEq/L). LGI1 protein is highly expressed in the hypothalamic region, especially in those cells producing ADH (antidiuretic hormone) and responsible for water retention (Irani *et al.*, 2012).

Although LGI1-IgGs are the commonest cause of LE, antibodies directed against other targets have also been associated with LE, including GABA-A and -B receptor, AMPAR, NMDA R, mGluR1 (metabotropic glutamate receptor1), glycine receptors, VGKC (Voltage-gated Kv1 potassium channel-complex) and CASPR2 (contactin-associated-protein-like-2) (Irani et al., 2010; Lai et al., 2010; Crisp, Kullmann and Vincent, 2016; Dalmau, Geis and Graus, 2017). Magnetic resonance imaging provides evidence of inflammation in the temporal lobe areas, and therapies with plasma exchanges or steroids significantly improves patient outcome for several weeks, indicating that the auto-antibodies are the principal cause of the pathology. Classic AEDs are not always effective as monotherapy (Zhang et al., 2019). Sodium-channel blockers, such as carbamazepine, lacosamide and phenytoin, are the most effective, with a time of action starting from one hour after administration up to a month. In contrast, the use of levetiracetam is strongly discouraged (Feyissa and López, 2017). LGI1 auto-antibodies have been generally reported to be IgG class 4, and this class does not generally activate the complement cascade. IgG4 titre is often associated with the severity of the disease,

and two IgG4s can split and re-combine to form a hybrid antibody recognising two different antigens. Prolonged exposure to pathogenic substances are likely to start the production of IgG4 and this may go along with the hypothesis that early cortical and basal ganglia abnormalities are the basis of the LE symptomatology, preceding the hippocampal inflammation (Crisp, Kullmann and Vincent, 2016). EEG analysis of LGI1-IgG patients, highlight a multiplicity of seizures types, such as focal motor and sensory seizures, but also subclinical seizures. The seizures originate from different parts of the brain (frontal, parietal lobe and especially temporal lobe) and, in some of the cases, are characterised by delta and then slow waves appearance up to 30 seconds, with muscle artefacts often present. Interictal events are also multifocal (Aurangzeb et al., 2017). Surprisingly, recent investigations highlighted a preferential asymmetry of glucose uptake in patients with LGI1 auto-antibodies when investigated with FDG-PET imaging (18F-fluoro-2-deoxy-D-glucose positron emission Tomography), indicating possible uneven LGI1 expression within the two hemispheres (Jang et al., 2018).

LGI1 auto-antibodies are responsible for the downregulation of LGI1 proteins at the synaptic cleft, but *in vitro* and *ex vivo* experiments highlight also other mechanisms of action. Investigation with COS7 cells over-expressing a transmembrane form of LGI1 and the postsynaptic ligand ADAM22, demonstrated that application of patient's serum specifically disrupted this link. Further experiments with primary hippocampal cells revealed that clusters of the GluA1 subunit of the AMPAR were reduced at the synapse, alongside a reduction of mEPSC amplitude attributable to reduction of AMPAR signalling (Ohkawa *et al.*, 2013). This condition was reversed when LGI1-IgGs were removed, indicating a possible mechanisms of action for the effects of plasma exchange in patients (Fukata *et al.*, 2010). Additional *ex vivo* evidence come from the stimulation of MF of the hippocampus and recording neurons in CA3 with bath application of patient's sera, which resulted in cellular hyperexcitation and epileptiform activity (Ohkawa *et al.*, 2013). Recently it has been reported that 72 hours application of LGI1 autoantibodies have neurotoxic effects, decreasing calcium signals in primary cultures and increasing apoptosis (Ayşit-Altuncu *et al.*, 2018).Previous reports have described several cases of

auto-antibodies in cats producing temporal lobe epilepsy with characteristic symptoms of facial automatisms, uncontrolled salivation, MTL inflammation and secondary severe motor seizures (Pakozdy *et al.*, 2014, 2015). Recently, a mouse model of LGI1 mediate LE has been created using an osmotic pump which injected auto-antibodies in the ventricles. Chronic (14 days) exposure caused decrease memory performance in the mice tested for novel object recognition test, without affecting other motor tests. In addition, it has been also reported that total and synaptic Kv1.1 and GluA1 subunits decrease, with a reduction of miniature EPSC frequency and LTP impairment in CA1 local circuits (Petit-pedrol *et al.*, 2018).

1.3.9 LGI1 conclusions

From the above sections it can be seen that a variety of models, preparations and time points of investigation have been used for the study of LGI1. These findings, often contrasting, introduce considerable heterogeneity that may explain the diverse findings described here. The scattered and non-uniform data available from animals of different ages, using diverse mutants or polyclonal IgGs and sera from multiple patients is additionally complicated by the different parts of the brain examined and by the brain developmental stage chosen. Therefore, it is plausible that the physiological abnormalities described in different zones might differ considerably from cerebral area to cerebral area. These factors, along and the short time-windows available before LGI1 KO mice die, highlight the difficulty in attributing a definitive mechanism by which LGI1 acts and do not provide a definitive explanation of how LGI1 elimination or reduction leads to such a strong epileptic phenotype.

Thesis Aims

My hypothesis is that acute reduction of LGI1 is sufficient to increase network excitability and that, in addition to the genetic and autoimmune reductions of LGI1, reduced LGI1 also occurs in other acquired epilepsies.

The specific aims are:

- To understand whether acute development of epilepsy alters LGI1 concentrations, and affects the excitability of hippocampal circuits
- To develop and validate a method for LGI1 acute downregulation
- To determine if acute alterations of LGI1 in hippocampal circuits is sufficient to alter network excitability *in vitro* and *in vivo*
- To elucidate the mechanisms behind the altered network excitability caused by acute downregulation of LGI1 protein

Chapter 2

2 General material and methods

2.1 Animals

Animal care and procedures were carried out in line with the UK Animals (Scientific Procedures) Act, 1986 and under the Home Office License PLL/PIL 11035/13691. C57 black/c (c57bl) male and female mice (3 weeks old) and Sprague Dawley (SD) male rats (200-300 grams) were shipped from Charles River UK, Ltd. and housed in the Institute of Neurology animal facility (Denny Brown Labs, UCL). Animals were kept at room temperature (RT) (22-25°C) and maintained on a 12/12 hours' dark/light cycle with free access to food and water. Experiments were carried out after a minimum period of 7 days of habituation.

2.2 Adeno-Associated Plasmid and Lentiviral Plasmids

Adeno-associated viral (AAV) vector for LGI1 was initially designed in the laboratory of the Prof. Dityatev (Magdeburg, Germany). pAAV-U6-GFP backbone was purchased from Cell Biolabs Inc. and the oligonucleotides for LGI1 were purchased from Dharmacon (GE healthcare). The backbone consists of 5.3 kb and has kanamycin resistance. Within the Left and Right ITR (Inverted Terminal Repeat) there is the MCS (internal multiple cloning site) and the mU6 promoter in the same orientation, following there is the GFP (green fluorescent protein) under pPGK promoter (Phosphoglycerate Kinase Mammalian Promoter) and a poly A sequence (Polyadenylation). ShRNA (Short Hairpin RNA) oligos were cloned between *SalI* and *EcoRI* restriction sites. The mice sense and antisense sequences of both shRNA-LGI1 and scramble are the following:

LGI1 and scramble sense and antisense sequences
LGI1
5'- GATCC**GTGTCTTCAATCTTGAATGT**<u>**TTCAAGAGA**</u>**ACATTCAAGATTGAAGACA**CTTTTTTG - 3'
3'- GC**ACAGAAGTTAGAACTTACA**<u>**AAGTTCTCT**</u>**TGTAAGTTCTAACTTCTGT**GAAAAAACTTAA - 5'
Scramble
5' - GATCC**GCGGCTGAAACAAGAGTTGG**<u>TTCAAGAGA</u>**CCAACTCTTGTTTCAGCCG**CTTTTTTG - 3'
3' – GCGCC**GACTTTGTTCTCAACC**<u>**AAGTTCTC**</u>**TGGTTGAGAACAAAGTCGGC**GAAAAAACTTAA - 5'

Table 1: Lgi1 and scramble sequences. *The sequence of nucleotides are the sites for the enzymatic restriction, underlined is the shRNA loop, and the bold letters represent nucleotides of the 19 nucleotides are the sequence forming the real stem of the active siRNA.*

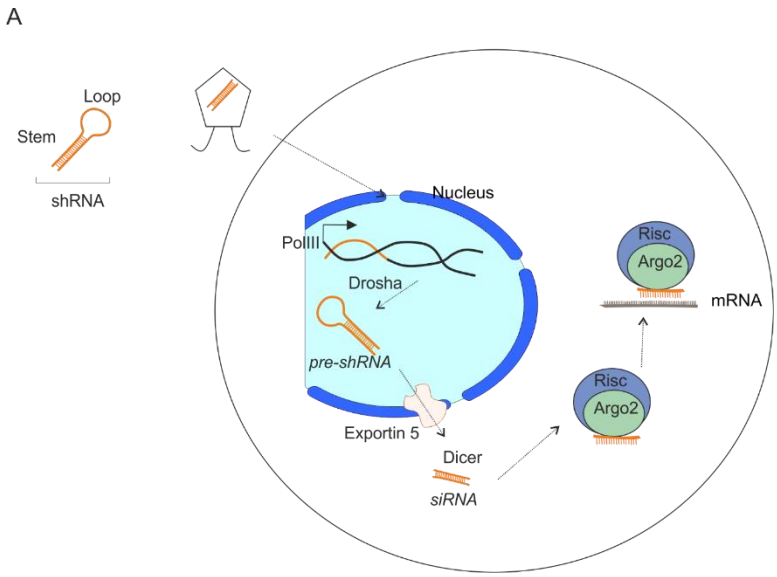

Figure 2.1:Simplified schematic representation of shRNA activity. *The viral particles delivered over the cells are entering the nucleus and stably integrating with the host DNA. After transcription by Pol III, the pre-shRNA undergoes a series of transformation process that will lead to its extrusion to the cytoplasm and to be incorporated in the RNA-*

silencing complex Risc-Argo2. The single stranded antisense siRNA is used as a negative filament to detect the mRNA of the targeted protein.

Jenna Carpenter from the laboratory of Professor Stephanie Schorge (DCEE and School of Pharmacy Department, UCL), kindly provided the lentiviral "pCCL_Flexed_MCS" backbone used for the subcloning procedure.

2.2.1 Subcloning into a Lentiviral backbone

AAV's and PCCL-Flexed's sequences chosen for the subcloning were cut by standard double enzymatic digestion with *EcoRI-HF* and *SalI-HF* (High Fidelity enzyme).

2.2.2 Restriction enzyme digestion

The "typical" digestion reaction was set up separately for each DNA's on ice (https://www.neb.com/tools-and-resources/usage-guidelines/optimizing-restriction-endonuclease-reactions). The proportions are as follow: 1μg of single DNA, 10 Units/ μg Restriction Enzyme, 1X NEBuffer in a total reaction volume of 50 μl in RNA-free water. The reaction occurred at 37°C for 1hr; no heat inactivation was needed.

2.2.3 Electrophoresis gel separation and DNA extraction

The DNA fragments were run through 0.8% agarose gel (Agarose - TAE (Tris-Acetate-EDTA (Ethylenediaminetetraacetic Acid) Buffer) Blend 1.0% Sigma Aldrich # A62360 for 50 min at 80V. DNA bands were visualised with GelRed® fluorescent nucleic acid gel stain (Biotium #41003), and extracted with a scalpel. The DNA bands were purified with the Wizard® DNA Purification Kit (Promega# A1120) according to manufacturer's

instruction, and quantified at the Nanodrop 2000 spectrophotometer (Thermo Fisher Scientific) as nl/µl.

2.2.4 DNA ligation

The ligation reaction requires 100ng of vector DNA, 1µl T4 DNA ligase enzyme, 2µl of 10X T4 DNA ligase buffer and *x* ng of insert DNA for a final volume of 20 µl filled up with sterile H_2O. The mass of the inset DNA is calculated with the formula:

$INSERT_{ng} = [(VECTOR_{ng} * INSERT_{kb\ size}) / VECTOR_{kb\ size}] *$ molar ratio (INSERT/VECTOR)

with Kb = kilobase. Generally, 100ng of vector DNA is taken for the reaction, meanwhile the molar ratio has to be decided according to the difference in size of the two DNAs to join. Reactions with small insert and big vector require high ratio (es 10:1), on the other hand, reactions with similar mass size for both insert and vector have similar ratio (es 2:1). All the elements of the reaction were gently mixed together and the ligation was set up at 4°C to avoid ATP degradation for the T4 ligase and ligase buffer. The ligation reaction was then carried out at 16°C for 16-18 hours before proceeding with the next step.

2.2.5 Bacterial Transformation and DNA amplification

0.5 µg/µl of DNA from the ligation reaction was mixed with 50µl Stbl3 competent cells (One Shot™ Stbl3™ Chemically Competent E. coli, Thermo Fisher # C7373-03) on ice for 30 minutes. The cells were then heat-shocked for 30s in a hot water bath (42°C), reincubated 3 minutes on ice and then placed for 1 hour at 37°C in the thermomixter after addition of warm S.O.C. medium (250 µl for each aliquot, Invitrogen #15544034) Next to a lit Bunsen, the cells were spread over an antibiotic-treated agar plates (imMedia™ Growth Medium, agar, kanamycin, Invitrogen™ #Q61120) with a sterile loop

and incubated face down at 37°C o/n. After 16-18 hours, the plates were removed from the incubator and put into 4°C if not used immediately for a maximum of 2 weeks.

Single, small and well-defined colonies were chosen to be amplified in antibiotic treated liquid agar (imMedia™ Growth Medium, liquid, kanamycin, Invitrogen™ #Q61020) tubes. The colony was inoculated in a 15mL tube with loose close cap and placed in a shaker incubator o/n at 37 °C. After 16-18 hours, if the media become a cloudy haze, 1mL was stored separately in a cryovial in-80°C as stock in 25% glycerol/ dH_2O solution. 2/3 of the remaining broth of each single tube was then taken and processed for extraction of DNAs through *Minipreps* kit (GenElute™ HP Plasmid Midiprep Kit, Sigma Aldrich #NA0200S). Afterwards, the DNA extract was used for a diagnostic enzymatic restriction digestion through a DNA separation gel (as previously reported). If the digestion was successful and the predicted bands were revealed, a single colony was then inoculated into a 1L flask with antibiotic treated liquid agar and placed in a shaker incubator o/n at 37 °C. The next day, the DNAs were extracted from bacteria using a *Maxiprep* kit (NucleoBond® Xtra Midi/Maxi Endotoxin Free, Machinery-Nagel # 40414.10). The pellet was generally resuspended into 50µl of TE buffer (Tris-EDTA) and quantified at the Nanodrop.

2.2.6 Primer design and DNA sequencing

Before virus production, shRNA-LGI1 and scramble DNAs were sent for sequencing to check whether the sequences were correct. Primers for the whole backbone and insert were chosen at a distance of 300-400bp (base pairs) each, forward and reverse to fully cover the whole plasmid. Primers were created in primer3.ut.ee. Desirable primer's characteristics are: 18-22 bases long, GC content between 50-55%, melting (annealing) temperature (T_m) between 50 and 60°C and a CG lock (2-3 final bases are C or G), but no regions with ≥4 identical nucleotides in a row.

The primers were ordered through Sigma Aldrich [0.05µmol] and upon arrival primers were initially resuspended in RNA-free H_2O to a stock concentration of 100pmol/µl. The working concentration used was 3.2pmol/µl. The plasmid DNA to be sequenced was diluted to 100ng/µl and 5µl were required for each DNA's reaction. The sequences were read with SeqScape software (Thermo Fisher) (**Figure 2.2**).

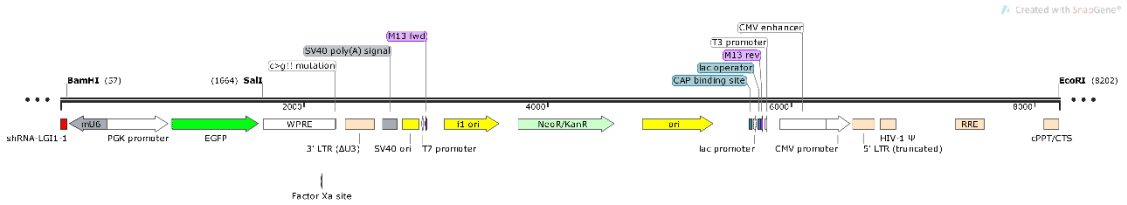

Figure 2.2: LV-shRNA-LGI1 map. *The final construct includes the AAV's MCS, mU6, pPGK and GFP into the third generation pCCL backbone containing kanamycin resistance gene.*

2.2.7 <u>In house lentiviral production</u>

LVs (lentiviruses) were produced by third generation technology (Palma and Naldini, 2002; Tagliatti *et al.*, 2016). HEK 293T cells in DMEM completed with GlutaMAX™ (Gibco #35050061) and pyruvate (100mM, Gibco #11360070) were used to harvest the viral particles. The day before transfection (day 0) 16-18 $*10^6$ HEK cells were plated in T225 flasks (#658170). On day 1, HEK cells were co-transfected in OptiMEM (Gibco # 31985-062) with DNAs in mass ratio 2:1:1,5:3 for pREV ((HIV-1) Regulator Of Expression Of Virion Proteins), pMDL (GAG, POL), pVSVG (VSV Glycoprotein G) and the vector of interest, respectively. 100µl of Lipofectamine 2000© was used every 100µg of total plasmid DNAs (Thermofisher Scientific #11668027). The mix was left over night (o/n) then replaced with equilibrated media. 48hr and 96hr later the HEK cells media was collected into 50mL Falcon tubes and quickly centrifuged for 3 minutes to separate the virus from cellular debris. The clarified supernatant was then filtered with a PVDF 0.45µm Durapore filter unit (Merck Millipore #SLHV033RS) into a 3-5 ultracentrifuge tubes

(previously washed in EtOH 70%) (Oak Ridge Centrifuge Tube, Thermo Scientific #3118-0050). The tubes were placed into a Beckman ultracentrifuge at 4°C and centrifuged for 2 hr at 32000 rpm for *in vivo* use. Once finished, the tubes were carefully extracted, marked the upper side of the base of each tube with a permanent marker to indicate the approximate area where the viral pellet was deposited during the ultracentrifugation and placed on ice. The supernatant was discarded into bleach and the tubes were left upside-down for 5 minutes to air dry. Ice cold PBS (Phosphate Buffered Saline, Thermo Fisher Cat #10010023) was added according to the dimensions of the pellet and the tube was left into a cold room o/n. the next day the pellet was resuspended with 3-5 triturations. The virus was then aliquoted in aliquots of 5µl sterile tubes (0.2mL flat cap PCR tubes, SLS #PCR1178), snap frozen into liquid nitrogen and moved to -80°C freezer in labelled 50ml falcon for long term storage.

2.3 Cellular cultures

2.3.1 Primary neuronal cultures

Glass coverslips (25 mm diameter, WVR international #ECN 631-1584) were washed with 95% EtOH for 2 hours at RT on a shaker. After, the EtOH was discarded and the coverslips were baked at 120°C o/n. PLL (poly-L-lysine hydrobromide, mol wt 30.000-70.000, Sigma Aldrich # P1274-25MG) was diluted to 1mg/ml in borate buffer (0.1M boric acid [Sigma Aldrich, # B6768], pH 8.5) and applied (200µl) over the glass coverslips inside a sterile hood. The drop was let o/n and then washed 2 times in dH_2O. Cortical and hippocampal primary neurons were derived from embryonic (E18) c57bl mice (Envigo). The mother was culled with CO_2 (2/3 O_2), then the belly was exposed and washed with 95% EtOH. A horizontal medium-lateral cut was made through the skin, along the diaphragm muscle, exposing the underneath uterus and extracting the embryos. Embryos were initially stored into a 50ml Falcon with cold Hybernate E

(Thermo Fisher # A1247601) and then transferred into 3ml culture dishes (60mm) with cold HBSS (Hank's Balanced Salt Solution, Thermo Fisher #H9394). The embryo was extracted from the amniotic sac, the head cut with small scissors and the skull peeled off with tweezers. The embryo was moved into a new dish and meninges were removed, left and right upper lateral cortex were taken with the use of recurve forceps, cut into small pieces and moved into a falcon containing fresh HBSS. The tissue was mechanically dissociated 7-8 times with a p1000 which was previously rinsed into DMEM-10% FBS to reduce sticking of the brain tissue (Dulbecco's Modified Eagle Medium, Thermo Fisher #41966029; Heat Inactivated Fetal Bovine Serum, Thermo Fisher #10082147). After that the dissociated cells were left to sit on ice for 5 minutes. The suspension was then moved into a new falcon, discarding the bigger pieces at the bottom, centrifuged at 1500 rpm for 2-5 minutes and the supernatant was discarded. The pellet was gently suspended into 1ml DMEM-10% FBS and cells were counted with Trypan blue exclusion method: initially cell suspension was diluted 1:10 with Neurobasal (Thermo Fisher #21103049), then was mixed 1:1 ratio with Trypan Blue dye (solution at 0.4%, Thermo Fisher #15250061). 10µl of the mix was placed into one of the two hemocytometer chambers and the four quadrant were counted at the microscope to estimate the number of viable cells (trans-lucid and white). Cells viability was averaged across the quadrants, then multiplied for the Trypan blue dilution factor (2), the initial Neurobasal dilution factor (10) and for the chamber volume factor (10.000). The number of cells/ml was then adjusted for the desired cellular density. Cells were plated directly on the coverslip in a drop of DMEM-10% FBS for one hour. Cells were kept at 37 °C in a humidified incubator containing 5% CO_2 and 95% oxygen. Complete Neurobasal medium containing 1%PenStrep (penicillin 10.000 U/mL - streptomycin 10mg/mL, Sigma Aldrich #P0781) 1% GlutaMAX^{TM} (Thermo Fisher, #35050061) and 2% B27 supplement (Gibco, #17504-044) was added to fill 2/3 of the well. Half media was replaced with fresh one every 7 days (Pacifici and Peruzzi, 2012; Dixon, Zhang and Lynch, 2015).

2.3.2 HEK 293 cells maintaining

Human embryonic kidney (HEK) 293 cells were grown in DMEM containing 1%GlutaMAX, 10% FBS and 1% PenStrep and split when they reached 70%-90% confluence. Cells were split every 4-5 days: media was removed, cells were washed 1x with PBS and cells were disaggregated using 0.25% Trypsin-EDTA (Thermo Fisher #15090046) and mechanical dissociation. Cells were then moved into a 15mL Falcon tube and centrifuge rapidly (1000rpm for 2 minutes). Supernatant was discarded and the cells were resuspended in 10ml of complete media. Just 1:10 of the mix was moved into a new t75 flask. Cultures were maintained in a humidified incubator (5% CO_2) at 37 °C and discarded after the 20^{th} passage.

2.4 Biochemistry (Western Blot)

2.4.1 Sample preparation for western blot

Samples (either Hek 293 cells, primary neurons or whole animal hippocampi) were lysed in RIPA buffer (Radioimmunoprecipitation assay buffer) (150 mM sodium chloride, 1.0% Triton X-100, 0.5% sodium deoxycholate, 0.1% sodium dodecyl sulfate, 50 mM Tris, pH 8.0. Sigma Aldrich #R0278-50ML) and protease inhibitor was added to the lysis mixture following the recommended concentration (Thermo Fisher, #A32963). Tissue/cells were initially mechanically disrupted by manual up and down with a pipette and then processed by a mechanical rotor type homogenizer (FastPrep-24, MP Biomedicals LLC) with the use of homogenizer beads (SLS Scientific Laboratory Supplies, # D1031-01). The samples were then centrifuged and the pellet discarded.

2.4.2 Protein quantification

Proteins were quantified by Bradford method with the use of BSA (Bovine Serum Albumine) (Pierce™ Bovine Serum Albumin Standard Ampules, 2 mg/Ml, # 23209. working concentration 0.12 µg/µl -2µg/µl from 0.25mg/ml stock concentration) as standard. Absorption was measured at 562nm using a spectrophotometer (FLUOstar Omega, BMG Labtech) and the sample concentration was extrapolated using a standard curve. Best fit linear regression was computed for each samples (dilution factor 1:10). Prior to loading, samples were boiled at 95°C for 5 minutes and 20µg of protein were loaded into each gel lane with Laemmli sample buffer (4x, Biorad, #D1031-01, 278Mm Tris-HCl, pH6.8, v/v 44.4% glycerol, 4.4% LDS, 0.02% bromophenolblue).

2.4.3 SDS-PAGE, antibody staining and detection

Samples were loaded into 10% Bolt Bis-Tris Plus Gels premade gels (Invitrogen, # NW00100BOX) and run for 70V-100V into a Mini Gel Tank (Thermo Fisher, #NW2000) into runner buffer (20X Bolt MOPS SDS (Sodium Dodecyl Sulphate) Running Buffer, Invitrogen, # B0001). SeaBlue prestain (Invitrogen, # LC5925) was used as ladder for the different molecular weight (9-150KDa (Kilo Dalton)). After run, the gel was transferred to a nitrocellulose membrane (0.2µm, Bio Rad, # 162-0112) by semi-dry method and blocked with 5% BSA (Sigma Aldrich, #A0281-1G) and then 3% milk in PBS (from lyophilised powder). Membrane was incubated with primary antibodies appropriately diluted in pbs or pbsT-0.1%milk at 4°C, o/n on a shaker. The next day, the membrane was washed 3 times with PBS and then secondary HRP (Horseradish Peroxidase) antibodies were applied for 1.30 hour in pbs or pbsT-0.1%milk at RT, on a shaking platform. Membrane was washed 3x with pbsT-0.1% milk and applied PierceM ECL substrate (Enhanced Chemiluminescence, #32106) for 5 minutes for detection. Pictures were taken by a ChemiDoc TM Imaging System (BioRad) and analysed with Image Lab

TM software (BioRad) for quantification of volume intensity of the revealed bands. Proteins were normalised over beta-actin of the same sample lane.

2.5 Imaging: Immunofluorescence

2.5.1 Free floating brain slices preparation

For immunofluorescence images from *in vivo* experiments, rats and mice were first deeply anaesthetised by use of isoflurane (4-3 % in 2 L/min O_2) then a sublethal dose of pentobarbital (140 mg/kg) was administrated intraperitoneally. Once unresponsive to toe and tail pinch, the animal was fixed on a surgical table for the perfusion. The chest was exposed, a needle was inserted in the left ventricle of the heart and a cut was made on the top right atrium to allow blood leakage. The animal was first perfused with heparin/PBS (0.8mg/ml, heparin sodium salt, Sigma Aldrich # H3393-10KU) to prevent the coagulation of the blood. Blood if present may cause auto fluorescence of the slices and unspecific antibody staining. Afterward, 4% PFA/PBS (paraformaldehyde/ phosphate buffered saline) (Santa Cruz Biotechnology # 30525-89-4) was utilised to fix the brain. The brain was then removed, left 1 day in 4% PFA at 4 °C and then cut at the vibratome (50 µm) and stored in 0.01% Na azide-PBS (Sigma Aldrich #S2002-5G) until used.

2.5.2 Immunofluorescence for free floating slices

Slices were washed 3 times with PBS solution (pH 7.4, Thermos fisher #10010023), permeabilised with 0.1%Triton TM X-100 solution for 10 minutes (ThermoFisher #28314), then washed 3x 10’ with PBS and incubated for 30 minutes with blocking solution (see specific protocol). Primary antibodies in blocking solution were used

following producers' recommendation and/or finding optimal concentrations, o/n at 4°C. The next day, slices were washed 3x10minutes with PBS, incubated 1hr at RT with secondary antibodies (see specific experimental paradigm), then washed 3x10minutes again before application of the neuronal stain (Hoechst 33342). A last 3x10minutes wash was done before mounting the slices over glass coverslips. After a few hours to dry, the slices were then mounted with Fluoroshield (Sigma Aldrich # F6182) and imaged as described in specific experimental paradigms.

2.5.3 Coverslips preparation and immunofluorescence protocol

For *in vitro* fixation, cells were quickly washed with sterile PBS and then fixed in 4% PFA solution for 20 minutes at RT. coverslips were washed 3 times with PBS solution, permeabilised with 0.1%Triton x solution for 10 minutes, then washed 3x5minutes with PBS and incubated for 30 minutes with blocking solution (see specific protocol). Coverslips were flipped upside-down on a drop of 50µl with primary antibodies in blocking solution (o/n at 4°C). The next day, slices were washed 3x5minutes with PBS, incubated 1hr at RT with secondary antibodies, then washed 3x5minutes again before application of the neuronal stain (Hoechst 33342). A last 3x5minutes wash was done before the coverslips were mounted upside-down on a droplet of mounting media (Sigma Aldrich # M1289) on a glass microslide (VWR #631-0107).

2.6 Live imaging: Propidium iodide staining

Propidium iodide (PI) dye (1ug/ml, Thermo Fisher #P3566) and Hoechst 33342 dye (4.5uM, Thermo Fisher #H1399) were incubated in the cell media for 20 minutes in the incubator. Coverslips were then imaged at with a Zeiss confocal microscope (1024x1024 resolution) using a 20X objective. Excitation wavelength for the PI was 535nm and emission peak at 617nm, excitation wavelength for Hoechst 33342 was 405 and

emission at 455nm, excitation wavelength for expressed EGFP was 488 and the emission at 515nm. Images were then analysed by automatic ROI detection plugin in ImageJ free software (https://imagej.nih.gov/ij/download.html).

2.7 Live cell calcium imaging

Calcium imaging experiments were performed with mouse embryonic (E18) cortical cultures between 21 and 23 DIV (*days in vitro*). Cells were initially incubated for 30 minutes at room temperature with 5 µM Fura-2-AM (acetoxymethyl) and 0.005% pluronic acid (ThermoFisher) in HEPES-aCSF solution (4-(2-Hydroxyethyl)-1-Piperazineethanesulfonic Acid) (125 mM NaCl, 2.5 mM KCl, 2 mM MgCl2, 1.25 mM KH2PO4, 2 mM CaCl2, 30 mM glucose and 25 mM HEPES, pH adjusted to 7.4 with NaOH). Cells were washed twice with new HEPES-aCSF and baseline was recorded for 10 minutes. After this time HEPES-aCSF was replaced with the same amount of solution containing PTX (picrotoxin) 10µM and recorded for further 10 minutes.

A 20x inverted objective on an epifluorescence inverted microscope (Olympus IX71) was used to take fluorescence images of [Ca2+] and variation. Measurements were performed in single cells using excitation light provided by a xenon arc lamp (Cairn Research, Kent, UK), the beam passing through a monochromator at 340 and 380 nm with bandwidth of 10 nm (Cairn Research, Faversham, UK). Emitted fluorescent light was detected by a cooled CCD camera (QImaging Retiga EXi, 1394) through a 510 nm long-pass filter (515 nm dichroic). The image scale size was obtained by dividing the camera pixel size (12 bit, 4x4 resolution), over the lens magnification (20X, Olympus). Images were initially processed using Andor software (Belfast, UK), Excel (Windows) and a Python script written by Dr. Marco Leite (UCL) (**Figure 2.3**).

The script cycles through all the individual cells and compute the baseline as the 5th per centile of the whole data set array. Each peak was detected as local maximum 20% greater than the average baseline. Active cells have been counted as those cells which

have at least 1 peak over 60 frames. Frequency of peaks was computed as total number of peaks divided the data size (60 frame). The coastline was obtained by averaging absolute difference between adjacent elements per frame.

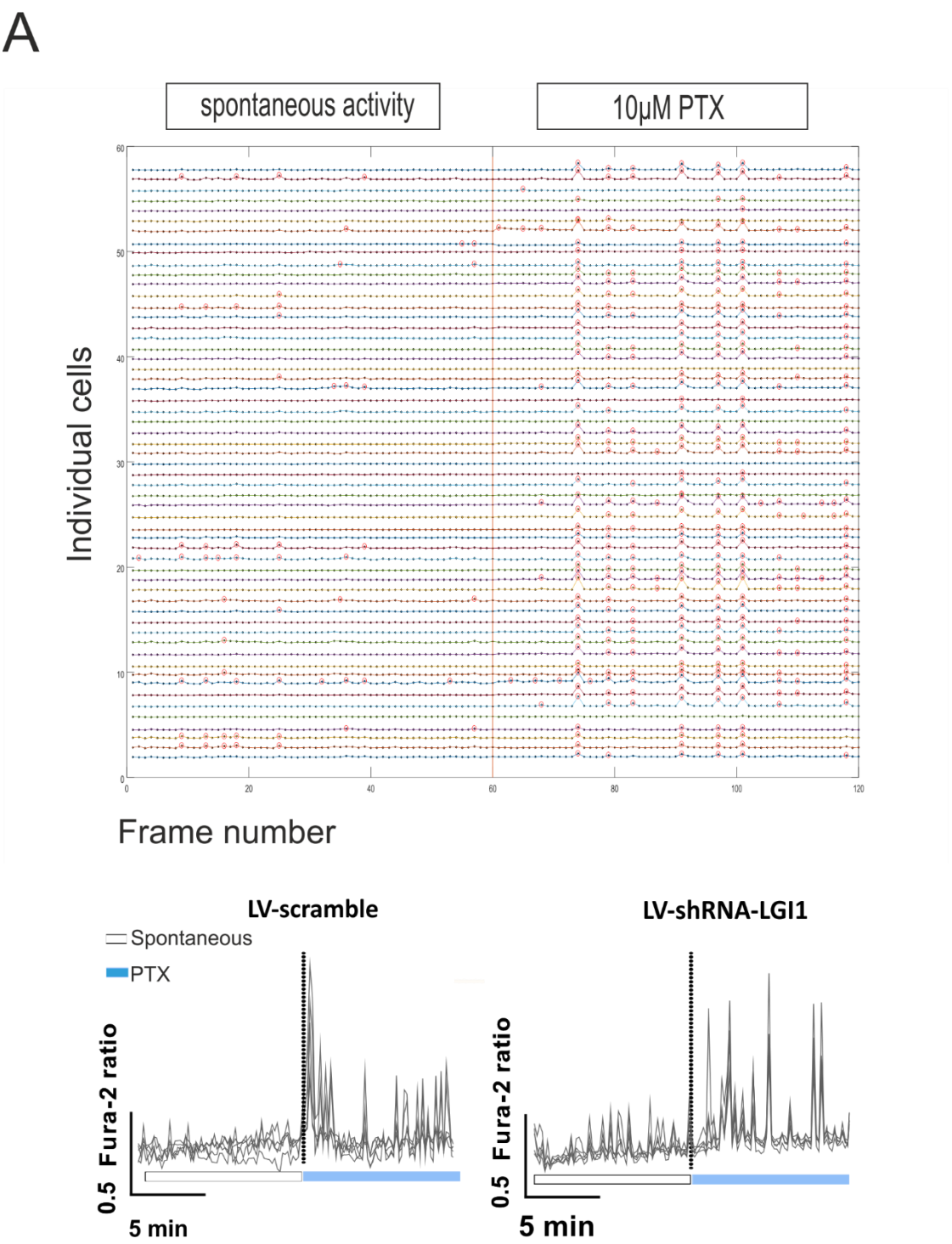

***Figure 2.3: Calcium imaging traces and analysis*. A)** Representative plot showing 340/380nm mean intensity for 120 consecutive frames (20 minutes). Each straight line

represents a single cell and the vertical orange line shows the moment in which PTX treatment was applied.

2.8 Multielectrode Arrays (MEA)

A single MEA device consisted of a 6-wells multielectrode arrays formed by 60-channel (54 recording electrodes plus 6 internal references) (MultiChannel Systems, MCS, Reutlingen, Germany). Each well was constituted of 9 recording electrodes plus one ground electrode on a glass base material. Each planar electrode diameter was 30µm and the interelectrode distance was 200 µm. Electrodes are made of TiN (titanium nitride). The MEA was connected to an amplifier by direct connexion between the amplifier's gold pins and the MEA contact pads. The signal arrived to the pc with a 68-pin MCS standard cable and digitised (25kHz sampling frequency) by the MC-Card (MEA-System). An integrated heating system was used to keep the MEA at 37°C during the time of recording (MCS) and a parafilm cap (Pechiney Plastic Packaging Company) was made in order to avoid evaporation and changes in the osmolality of the media (Blau *et al.*, 2009). The bath was grounded with a silver chloride wire wrapped around one of the name-pin of the MEA device and placed in well A for all the experiments.

MEAs were sterilised by use of 1% solution of Terg-a-zyme (Sigma Aldrich #Z273287) in distilled water o/n on a shaking platform. The next day were then washed in EthOH for a few seconds and UV under the hood. MEAs coating was done by placing a 30 µl drop of laminin (50ug/ml, ThermoFisher # 23017015) and PLL (30.000-70.000 MW, Sigma Aldrich # P2636-25MG) at ratio 1:2 in borate buffer at the centre of the device. After several washing with dH_2O (distilled water), the device was left to completely air-dry for several minutes under the hood (Colombi et al., 2013).

Data analysis was performed with Spycode working environment written in Matlab© (The Mathworks, Natick, MA, USA) and kindly provided by Dr. Michela Chiappalone's lab in

the Italian Institute of Technology (IIT), Genoa, Italy (Bologna et al., 2010). Initially, the files were converted from mcd file to MAT file. Secondly, the MAT files were filtered offline by high pass Butterworth filter (>300 Hz, gain 1200, resolution 16 bit) and the files of the six wells were divided and individually analysed. Then, the spike timings were extracted using a threshold method (10 standard deviations, 200mV artefact threshold) and used to compute the firing rate and the burst rate of each electrode. The mean firing rate was calculated as the average number of spikes for a certain time window measured among all active electrodes. The firing rate threshold was 0.02 spikes/second, with peak lifetime period set as 2ms, and refractory period 1ms. The mean bursting rate was defined as the detection of a given number of spikes in a given time window (a few milliseconds up to 1minute). The bursting rate of each channel was calculated using the logarithmic Inter Spike Interval Histogram method (Selinger et al., 2007; Pasquale, Martinoia and Chiappalone, 2010). A threshold of 0.4 burst/min was used to define if a channel was active, meaning that for a channel to be considered active it needs to have at least 4 burst for each recording period to allow a reliable bursting rate estimation. Additional bursts parameters were extracted such as the mean burst duration (ms) and the mean frequency intra bursts (spikes/s) (Colombi et al., 2013).

2.9 Solutions for electrophysiology

2.9.1 Solutions (for whole cell voltage clamp and LFP experiments)

Sucrose cutting solution was used for LFP and whole cell experiments to perfuse the animal and cutting the brain contained (mM): sucrose (105), NaCl (60), $NaHCO_3$ (26), Glucose (15), NaH_2PO_4 (1.25), KCl (2.5), ascorbic acid (1.3), sodium pyruvate (3), $CaCl_2$ (0.5), $MgCl_2$ (7).

Ringer solution was used for LFP experiment as slice storage and recordings in LFP and whole cell experiments (mM): NaCl (125), $NHCO_3$ (26), Glucose (15), NaH_2P0_4 (1.25), KCl (2.5), $MgSO_4$ 7 H_2O (1.3), $CaCl_2$ (2). Both solutions were bubbled with 95% O_2/5% CO_2 to have 7.4 pH and osmolality 305-310.

2.9.2 Whole patch clamp Internal solution: potassium gluconate (K-Glu).

The solution contained (mM): K-gluconate (135), KCl (4), Hepes (10), Mg-ATP (4), Na-GTP (0.3), Na_2-phosphocreatine (10). The pH was 7.3 and mOsm: 291-295. The solution was stored at -20°C until single aliquots were used. 7.4 pH.

2.10 Acute preparations of *ex vivo* mouse slices

5-6 weeks old male mice were deeply anesthetised with isofluorane (3% in oxygen, 2 L/min) injected with 300µl sublethal dose of pentobarbital IP (140 mg/kg) Once unresponsive to toe and tail pinch, the animal was fixed on a surgical table for the perfusion. The heart was exposed, a needle was inserted in the left ventricle of the heart and a cut was made on the top right atrium to allow blood leakage. The animal was then perfused with 25ml of ice cold sucrose solution. Animal was decapitated, the brain removed and placed in a glass petridish filled with bubbled ice cold sucrose solution in order to extract the intact hippocampi. Transversal slices (400 µm) were embedded in a 3% agar support, angled at 30° with respect to the dorso-ventral axis, and slowly sliced with a Leica VT1200 vibrating blade microtome. The slices taken for the experiments were those from 1/3 to 2/3 of the hippocampus (central part). Isolated hippocampal transverse slices were then quickly transferred to a submerged chamber (95% O_2, 5% CO_2) placed into a warm bath (34°C) for 20 minutes and then moved at room temperature for 60 min in carbonated standard recording aCSF before experiments started (**Figure 2.4**).

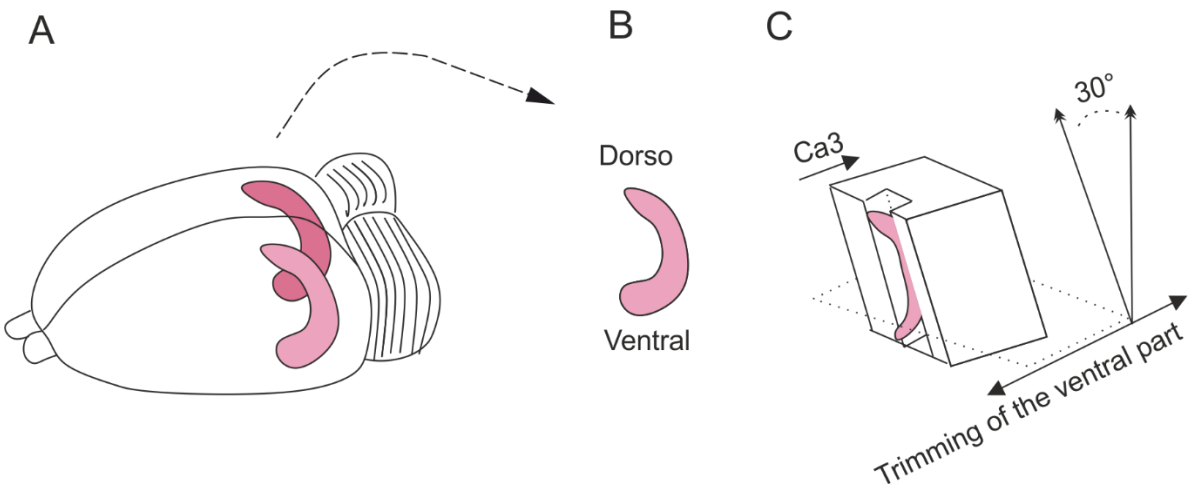

Figure 2.4: Schematic hippocampal extraction for acute slicing and transversal cut.

A) *the brain was cut into half following the hemisphere lines, the midbrain was removed and* ***B)*** *the hippocampi were extracted using a modified glass pipette with curved tip to not damage the tissue.* ***C)*** *single hippocampi were then gently flattened and moved into a pre-prepared 3% agar support "E" shaped with the CA3 area against the agar surface. Agar and hippocampus were then trimmed in their bottom part to have a flat surface and then super-glued to the metallic plate. This construction was then quickly submerged into cold bubbled sucrose-aCSF and angled of 30° with respect of the Leica magnetic platform.*

2.11 Intracellular recordings: whole cell electrophysiology

Slices were submerged into the chamber of an upright Olympus BX50WI microscope. Slices were continuously perfused and bubbled in extracellular recording solution (23-35°C) and visualised with 10X and 40X objectives (Olympus) under DIC (Differential Image Contrast) visualisation. The recordings were performed with multielectrodes made of borosilicate thin glass (4-6 MΩ, vertical puller Narishige PC-10, capillaries #GC150T-4), filled with filtered cold K-gluconate solution and connected with an Axon Multiclamp 700B amplifier (Molecular Devices). Axon-Instrument CV-7B head stage were mounted

over a Luigs & Neumann micromanipulators (Mini25) and setup. Data were acquired at 10kHz and filtered at 2kHz (Bessel) using WinEDR (John Dempster, University of Strathclyde). Neurons were sealed and opened in voltage clamp mode. GFP+ cells were identified by excitation light at 488nm wavelength (ThorLabs). Cells with RMP (resting membrane potential) above -55mV, access resistance more than 20 MΩ, bridge balance more than 10 MΩ and leak current higher than 200 pA were discarded. Series resistance was monitored at the beginning and at the end of the experiment with a negative (-5mV) voltage step and cells were discarded if it changed by more than 20%. Recording were not corrected for liquid junction potentials.

2.11.1 Voltage clamp

VC (voltage clamp) mode was employed to control the voltage of the patched cell membrane and to record transmembrane currents at a constant voltage. The neurons, were approached by the pipette with a small positive pressure, to prevent the tip clogging. A pulse of - 5mV was given in order to monitor the formation of the GΩ (giga seal). Then, the pipette fast capacitance compensation was auto-adjusted before membrane rupture. After breaking in with gentle negative brief pressure, the cell capacitance was auto-compensated before moving into current clamp mode. Neurons were maintained at -70mV for the whole time of the recording.

2.11.2 Current clamp

CC (current clamp) mode was employed to command and record changes in voltage of the patched cellular membrane by injection of a diversity of current pulses. In this configuration, the bridge was auto-balanced through an automatic algorithm. This method is able to detect changes in transmembrane potential following ion channel

activity (Instruments, 2010). pA current injection was manually monitored and corrected for the whole time of the experiment.

2.11.3 Whole cell data analysis

Recordings were analysed using a script written by Dr. A. Snowball in Python 3. The input resistance (IR) was computed by finding the linear coefficient of the relationship between the change in membrane voltage and the change in input current; an affine least squares fit to three progressive current steps was used for this purpose. The approximate cell capacitance was computed as *capacitance* = *tau* / *IR,* whereby the time constant *tau* was found by fitting a single exponential function to the time points where the membrane voltage was between 10% and 95% of the initial charging decay slope of a negative hyperpolarizing current step. Action potentials were identified if the voltage signal crossed a threshold of 0V for at least 200µs. The time of AP initiation was defined as the moment the voltage time derivative crosses 20 mV/ms. Inter-spike interval times were computed based on AP initiation times. The AP half width was calculated as the time length between the voltage crossings of the half potential between the AP initiation and the maximum voltage (Kerrigan, Brown, & Randall, 2014).

2.12 Extracellular recordings: Local Field Potential (LFP)

Extracellular local field potential was used to record mossy fibres – CA3 network activity in response to extracellular stimulation (**Figure 2.5 A**). Data acquisition: the same setup used for whole cell patch clamp was also used for LFP experiments (see previous section). Slices were left to recover 1hour at room temperature in bubbled recording solution (95% O_2 5% CO_2) before being placed for further 1hour in the recording chamber of the electrophysiology setup. Field EPSP were obtained by external stimulation of mossy fiber pathway (over the dentate granule cell layer) using a bipolar stimulation

electrode (stainless steel, FHC). The stimulus intensity was adjusted as 1/3 of the maximum field excitatory postsynaptic potential (fEPSP), delivered for 80 µs and measured using a constant current stimulus isolator (DS3, Digitmer, Hertfordshire, UK). The recording electrode was made of borosilicate glass (1-3 MΩ) and filled with the same extracellular solution. Data were acquired at 20kHz and filtered at 2kHz using WinWCP (John Dempster, University of Strathclyde).

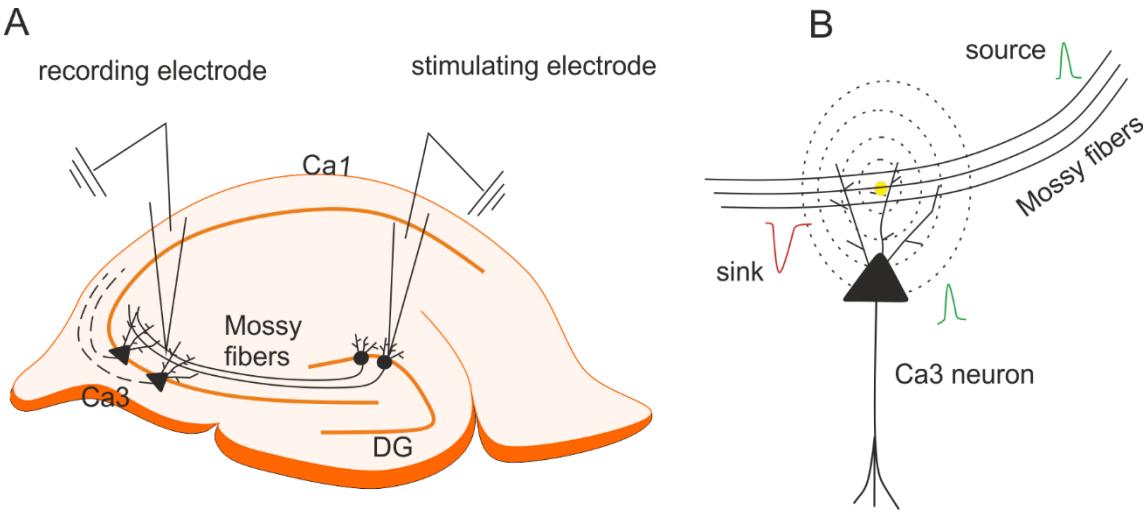

***Figure 2.5: Hippocampal transversal slice section and diagram of the sink and source currents among MF and CA3 neurons*. A)** acute transversal hippocampal slices showing the stimulation electrode location on the granule cells and the recording electrode over the stratum lucidum of the CA3. **B)** schematic illustration for source and sink of fEPSP. The negative slope is due to positive ions (sodium) entering the dendritic branches and axonal membranes, hence inner side of the neurons is transiently positive, meanwhile the extracellular space stays briefly negative (Mary M. Heinricher, 2004). Images modified from (Einevoll et al., 2013).

2.12.1 fEPSP data analysis

The peak amplitude of the recordings was analysed with Clampfit™ software in combination with bespoke Python 3 code written by Dr. Marco Leite. The delta amplitude

and slope were calculated based on the maximum and the minimum points of the voltage signal between two cursors manually placed just before the beginning of the decay slope and just after the maximum of the decay slope.

2.13 *In vivo* perforant path surgery and stimulation

For all the experiments, SD male rats of 250-310g were used after a week of habituation in the animal facility.

2.13.1 Electrodes preparation

Prior to the surgery procedure, all the electrodes and electrode components were purchased from Invivo1 (Plastics One Inc, Bilaney Consultants UK Ltd., UK). Initially, stimulation electrodes (E363/3, 0.15mm diameter), reference electrodes (E363/0) and recording electrode (E363/1, 0.25mm diameter) were prepared as followed: the bipolar stimulation electrode was made out of two stainless steel polyimide-coated electrodes twisted together. One of the electrode's tip was cut of about 1mm shorter that the other one and kept separated of ~0.5 mm to avoid short circuit. Both stimulation and recording electrode tips were exposed of about 1mm coating. The gold plated socket reference electrode was soldered to a silver wire (0.125mm diameter).

2.13.2 Perforant path surgery

After weighing, the animal was put asleep in an anaesthetic chamber by use of isoflurane (4 % in 2 L/min O_2). The animal was then moved to a stereotaxic frame (David Kopf Instruments, USA) over a heat-mat for surgery and the isoflurane reduced to 2%. Eyegel (Viscot Tears) was applied over the eyeballs and meloxicam (Metacam Henry Schein

Animal Health (HSAH), 0.2 ml 5 mg/ml) was given via subcutaneous injection. After confirming that there was no reaction to the toe and tail pinch, a small area on the head of the animal was shaved, cleaned with iodine (Videne, MidMeds Ltd., UK) and exposed the surface by cut of 1 cm^2 skin area. The craniotomy comprehends the drilling of 5 burr hole in total using a stereotaxic drill (Model 1471, David Kopf Instruments, USA) with ball mill drill bit measure #3 (WPI – 501855). The first burr hole (Antero Posterior [AP] -0.81cm from the bregma; Medio Lateral [ML] -0.44 cm from the bregma) was for the insertion of the bipolar stimulating electrode able to triggers subthreshold stimuli to the perforant path area. A second hole was drilled for the insertion of a recording electrode (AP -0.4; ML -0.25) in the DG of the hippocampus to record the resulting population spike of the pyramidal cells. Lastly, two burr holes were drilled in order to insert screws that will help holding in place for the dental cement. A last burr hole was inserted for the reference electrode (**Figure 2.6A**) The right Z position of the recording electrode was determined by lowering slowly the recording and the stimulating electrodes until maximal population field excitatory postsynaptic potential was achieved (**Figure 2.6B**). A single pulse stimulus of 3.5 mA and 150 μs width was delivered from a Neurolog system (Digitimer Ltd, Welwyn Garden City, UK) and a stimulus isolator (Digitimer, UK). Recordings were bandpass-filtered at 0.1-50 Hz. The presence of positive going field potentials with >2 mV population spike indicated that the electrodes were correctly positioned. After this, electrodes and ground were inserted into a six-channel holder (#MS363, Invivo1, Plastics One, UK) and this was fixed with dental cement (Kemdent, Swindon,UK). Buprenorphine (Buprevet, HSAH, 0.2 ml 0.2 mg/ml) was administered towards the end of the procedure as Dr. Pishan Chang (personal communication) observed a decrease in population spike amplitude if Buprenorphine was administered at the beginning of the procedure. Lastly, saline solution (2.5ml, HSAH, 0.9% w/v NaCl) was administered at the end of the procedure.

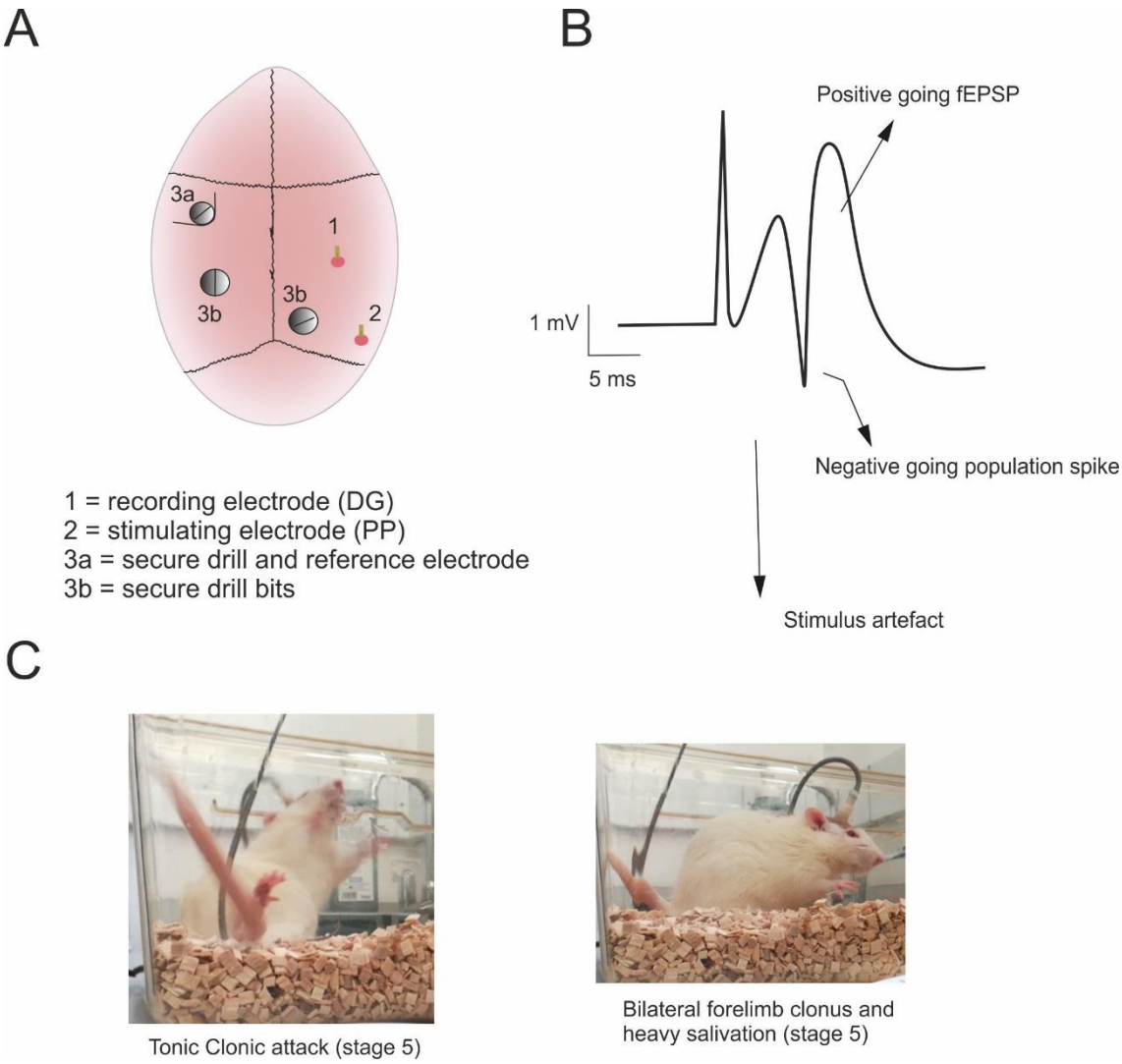

Figure 2.6: The perforant path model of acquired epilepsy **A)** Schematic representation of the perforant path surgery circuit and electrodes implanted **B)** Typical population spike shape recorded in DG upon perforant path stimulation **C)** Spontaneous seizure of a stimulated rat after 2hr stimulation in the recording chamber (Modified Racine scale 5) (**Figure 2.6C**)

2.13.3 Perforant path stimulation

After 7 to 10 days of care post-surgery, the animal underwent the stimulation procedure for the induction of status epilepticus: the six channel holder on the animal's head was

connected to the 6 channels via a 363/363 plug cable (Plastic 1) which allowed the animal to move freely for the whole time of the induction.

The stimulation was delivered through Spike 2 software (CED, Cambridge, UK), connected to a Hum Bug Noise Eliminator (Digitimer Ltd.), band pass-filtered (0.1-50 Hz) and digitised at 100 Hz (CED micro 1401, Cambridge, UK).

The first 10-20 minutes were recorded as baseline. After this time, two hours' 50 μs, monopolar pulses at 20 Hz stimulation was delivered (intensity was set to that which elicited 2/3 of the maximum amplitude of the population spike with a single stimulus). During this stimulation time, the 20Hz stimulation triggered self-sustaining status epilepticus which was monitored and recorded for the following three hours. Behavioural seizures were graded according to the Racine scale (see Table 2, Results 3.1) every 10 minutes. At the end of this time, saline (5 ml) and diazepam (20 mg/kg I.P., Hameln Pharmaceuticals Ltd) was given to the animal and the rat was monitored for 20-30 min to ensure SE stopped.

2.13.4 In vivo stereotaxic injection of substances (in rats and mice)

Male Sprague-Dawley rats (300 g) were anesthetised with isoflurane (5% in 2 L/min O_2), the animal's head was shaved with an electric small shaver (Wella, UK) and then placed in a stereotaxic frame (Kopf Instruments, USA). Eyegel (Viscot Tears) was applied on the animal's eye bulb and it was injected with Metacam (1.3 mg/kg) and Buprenorphine (0.2 mg/kg, 40 minute since onset, 12 hours analgesia, Temgesic, Scherig-Plough, UK) subcutaneously. The head's skin was cleaned with iodine (Videne, MidMeds Ltd., UK) and the skull exposed. Isoflurane was then decreased to 2-3% in 2L/min O_2 and the animal's breath was monitored through all the procedure to avoid gasping. Three burr holes were drilled unilaterally with a 1.2mm diameter ball mill carbide drill bit (World Precision Instruments (WPI)) at high speed and according to the coordinates from bregma suture: dorsal hippocampus (Medium Lateral [ML] -2.5; Antero Posterior [AP] -

3.6; Dorso Ventral [DV] -3.00), central hippocampus (ML -4.2; AP -4.5; DV1 -8.00; DV2 -3.30) and ventral hippocampus (ML -5.00; AP -5.30; DV1 -7.10; DV2 -4.40). The coordinates were adjusted in proportion to the distance between the bregma and lambda sutures over a max ML distance of 4.00mm.1µl of each virus was injected using a Hamilton syringe at the speed of 100 nL/min and waited 5-10 min before slowly withdrawing the micropipette to avoid backflow of the virus to the surface. The skin was then sewed (Vicryl rapide ™ (polyglactin 910), 3-0, #W9931, Ethicon ®), saline solution (2.5 ml) was administered and the animal was monitored until awake.

C57bl WT male mice (4 weeks old, 16-18 gr) were anesthetised with isoflurane (3% in 2 L/min O_2), the animal's head was shaved with an electric small shaver (Wella, UK) and then the animal was placed in a stereotaxic frame (Kopf Instruments, USA) and kept warm over an electric heat-mat. A small amount of eye gel (Viscot Tears) was applied on the animal's eye bulb and then it was injected with Metacam (0.13 mg/kg) and Buprenorphine (0.02 mg/kg, 40 minute since onset, 12 hours analgesia, Temgesic, Scherig-Plough, UK) subcutaneously. The head's skin was cleaned with iodine (Videne, MidMeds Ltd., UK) and the skull exposed. Isoflurane was then decreased to 1-2% in 2L/min O_2 and the animal's breath was monitored through all the procedure to avoid gasping. One burr hole was drilled bilaterally with a 1.2 mm diameter ball mill carbide drill bit (#501819, World Precision Instruments (WPI)) at high speed and according to the coordinates from bregma suture (mm): (ML1 –2.54; AP1 –2.75; DV1 -2.35; ML2 -3.1; AP2 -2.75; DV2 -2.8). The coordinates were adjusted in proportion to the distance between the bregma and lambda sutures over a max ML distance of 4mm. 1µl of each virus were injected to the speed of 100nL/min. Before withdrawing of the micropipette 5 minutes were to avoid backflow of the virus to the surface. The skin was then sewed , saline solution (0.5 ml) was administered and the mouse monitored until awake (Counsell *et al.*, 2018).

2.14 Intraperitoneal injection of kainic acid and behavioural Racine score

Kainic acid 50mg/ml stock powder (KA, Tocris Bioscience #0222) was dissolved in dH_2O to a concentration of 10 mg/ml. KA was further diluted in 0.9% sterile saline solution for a single dose of 5 mg/kg for each injection. Mice were injected intraperitoneally once every 30 minutes until they reached stage 5 of a modified Racine scale (Tse *et al.*, 2014) or reached a maximum dose of 45mg/kg. Once that the mouse reached stage 5 for a consistent amount of time (30 minutes) or was evaluated as in continuous status epilepticus, the animal was sacrificed as human endpoint. Behavioural observations were taken every 10 minutes by a blinded observer (Dr. Gabriele Lignani, UCL). The scores were then analysed in a blind fashion with Microsoft Excel and GraphPad© Prism6.

2.15 Statistics

All the data were expressed as mean values ± SEM (standard error of the mean), if not stated otherwise. SEM was calculated as the ratio between the standard deviation of the population over the square root of the number of observations. Student's unpaired t-test was used to assess difference between two independent normally distributed populations. Paired t-test was used in case of repeated t-test measures from matched groups. Analysis of the variance (ANOVA)'s test coupled with post-hot correction, was used when 3 or more normally distributed data were compared. Normal distribution of the data was assessed using the Kolmogorov–Smirnov normality test. Data not normally distributed were calculated with Mann-Whitney test when two groups were compared. Range and IQR (inter quartile range) were used to indicate as measure of dispersion of the data around the median (Norman and Streiner, 2000).

According to the basic formula for sample size known as Lehr's equation, the n required was calculated as follow $n = 16 / \Delta^2$, with Δ (delta) = δ (effect size) / σ (standard deviation)

and assumed equal sample size and homogeneous variance. The numerator is chosen as two sample comparison and with a power of 80%.

The data were represented by box and whiskers graphs: bars symbolised minimum and maximum value, box edges were the 25^{th} and 75^{th} percentiles, the horizontal central line represented the median, the "+" symbol represented the mean. Statistical analysis was done by employing GraphPad© Prism 6 software, Microsoft Excel 2010 (Windows), Matlab © (The Mathworks, Natick, MA, USA), Clampfit Axon pClamp™ and Python 3.1© (open source software www.python.org/) with Anaconda© AI/ML enablement platform.

Chapter 3

3 Lgi1 protein is altered in an *in vivo* model of chronic epilepsy

3.1 Summary

In this chapter I asked whether a reduction in LGI1 is associated with forms of acquired epilepsy, in particular epilepsy that develops post-status epilepticus, and whether this has any impact on circuit function.

I used a perforant path model of epilepsy which involves just the use of electrical stimulation. I then investigated if LGI1 concentrations were altered after establishment of SSSE and if this altered hippocampal physiology.

3.2 Introduction

Mutations in LGI1 gene either preventing the release of LGI1 or causing abnormal LGI1 monomers, lead to a familial form of epilepsy (ADTLE) (Kalachikov *et al.*, 2002). KO animals for LGI1, are lethal within a few weeks after birth (Chabrol *et al.*, 2010; Fukata *et al.*, 2010; Yu *et al.*, 2010). There is substantial evidence that there is an important developmental component in these epileptic syndromes (Zhou *et al.*, 2009).

However, LGI1 has been also associated with an acute, acquired aetiology of epilepsy, autoimmune limbic encephalitis, in which the onset of this disease is typically after development (Irani *et al.*, 2010). This suggests that there must also be an acute epileptogenic effect of LGI1 down-regulation.

To address this, I used a well-established model of post-status epilepticus epilepsy. A drawback of many epileptic models, is that they require the use of a chemoconvulsant agent, which makes it unclear whether any pathophysiological change (in our case the hypothesised change in LGI1) is due to the chemoconvulsant itself or the electrical activity of the seizure (Sloviter, 1983).

In order to avoid this potential confounder, I used a perforant path model of epilepsy which avoids the need for a chemoconvulsant to see whether the electrical activity, in particular SE, can results in reduction of LGI1(Walker *et al.*, 1999). Importantly this model is associated with the development of chronic epilepsy (Khalil *et al.*, 2017).

3.3 Hypothesis

My hypothesis here is that acquired epilepsy can be associated with a reduction in LGI1, which results in changes in hippocampal circuit excitability.

3.4 Experimental paradigm

Animals were divided into three groups: animals that underwent perforant path surgery and stimulation (called “epileptic” from now on), animals that underwent surgery but not stimulation (“sham”) and animals that had neither surgery nor stimulation (“naïve”). The ipsilateral (right) and contralateral hippocampi of epileptic and sham animals were extracted three weeks after the procedure or the induction of SE and snap frozen in liquid nitrogen. Hippocampi from SD rats of similar weight were used as control animals and treated with the same method. Lysates from all hippocampi were diluted in 5M Urea (Sigma, U5478) solution and 20µg of samples were loaded in each well of a run SDS PAGE gel (Sodium Dodecyl Sulphate - Polyacrylamide Gel Electrophoresis) (10% Bolt). Samples were transferred to a nitrocellulose membrane by semi-dry method and blocked with 5% BSA and then 3%milk in PBS. Membranes were incubated with 1:250 anti-LGI1 in pbs (Santa Cruz c-19), 1:2000 anti β-actin in pbs (Sigma, #A2220-200UL) o/n. The secondary HRP antibody used were donkey anti-goat (1:2500, Santa Cruz, sc-2020) and donkey anti-mouse (1:4000, 2B scientific # 43R-1308) in pbs and were incubated for 1.30h at RT shaking. Thermo Scientific Pierce^{M} ECL substrate (#32106) was used for the detection. Pictures were taken by a ChemiDoc ^{TM} Imaging System (BioRad) and

analysed with Image Lab ™ software (BioRad) for quantification of volume intensity of the revealed bands. LGI1 was normalised over beta-actin of the same sample lane.

The *in vitro* electrophysiology was performed by Nicola Hamil. In brief, horizontal hippocampal slices (350 µm) from sham and epileptic rats were sliced using a Leica VT 1200S (GmBH, Germany) at 0.16 mm/sec in high sucrose aCSF containing (in mM): 87 NaCl, 2.5 KCl, 7 $MgCl_2$, 75 sucrose, 1.25 NaH_2PO_4,26 $NaHCO_3$, 0.5 $CaCl_2$, 25 glucose (osmolarity 316 mOsM), stored in a holding chamber at 37 ˚C for 20 minutes then transferred to a gas/fluid interface chamber at room temperature. Slices were maintained in aCSF and experiments were carried out in a submerged recording chamber perfused with the same solution. All solutions were continuously gassed with 95 % O_2 and 5 % CO_2. Field excitatory post synaptic potentials were recorded using glass microelectrodes filled with aCSF (~1 MΩ) positioned in the middle molecular layer of the dentate gyrus or stratum radiatum of CA3 or CA1. A bipolar stainless steel stimulating electrode (~8 - 10 MΩ) was used to deliver < 1 mA pulses to the medial perforant path (MPP, 200µs), mossy fibres (MF, 200µs) or Schaffer collaterals (SC, 400µs) every 20 seconds. Electrode position and stimulus intensity were adjusted to maximize the fEPSP without observing contamination from population spikes. Slices were discarded when the response obtained was < 1 mV. Stimulus intensity was reduced to elicit ~75 % of the maximal response and paired-pulses were applied at an appropriate interstimulus interval; 20ms at the MPP, 50ms at the MF and 20ms at the SC. A frequency facilitation protocol was used to confirm MF activation. Stimuli were applied at 0.05Hz for 10 minutes, 1Hz for 10 minutes and then 0.05Hz for 10 minutes. If frequency facilitation was not observed, electrodes were repositioned. Paired-pulse ratio was calculated as the amplitude of the test pulse expressed as a percentage of the amplitude of the conditioning pulse.

3.5 Results

3.5.1 The perforant path stimulation model reliably induced status epilepticus

10 days after surgery, the rats underwent the stimulation paradigm (**Figure 3.1A**). After a short period of baseline (**Figure 3.1B**), 20 Hz stimulation was applied (**Figure 3.1C**), the intensity of the stimulation was adjusted to have 2/3 of maximum population spike and continued for a period of 2-3hours. Self-sustaining status epilepticus (**Figure 3.1D**) was induced in 4 (rat 1, rat 2, rat 3, rat 4) out of 5 (rat 5) stimulated rats (success rate 80%). In the one failure (rat 5), there was neither electrographic nor behavioural evidence of self-sustained status epilepticus.

Conversely, in the other 4 rats (rat 1, rat 2, rat 3, rat 4), the behavioural changes (stage 2 and 3) started between 10 and 30 minutes after the start of the 20 Hz stimulation and reached stage 5 within 50 minutes on average (mean = 52.5 ± 5.82 minutes) from the beginning of the protocol (**Figure 3.1E**). After the 2 hours stimulation period, the EEG demonstrated repetitive spikes for the whole duration of the post stimulus recording period (**Figure 3.1D**), and there were repetitive seizures that varied from stage 3 to stage 5 with periods of immobility in between (**Figure 3.1E**) (number of stage 5 seizures/hour after stimulation: 3 = ± 1 with a mean behavioural duration time: 61 ± 5.2 seconds (from Khalil *et al.*, 2017).

RACINE SCALE	
Stage 1	Mouth and facial movements, immobility
Stage 2	Head nodding
Stage 3	Forelimb clonus
Stage 4	Seizures characterised by rearing
Stage 5	Full motor seizure with loss of postural control

***Table 2: Modified Racine scale**. Behavioural animal seizure scale (Racine, 1972).*

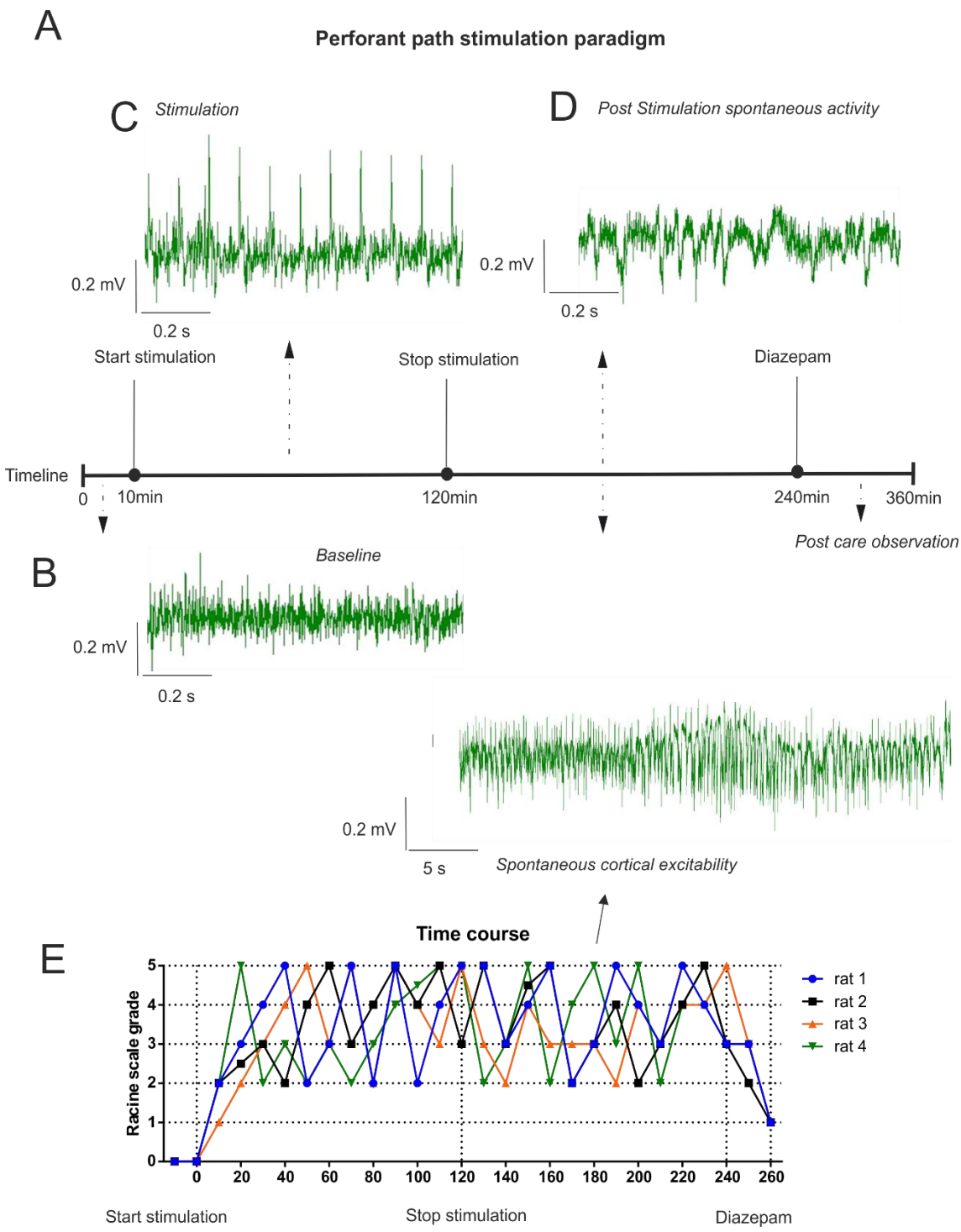

Figure 3.1: Electrical stimulation of perforant path fibres and relative behaviour.

A) *representative perforant path stimulation timeline and EEG traces of implanted rat:* ***B)*** *baseline,* ***C)*** *stimulation (20 Hz) and* ***D)*** *post stimulation spontaneous activity.* ***E)*** *Representative behavioural time course of each stimulated rat during PPS (perforant path stimulation) with a short representative traces of spontaneous cortical excitability.*

3.5.2 LGI1 expression levels decrease in animals with acquired chronic epilepsy three weeks after SE

It has been previously demonstrated in the laboratory that after the first week of the induction of the SE, the rats develop chronic epilepsy (Walker *et al.*, 1999; Khalil *et al.*, 2017). Hence, I first choose to examine the levels of LGI1 protein 21 days after the perforant path stimulation procedure. LGI1 was significantly reduced in the ipsilateral side of the hippocampi of epileptic rats (rat 1, rat 2, rat 3, rat 4), compared to that in the hippocampi from Sham (rat 6, rat 7, rat 8, rat 9) and Naïve animals (rat 10, rat 11, rat 12, rat 13) (Naïve vs. Epileptic: average reduction = 48.6%, LGI1 mean epileptic quantification = 0.51 ± 0.02; Sham vs. Epileptic: average reduction = 27.5% reduction, LGI1 mean sham quantification = 0.78 ± 0.04, p=0.001 two tailed Student's t test corrected for multiple comparisons. **Figure 3.2D**). Interestingly, the Sham animals were significantly different from the naïve controls (Naïve vs. Sham: mean = 21.1% reduction, p=0.001 two tailed Student's t test corrected by multiple comparison).

Conversely, on the contralateral side, the levels of LGI1 protein in epileptic animals were not significantly affected (Naïve vs. Epileptic: average reduction = 14%, LGI1 mean epileptic quantification = 0.86 ± 0.21; Sham vs. Epileptic: average reduction = 0.07%, LGI1 mean sham quantification = 0.86 ± 0.08; p>0.5 two tailed Student's t test corrected for multiple comparisons (**Figure 3.2E**). However, this result may have been biased by a clear outlier in the sham treated (**Figure 3.2E**). Nevertheless, even when I eliminated this outlier, there was still not significant difference between sham and epileptic (Sham vs. Epileptic: average reduction = 35%, LGI1 mean epileptic quantification = 0.65 ± 0.04, p=0.09 two tailed Student's t test corrected by multiple comparison, n=3).

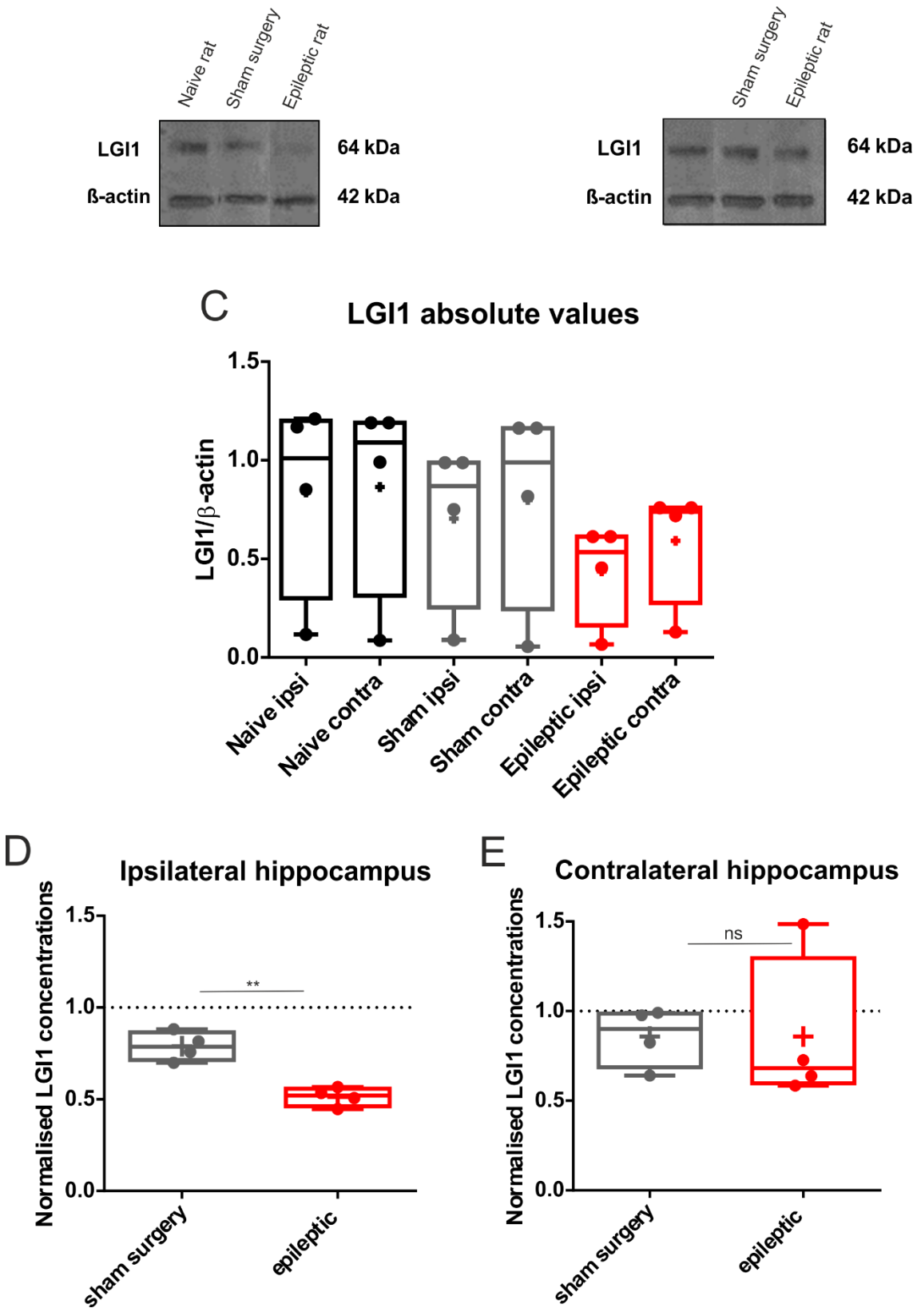

Figure 3.2: LGI1 protein is reduced in ipsilateral hippocampi of epileptic animals. ***A)*** *LGI1 expression in the ipsilateral and* ***B)*** *contralateral side of the hippocampus from rat lysates. Upper bands were revealed with LGI1 antibody and lower bands with β-actin ab.* ***C)*** *show the absolute quantification of LGI1 concentrations in each condition.* ***D)*** *LGI1*

*relative quantification in the ipsilateral and **E)** contralateral side of the hippocampus for sham and epileptic rats. Each measurement of band intensity is normalised by the respective ipsi- and contralateral naïve control (blots n=4; each sample: Naïve rat n=4, sham n= 4, epileptic n=4).*

3.5.3 Blocking Kv1.1 with α-Dendrotoxin has less effect on paired pulse ratio in epileptic animals

Secondly, we investigated whether there were any associated functional changes in the major hippocampal pathways in epileptic animals that would lead to a modified excitability of the neuronal network. These changes were investigated by Dr. Nicola Hamil (UCL) who performed paired pulse experiments in the three major hippocampal sub-fields, dissecting the field connections: medial perforant path – DG, Mossy fibres – CA3 and Schaffer collaterals –CA1.

Since loss of LGI1 should have a direct effect on presynaptic Kv1.1 expression and function (see Chapter 1), we asked if loss of LGI1 had an effect on synaptic plasticity. To address this question, Dr. Hamil acutely applied α-Dendrotoxin (300nM) in hippocampal slices from sham and epileptic animals to investigate whether they have similar susceptibility to this blocker. α-Dendrotoxin is a specific blocker for Kv1 family (Harvey and Robertson, 2004). Short term plasticity was tested using a paired pulse protocol which is dependent upon presynaptic potassium channel modulation (Geiger and Jonas, 2000). Our results show that α-Dendrotoxin is able to reduce PPR (paired pulse ratio) in hippocampal control slices, but this ability is reduced or lost in slices from epileptic animals (**Figure 3.3**).

We examined the ability of Kv1 to modulate the inhibition of paired pulse ratio in all the subfield of the hippocampus: DG, CA3 and CA1. Fig 3.3A shows that PPR at the Schaffer collateral is strongly reduced after application of α-DTX in Sham animals, but this

difference disappears in epileptic animals (**Fig 3.3B)** (SC-CA1 change PPR before after α-DTX application: Sham = 76.9 ± 2.84%; Epileptic = 91.36 ± 4.58. p = 0.01 two tailed Student's t test. Sham rats n = 5, sham slices n = 5, epileptic rats n= 5, epileptic slices n = 5)

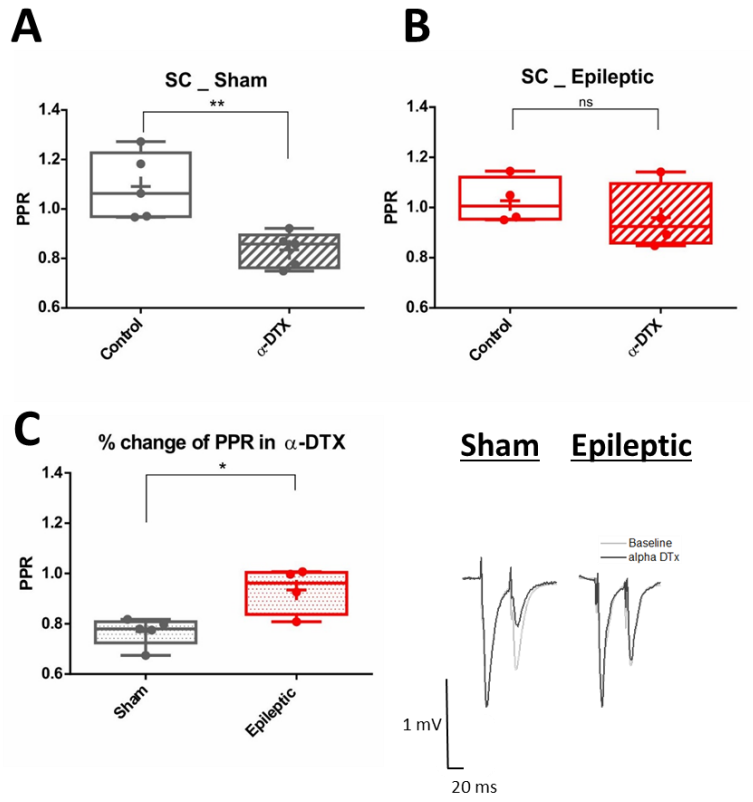

Figure 3.3: Modulation of paired pulse ratio by Kv1 in Schaffer collaterals to CA1 connections. A) *Paired pulse ratios from sham animals and* ***B)*** *PPS animals for stimulated Schaffer collaterals to CA1.* ***C)*** *% of change in PPR between baseline and α-DTX in sham and epileptic animals. Representative PPR traces: light grey represents the baseline, while black are the traces post application of α-DTX (data performed and quantified by Dr. N. Hamil)*

Fig 3.4 A shows that PPR at the Mossy Fibers is also markedly reduced after application of α-DTX in Sham animals, while this difference also disappears in epileptic animals (**Fig 3.4 B)** (MF-CA3 change PPR before after α-DTX application: Sham = 53.14 ± 1.83%;

Epileptic = 112.36 ± 6.8%; p = 0.0001 two tailed Student's t test. Sham rats n = 3, Shamslices n =3, epileptic rats n= 4, epileptic slices n = 4.)

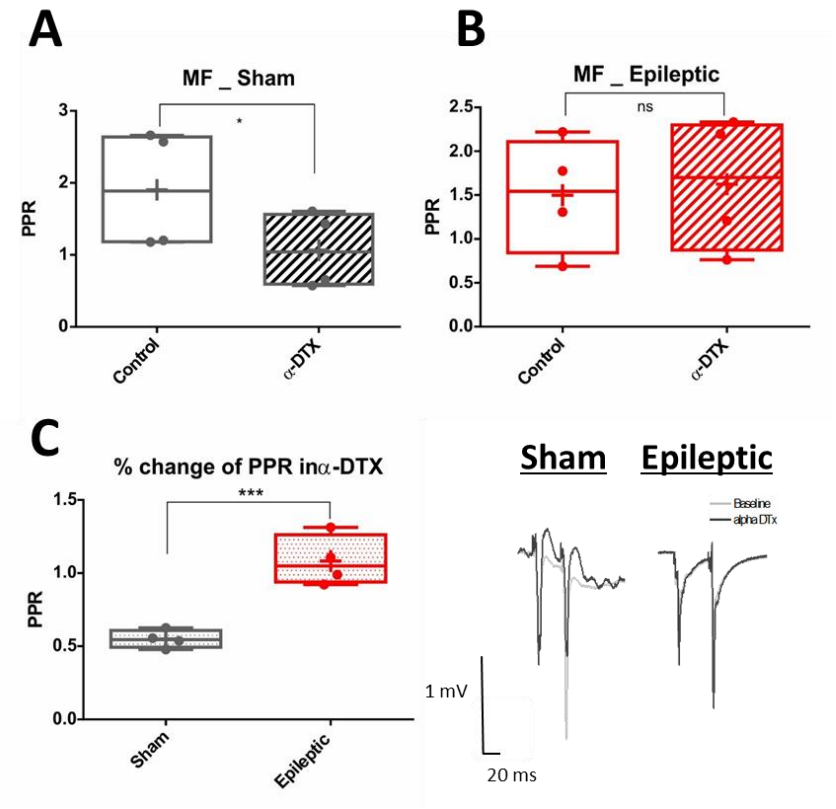

Figure 3.4: Modulation of paired pulse ratio by Kv1 in MF to CA3 connections. A) *Paired pulse ratios from sham animals and* ***B)*** *PPS animals for stimulated Mossy fibers to CA3.* ***C)*** *% of change in PPR between baseline and α-DTX in sham and epileptic animals. Representative PPR traces: light grey represents the baseline, while black are the traces post application of α-DTX (data performed and quantified by Dr. N. Hamil)*

Lastly, **Fig 3.5A** shows that PPR at the Mossy Fibers is significantly reduced after application of α-DTX in Sham animals, but this difference is less marked in the group of the epileptic animals (**Fig 3.4B)** (MMP-DG change PPR before after α-DTX application: Sham = 75.12 ± 1.22%; Epileptic = 84.34 ± 2.75%. p = 0.01 two tailed Student's t test. Sham rats n = 5, sham slices n = 5, epileptic rats n= 5, epileptic slices n = 5). (**Figure 3.5**).

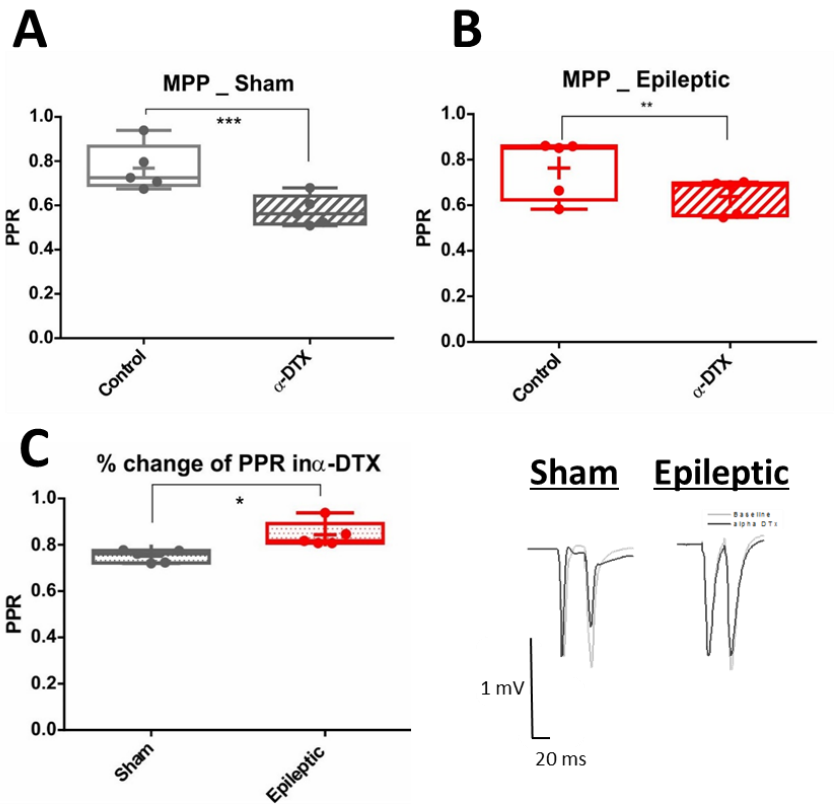

Figure 3.5: Modulation of paired pulse ratio by Kv1 in MPP to DG. A) *Paired pulse ratios from sham animals and* ***B)*** *PPS animals for stimulated Medial Perforant Path (MPP) – DG. The medial perforant path is characterised by paired pulse depression, with higher release probability within the first pulse, as compared to the lateral perforant path which is considered to be facilitating* ***C)*** *% of change in PPR between baseline and α-DTX in sham and epileptic animals. Representative PPR traces: light grey represents the baseline, while black are the traces post application of α-DTX (data performed and quantified by Dr. N. Hamil)*

3.6 Discussion

Previous work has shown that upon continuous subthreshold electrical stimulation of the DG, animals have a high probability to develop self-sustained status epilepticus (Bumanglag and Sloviter, 2008), and subsequent epilepsy. In my experiments, I

examined whether 3 weeks after post stimulation period, the concentrations of the extracellular brain protein LGI1 are affected. First, this time-point was chosen because I wanted to measure the chronic changes happening in the brain after induction of SE. The early phase activity-dependent remodelling of LGI1 was not the purpose of this initial experiment. The process is stabilised around one-week post PPS. Secondly, during the third week, in this model, the number of seizures reach a stable plateau, becoming constant over time (Khalil *et al.*, 2017).

The perforant path model is a reliable model of acquired epilepsy, and in my experience I had 80% success rate. One rat failed to go into self-sustaining status epilepticus; this could have been due to technical issues with electrode implantation or something intrinsic to the rat. In theory this latter explanation could have biased the results because such a “selection process” does not occur for the sham control.

In my experiments, I found that there was a difference in LGI1 expression in the ipsilateral hippocampus of epileptic animals, but not in the contralateral side. Interestingly, the contralateral hippocampi, despite heavily interconnected with the ipsilateral one through commissural fibres (Swanson, Wyss and Cowan, 1978), does not show a clear reduction in LGI1 as the ipsilateral side. These results might be influenced by one outlier in the epileptic data set, or by the low number of animals used for this experiments. More *n* would be required to increase the statistical power.

The protein detection method had initially several problems in revealing LGI1. In fact, LGI1 single proteins are organised in a tight chain of multimers, which in turns directly bind the trans-synaptic proteins ADAM22 and ADAM23 (Owuor *et al.*, 2009; Fukata *et al.*, 2010). A classic RIPA buffer with 0.1% SDS was not sufficient to reveal clearly the bands. With the use of the chaotropic agent Urea (5M and 2.5% SDS) the hydrogen bonds of the macrosctructure were successfully denaturated and it was then possible to reveal LGI1 band with the described detection system (Chabrol *et al.*, 2010). The validity of the primary antibody for LGI1 could not be tested in K.O. animals for lack of availability of the brain material. Nevertheless, the detection of a single band at ~64kDa and the use

of an shRNA for LGI1 described in the next chapter, assured that the detected protein was indeed LGI1.

Furthermore, the measurement of LGI1 protein in this precise time window does not exclude that 1) degradation and production of LGI1 might change within weeks and 2) that the LGI1 mRNA was also affected. The downregulation observed in my experiment cannot be directly attributed to any specific subtype of LGI1 protein present in the adult brain. It could be either a downregulation of the newly synthesised LGI1 or an increase in its degradation before secretion. Lastly, LGI1 proteins might be removed from the monomers already present at the synapse and for which there would be a faster degradation than normal, but an unvaried production. Extraction of pure ECM fraction from brain lysates is not yet possible with the standard centrifugation systems (Naba, Clauser and Hynes, 2015), hence the LGI1 measured here is the total amount of LGI1 present both in cellular bodies and external environment.

In my experiments, it is clear that the damage induced by the surgery and the presence of the implanted electrodes are sufficient to provoke a decrease of LGI1 in the hippocampi (but not seizures). A possible explanation would be due to neuronal death caused by focal inflammation of the hippocampus due to the surgery and this could be tested in a future by performing immunostainings of the hippocampus and perforant path areas for activation of astroglia and microglia form with the markers. Neuronal death is also an important player in the process of epileptogenesis. In the epileptic animals, this is probably initially due to the forced and repeated granule cells discharge triggered by the electrode stimulation (Bumanglag and Sloviter, 2008). During this initial time and for the 2-3 following days, it has been reported that there is prominent cellular loss in the hilus and then, to a lesser degree, in CA1 and CA3 regions (Sloviter, 1983) as well. LGI1 was normalised over beta actin, a cytoskeletal protein which might also be subject to abnormal degradation after an epileptic insult. Despite this, the amount of this marker across all the samples was comparable and the signal was lower than saturation threshold. In a previous work, it has also been shown that beta-actin is a reliable

endogenous control in the hippocampus, confirmed also by QPCR experiments (Ribeiro *et al.*, 2008).

In my work, LGI1 was reduced by ~50% in the ipsilateral side of the whole epileptic hippocampus (**Figure 3.2 A, D**). LGI1 concentrations in the different areas of the hippocampal formation are not homogeneous, being more abundant in DG and CA3, followed by CA1. Future works might be directed at determining regional differences in LGI1 downregulation, extending the research also to the entorhinal cortex and perforant path fibres which also have been found positive to LGI1 staining in adult brain (Herranz-Pérez *et al.*, 2010).

Having found a reduction in LGI1, we asked if this was associated with a change in Kv1.1 function and/or expression. Previous work indicates that LGI1 protein is able to govern the density of Kv1.1 at the synapses and that KO animals for LGI1 display fewer Kv1.1 channels. The lack of Kv1.1, in turn, affects intrinsic neuronal excitability in pyramidal neurons (Seagar *et al.*, 2017).

In our experiments, blocking of Kv1 channels affects PPR predominantly in Sham animals, and to a lesser extent in epileptic ones. Yet the PPR under control conditions is largely unchanged between epileptic and control animals. These results could be explored further and confirmed by analysis of peak current, though this suggests that despite the loss of Kv1 channels, homeostatic mechanisms in epileptic animals are able to maintain the PPR. Nevertheless, the loss of Kv1.1 can have a large impact on short-term plasticity which is further explored in chapters 5 and 6.

In conclusion, the data collected and showed in this chapter support my initial hypothesis for which LGI1 is reduced in acquired epilepsy, together with other extracellular matrix proteins and ion channels. This downregulation may be a common pathogenic mechanism in genetic epilepsy, autoimmune epilepsy and other acquired post status epilepticus epilepsies.

In my next chapter I will study whether an acute reduction of LGI1 in cultures affects neuronal network and cellular excitability.

Chapter 4

4 *LGI1* knock down as a valuable approach for *in vitro* study of altered *LGI1* expression

4.1 Summary

In this chapter, I will initially confirm the presence of LGI1 in primary neuronal cultures with the use of specific antibodies against LGI1 antigens. Afterwards I aim to produce and validate a lentiviral construct able to deliver a retroviral short hairpin RNA (shRNA) for LGI1 that can be used to acutely reduce the amount of LGI1 in neuronal cultures. Since it has been previously shown that there is a close relationship between epileptic bursts, action potentials and calcium waves I firstly aim to monitor calcium signals in a network of neurons treated with LV-shRNA-LGI1 and, secondly, to record spikes and burst activity with fine temporal resolution by use of Multielectrode Arrays (MEAs). Lastly, I will investigate whether reduction of LGI1 affects neuronal viability and changes the number of active excitatory synapses.

4.2 Introduction

The role of LGI1 protein has been mostly studied during the development of the brain and its circuits (Chabrol et al., 2010, Fukata et al., 2010). The few attempts to investigate the acute physiological role of LGI1 in brain circuits and acute pathological impairments of LGI1 relied on the creation of transgenic animals such as a conditional post-natal KO rats for LGI1 in the whole forebrain of excitatory (CamkIIα) neurons, of parvalbumin positive - GABAergic neurons (Boillot *et al.*, 2014) and by the use of a morpholino to knock down *LGI1a* in a zebrafish (Teng *et al.*, 2010). These models do not easily

distinguish a chronic/developmental role for LGI1 from the acute network effects of a reduction in LGI1. This is particularly important because there are human diseases which result from an acute reduction in LG1 due to autoantibodies directed against LGI1.

Nevertheless, there is a lack of cellular electrophysiological recordings and information about the importance of LGI1 in specific brain circuits in many of these studies.

For instance, recordings from CamkIIα KO neurons in transgenic mice would help understand the effects of acute loss of LGI1 on the global population of excitatory neurons in the brain. It could also mimic the general effects of auto-antibodies against LGI1 in the brain. Such antibodies have been detected in patients with autoimmune encephalitis, but yet it is unknown whether the disruption of this protein in the brain or solely the associated inflammatory response play a major pathological role (Irani *et al.*, 2010).

Hence, my aim is to validate an acute method to downregulate LGI1 *in vitro* and explore the functional consequences.

4.3 Hypothesis

The hypothesis I want to test is that the acute reduction of LGI1 increases the excitability of neuronal networks *in vitro*.

4.4 Experimental paradigm

Auto-antibody staining:

For the auto-antibody staining, I used mice hippocampal cultures (40K cells/well) at DIV 21. The cultures were incubated with 0.5mg/ml of IgGs in 10%BSA-HBSS for 30 min on ice. Coverslips were then gently washed 3 times in HBSS for 5 minutes and then fixed for 15 minutes with PFA. Coverslips were washed 3 times in HBSS for 5 minutes each and blocked in a solution containing 10% BSA in PBS for 30 minutes. The secondary antibody (donkey anti-human IgG, Fcy fragment (H), Alexa Fluor® 594 , # 709-585-098,

Jackson Immuno Research Laboratories Inc.) was incubated for 1hr at RT. After 3 x 5 minutes washes with HBSS, the coverslips were incubated with Hoechst 33342 neuronal dye (1:5000 in PBS) for 5 minutes. Coverslips were washes again 3 times with HBSS for 5 minutes each time, then each coverslip was mounted upside down on a glass microslide. The coverslips were allowed to dry o/n on a planar surface and then imaged with a Zeiss confocal microscope (1024x1024 size).

ShRNA subcloning and in house virus production:

AAV-LV-shRNA-LGI1 and scramble were subcloned into a LV (lentivirus) backbone by double restriction enzyme digestion between *SalI* and *EcoRI* restriction sites (see methods and experimental paradigm). LV-shRNA-LGI1 and LV-scramble inserts (~1670 bp) and pCCL__Flexed_MCS backbone (~5000 bp) were extracted from the separation gel and ligated in ratio 5:1 and 3:1 with a negative control lacking of the insert to check for the ratio of false positive colonies. Ligation mixes were left at 16°C for 16-18 hours o/n.

The final plasmid DNA concentrations obtained from inoculation into LB broth (Luria broth) with kanamycin resistance and extraction with *maxipreps* were shRNA-LGI1 = 2313.8 ng/µl, scramble = 3630 ng/µl. Since my vector is a third generation system, the transfer plasmid had to be coupled with pREV, pMDL packaging plasmids and with pVSVG envelope plasmid (Dull *et al.*, 1998). All these plasmid DNAs were amplified and purified with *maxipreps* prior to *in house* production, getting to a final yield of pREV =3651.6 ng/µl, pMDL =5140.5 ng/µl, pVSVG = 4592.6 ng/µl. Lastly, the molar ratio used for *in house* production of lentiviral particles was 2:1:1,5:3 (respectively for pREV, pMDL, pVSVG and the DNA of interest). In my case this was equivalent to pREV =6.2 ug/flask, pMDL =12.5 ug DNA /flask, pVSVG = 9 ug/flask, shRNA-LGI or scramble = 32 ug/flask).

Sample preparation for western blot:

Embryonic mice cortical neurons (E18) were plated (1million cells in 60mm petri dish) and transduced at DIV1 with LV-shRNA-LGI1 or LV-scramble. After 20 DIV the media was removed and neurons were quickly washed with PBS. Each culture condition was scraped by using a cell scraper, lysed in 100µl of RIPA buffer and quickly collected in an Eppendorf tube and placed into ice. Cells were initially broken by mechanical disruption with a 26-gauge needle syringe and spun down in a centrifuge at 14500 rpm for 30 minutes, the pellet was discarded.

The samples were quantified by Bradford as described in the general methods and for each sample 20 µg of proteins were loaded.

HEK transfection for overexpression of LV-EF1α-LGI1-ires-dscGFP construct (Elongation Factor 1-*Alpha* 1) and sample collection (western blot experiment positive control):

HEK 293 cells (~70% confluence) were transfected o/n with a mixture of 2.5 µg of *LV-EF1α-LGI1-ires-dscGFP* DNA (kindly donated by Dr. Albert Snowball, Prof. Stephanie Schorge's lab) and 5µl lipofectamin2000© (Thermo Fisher, # 11668030) into 1000µl of new media in each of the 35mm well. The next morning the media was replaced with fresh Optimem (Thermo Fisher, #11058021) and 24hr afterwards the media was collected, spin down to remove cellular debris (1000rpm, 2 minutes), filtered by centrifugation with Amicon Ultra-15 Centrifugal Filter Unit (Merck, #UFC903024, >30KDa) at 4000 rpm for 15 minutes (4°C) and stored in -80°C until used. The cells were scraped as described for neuronal cultures and also stored in -80°C until used. When thawed, cells and media were prepared as described for neuronal cultures.

SDS-PAGE and western blot:

Samples were run for 3hr at 70V and then transferred to a nitrocellulose membrane by semi-dry method and blocked with 5% BSA and then 3%milk in PBS. Membranes were incubated with 1:250 anti-LGI1 in PBS (Santa Cruz c-19), 1:2000 anti β-actin in PBS

(Sigma, #A2220-200UL) o/n. The secondary HRP antibody used were donkey anti-goat (1:2500, Santa Cruz, sc-2020) and donkey anti-mouse (1:4000, 2B scientific # 43R-1308) in PBS and were incubated for 1.30h at RT shaking. Thermo Scientific PierceM ECL substrate (#32106) was used for the detection. Pictures were taken by a ChemiDoc TM Imaging System (BioRad) and analysed with Image Lab TM software (BioRad) for quantification of volume intensity of the revealed bands. LGI1 was normalised over beta-actin of the same sample lane.

Live calcium imaging setup and settings:

Calcium imaging experiments were performed with mice embryonic (E18) cortical cultures between 21 and 23 DIV. Cells were initially incubated for 30 minutes at room temperature with 5 µM Fura-2-AM and 0.005% pluronic acid (ThermoFisher) in 500µl HEPES-aCSF solution (see methods for recipe). Cells were washed twice with new HEPES-aCSF and 340/380nm exposure time was adjusted so that the ratio of the detected intensity was ~1. Baseline was recorded for 10 minutes. After this time HEPES-aCSF was replaced with the same amount of solution containing PTX (picrotoxin) 10µM and recorded for further 10 minutes. Images were acquired with a frame interval of 10 seconds.

Propidium iodide incubation time and concentrations:

Embryonic (E18) mice cortical cultures (400k cells/coverslip) were transduced at DIV1 with LV-scramble virus or LV-shRNA-LGI1 virus. At DIV21 cultures were transferred in a metallic chamber and incubated with propidium iodide dye (1ug/ml, Thermo Fisher #P3566) and Hoechst 33342 dye (4.5uM, Thermo Fisher #H1399) for 20 minutes in the incubator. Coverslips were then washed and Neurobasal A complete media was replaced with HEPES-aCSF (500 µl). Intensity, gain, laser power and pinhole remained constant along all the experiments and different preparations. The experiments were performed in triplicates for a total of 3 different preparations, and blinded to the treatment

group. The particle size detected were between 10 and 300 pixels for both treatments. Mortality rate was calculated as (total number of PI detected particles over total Hoechst particles) x 100.

Multielectrode arrays:

The neurons were plated in the centre of the device on the day of cell preparation and recorded by MEA 2100 system with integrated amplifier and connected to a temperature controller (Multichannel Systems, Reutlingen, Germany and www.multichannelsystem.com). The neurons plated were derived from mice E18 embryonic cortical hippocampal cultures mice at the concentration of 45K neurons per well. Neurons were transduced at DIV1 and the 6 wells were equally divided by treatments. After 16/18 h post transduced, the media was completely replaced and the neurons were left grown up to 21DIV. Recording protocol was organised in 5-minute recovery followed 10 minutes recording. Data were collected for processing by use of Spycode software (Matlab) kindly donated by Ilaria Colombi (Dr. Michela Chiappalone's lab, Italian Institute of Technology (IIT), Italy) together with Excel (Windows) and GraphPad Prism7 were used for data analysis. Ten standard deviation of the noise was defined as threshold to detect single extracellular spikes.

4.5 Results

4.5.1 LGI1 protein is present into in vitro neuronal primary cultures and can be detected by auto-antibodies from patients with limbic encephalitis

Auto-antibodies are immunoglobulins (IgG) that “attack” antigens coming from the same host which is producing them. These IgG can be a mixture of auto-antibodies against big complexes of proteins (VGKG-ab) or can be very specific for single protein epitopes, such as those for LGI1 or CASPR2 encephalitis (Crisp, Kullmann and Vincent, 2016).

Since the commercial antibodies against LGI1 available are not specific when used for immunohistochemistry and immunofluorescence assays, I decided to use auto-antibodies coming from patients with limbic encephalitis against LGI1 to confirm the presence of LGI1 in neuronal primary cultures. The antibodies were a donation from Prof. Sarosh Irani’s lab in Oxford, UK.

I received 2 samples of autoantibodies: 1 from patients and 1 from healthy control patients in the following concentrations (stock in -20°C):

- LGI1.1 = 2.9 mg/ml
- HC1 = 5.7 mg/ml

The autoantibodies preparations were initially dialysed against PBS by Dr. Melanie Ramberger, postdoc in Prof. S. Irani’s lab. The cultures, at DIV21, were incubated for 30 minutes on ice with 0.5 mg/ml of each auto-antibody. After fixation with PFA on ice, the coverslips were imaged using a donkey anti-human Fc as secondary antibody. The experiments were performed in triplicates from two preparations, and I was blinded to the treatment group. The images were taken with the same laser intensity and settings using a Carl Zeiss ZEN microscope. Analysis of the whole picture intensity was done by measurement of the intensity (mean grey value), using ImageJ free software. Pictures were adjusted to have the same brightness intensity value (210) for both controls and anti-LGI1s, and propagated to all the other images.

The results show that the cultures incubated with auto-antibodies from patients with LGI1 encephalitis, have higher binding affinity than control patients (anti-LG1 mean = 0.19 ± 0.01; HC (healthy control) antibody mean = 0.07 ± 0.01; n = 6 coverslips for both conditions; two tailed Student's t test p <0.0001) (**Figure 4.1A, B**).

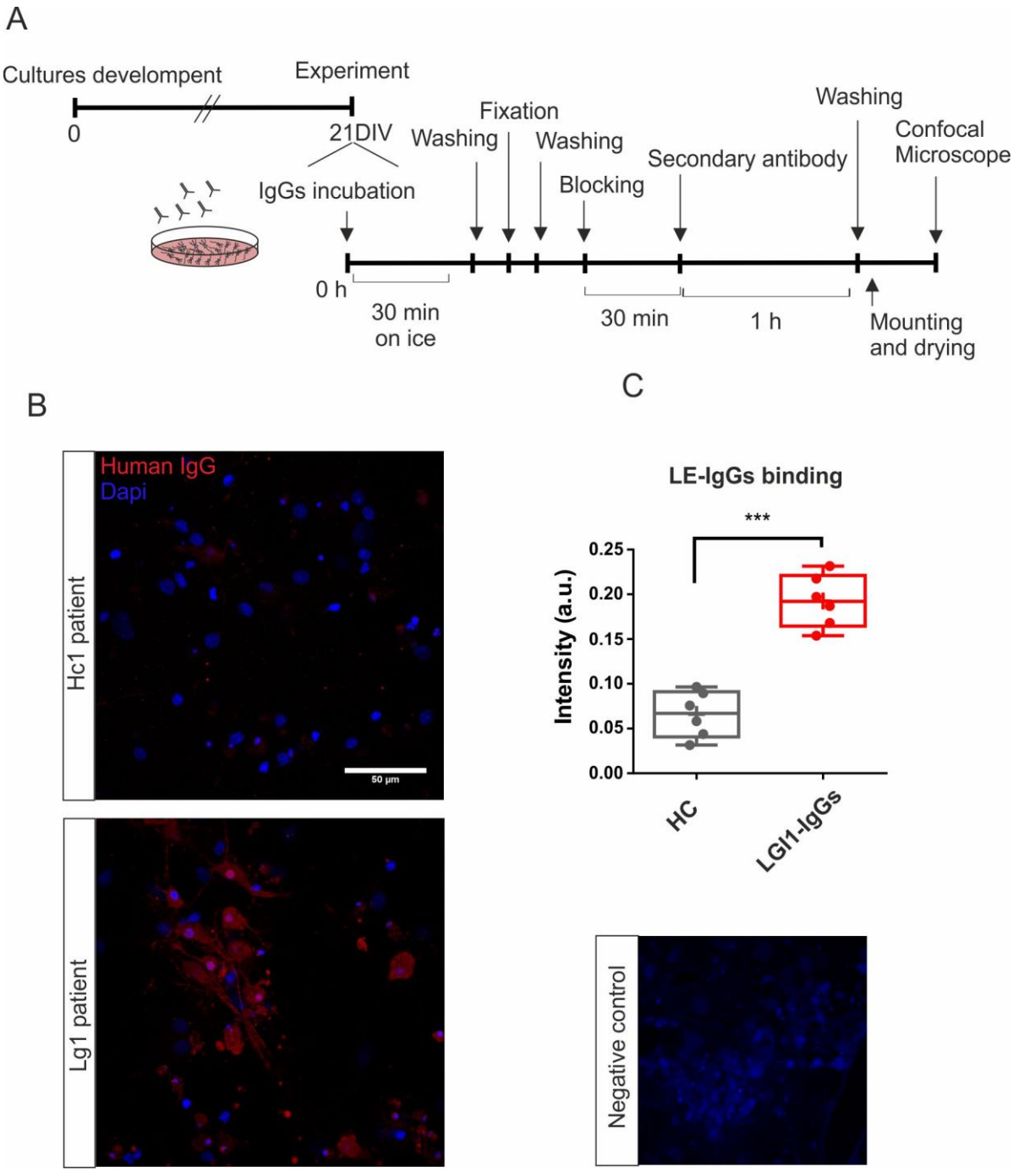

Figure 4.1: LGI1-IgGs from encephalitic patients bind LGI1 protein in mouse primary cultures. A) *experimental time line* ***B)*** *two representative images of primary neuronal cultures treated with auto-antibodies from healthy patients and with auto-LGI1*

antibodies. The image on the bottom right hand side shows a negative control for the secondary antibody (donkey anti-human Fc (H) (n =6 coverslips for each condition). Scale bar = 50µm (40X). ***C)*** *quantification of IgG signal in control and LE (limbic encephalitis) patients.*

4.5.2 LV-shRNA-LGI1 construct is efficiently expressed both in vitro and in vivo

In my experiments, the acute reduction of LGI1 was achieved by silencing RNA methodology. In particular, an shRNA (short hairpin RNA) is a double stranded sequence of about 20 nucleotides (called stem) with a short 4-11 hairpin-loop, extremely specific for the targeted RNA and able to block the greatest majority of the cellular post-transcriptional processes (Chris B. Moore *et al.*, 2010). shRNA are able to enter the cell, integrate into the host DNA and, after being transcribed, the Drosha enzyme processes the initial precursor to a *pre-shRNA*. This intermediate RNA is then transferred to the cytoplasm by Exportin-5 where another processor enzyme, Dicer, eliminates the hairpin and convert the shRNA to a short double stranded siRNA. The antisense strand is then loaded into the RISC complex and used as a stamp for specific degradation of the target mRNA mediated by the RNAse-H Ago-2 (www.labome.com) (**Figure 2.1** Methods).

The AAV-shRNA-LGI1 and AAV-scramble were a donation by Prof A. Dytiatev's group in Magdeburg. The initial shRNA was made into an adeno-associated viral vector (AAV) backbone which I then subcloned into a lentiviral vector (LV) by double restriction enzyme digestion (see methods and experimental paradigm). The designed shRNA sequence had 19 nucleotides which are meant to be highly effective and prevent the occurrence of any RNA-protein kinase dependent (RPK) inflammatory response (Reynolds *et al.*, 2004). The shRNA (and scramble) functional sequence was composed of the selected shRNA for LGI1 mRNA under the control of mU6 promoter. The mU6 promoter is a typical promoter in RNA strategies, including silencing approaches with shRNA (Chris B Moore *et al.*, 2010). mU6 is also active in all cell types, so that the

silencing is not restricted to a specific cell sub-type but a specific area (Sandy, Ventura and Jacks, 2005).The reporter gene was EGFP under the universal promoter PGK. NeoR/KanR (Neomycin/Kanamycin Resistance Gene) was used in the initial bacterial amplification and selection. Scramble sequence was used as negative control and toxicological control. Scramble structure was designed as a rearranged sequence with the same molecular weight of LV-shRNA-LGI1 base composition to control for potential off-target effects (dharmacon.horizondiscovery.com). Before production and for checking possible mistakes and mutations, the final plasmids were sent for sequencing (performed by Sourcebioscience). LV-shRNA-LGI1 and control were successfully able to express their reporter gene when transfected by Lipofectamine 2000© method in HEK (**Figure 4.2B** left panel).

The home-made production resulted in viruses with poor infection unit/ml though (IU/ml) (LV-shRNA-LGI1 $1.17E^{+06}$ IU/ml and LV-scramble 3.25 E^{+06} IU/ml). The titre was calculated using the formula

$$Titre = \frac{MOI \ * \ \text{num cells}}{\text{ml}}$$

with MOI = 5 (multiplicity of infection i.e. the virus particles for each infected cell), and performed in triplicate with serial dilutions of the viruses in primary cultures. Transduction in neuronal cultures first (**Figure 4.2B** central panel), and then injection into rodent hippocampus (**Figure 4.2B** right panel), evidenced that the LV-shRNA-LGI1 was too low for reliable expression *in vivo*.

Because of the poor infection units, a company (VectorBuilder) was asked to produce a high and ultra-purified virus (LV-shRNA-LGI1 titre 3.08 x 10^9 IU/ml; LV-scramble titre 4.25 x 10^9 IU/ml). The commercial virus was able to be highly expressed both in primary cultures (**Figure 4.2C** left and central panel), and in DG/CA3 area of the hippocampus (**Figure 4.2C** right panel). This decision was taken with the possibility of using the virus for *in vivo* animal models (described in chapter 5).

4.5.3 LV-shRNA-LGI1 virus reduces endogenous LGI1 protein in vitro

In order to validate the shRNA-knock down efficiency, I transduced primary neuronal cultures at DIV1 with both LV-shRNA and LV-scramble, and collected them at DIV21 for quantification of LGI1 protein. The experiments were performed in duplicates for a total of 4 different preparations and I was blinded to the treatment group.

LGI1 levels were reduced on average by 38.2 ± 0.05% in LV-shRNA-LGI1 cultures compared to LV-scramble ones (LV-scramble mean = 0.9548 ± 0.08495; LV-shRNA-LGI1 mean = 0.5728 ± 0.05751; p=0.005 two tailed Student's t test). All the intensity values were initially normalised over the endogenous LGI1 level in untreated cultures, then averaged and plotted (**Figure 4.2D, E**). This intra-blot normalization was done in order to reduce the variability of the signals detected due to the very different background of each blot.

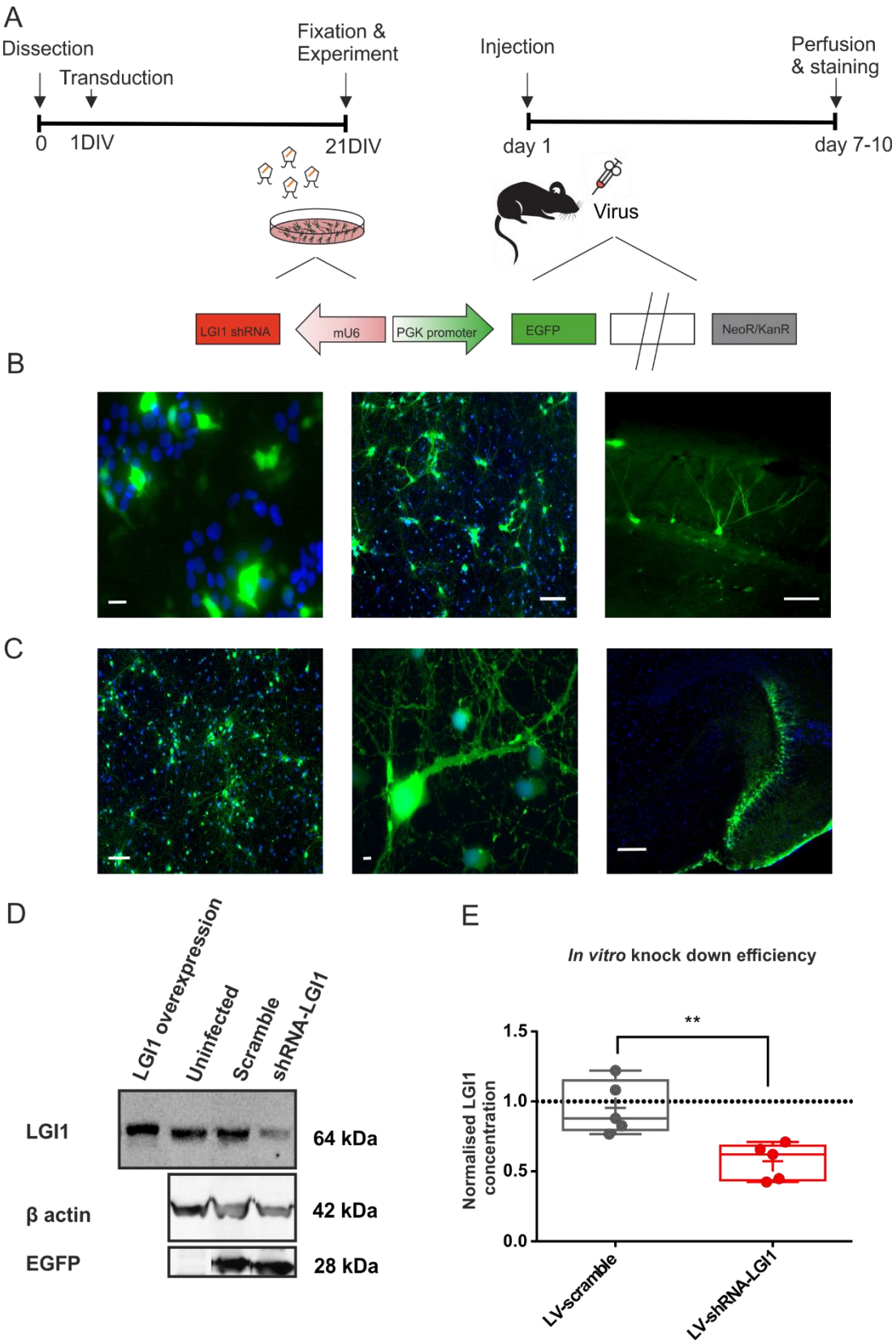

Figure 4.2: LV-shRNA-LGI1 expression and downregulation efficiency. A) *experimental paradigm and time line for cell cultures and hippocampal injections in rodents. LV-shRNA-LGI1 sequence plasmid: LGI1 shRNA is under the promoter mU6 (murine U6 small-non-coding-RNA), meanwhile the EGFP (enhanced green fluorescent*

*protein) is under the independent promoter PGK (phosphoglycerate kinase). NeoR/KanR (Neomycin/Kanamycin Resistance) (**B)** (from left to right) HEK 293T cells positive to endogenous EGFP expression (green) after transduction with LV-shRNA-LGI1 plasmid (40X scale bar = 10µm) (in blue: Hoechst 33342 neuronal dye); primary cultures of hippocampal neurons transduced with in-house LV-shRNA-LGI1 virus (10X, scale bar = 100µm); in vivo expression of in-house LV-shRNA-LGI1 virus in hippocampus of adult rats (10X, scale bar = 100µm); **C)** (from left to right) primary hippocampal cultures positive to commercially produced LV-shRNA-LGI1 virus (10X, scale bar = 100µm); zoom section (63X scale bar = 10µm) neurons and projections; in vivo expression of commercially produced LV-shRNA-LGI1 virus in the hippocampus of adult mice (10x, scale bar = 100µm). **D)** LGI1 expression in neuronal cultures. First lane is the overexpression in HEK293 media of LGI1 peptide with the expression vector LV-EF1α-LGI1-ires-dscGFP. The second lane is the endogenous level of LGI1 in untreated primary cultures, the third lane shows the levels of LGI1 in cultures transduced with scramble virus and the fourth and last lane shows the levels of LGI1 in cultures transduced with shRNA-LGI1. The β-actin and EGFP signals are also shown. LGI1 intensity was normalised by β-actin levels. EGFP intensity was detected to evaluate that the reporter gene was also expressed at the same time as the shRNA and hence could be a reliable source of transduction rate. LV-Scramble and LV-shRNA-LGI1 were normalised compared the LGI1 concentrations in untreated cultures. **E)** Quantification of LGI1 concentrations detected by western blot method. $p<0.01$ Student's t test (blots n=5; blot preparations: untreated cultures n=5, LV-scramble n= 5, LV-shRNA-LGI1 n=5).*

4.5.4 LV-shRNA-LGI1 transduced neurons are spontaneously more active than control

A reliable and straightforward approach to measure neuronal activity comes from the use of fluorescent indicators for *in vitro* assays. These phenotypic assays are of mid-level

complexity and are a suitable biological settings to help bridge RNAi molecular mechanisms of action with *in vivo* physiology (Pacico and Meur, 2014).

To test whether the downregulation of LGI1 alters the physiological state of the neurons, I measured calcium signals in primary neuronal cultures transduced with LV-shRNA-LGI1 and LV-scramble virus by live calcium imaging. It is well documented that epileptic bursts and action potentials correlate with calcium transients in cultures (Kovac *et al.*, 2014).

The cultures (400K cells per each coverslip) were transduced at DIV1 with 5 MOI of the commercially produced virus, which was consistently able to infect ~50% of the neurons on the coverslips. After 21-24 DIV, the coverslips were moved to a metallic chamber and incubated with 5µM of Fura-2-AM and 0.005% pluronic acid in HEPES-aCSF for 30 minutes at RT. The coverslips were then placed under the microscope and the chamber fixed, so that drifting artefact would be avoided. Between 30 and 80 ROI (region of interests) were circled around the bright and visible cellular bodies for each condition, then ratiometric fluorescent calcium signals were detected with a 20X CCD camera at 340 and 380 nm (see methods).

In my set of experiments, I first chose to measure spontaneous calcium transients in LV-shRNA-LGI1 treated cells and control. Hence, I recorded calcium signals during 10 minutes of spontaneous baseline and then 10 minutes after the application of PTX-HEPES-aCSF solution (**Figure 4.3 A**). It has been previously reported that blocking of GABA-A receptors by use of 10µM PTX is able to increase neuronal excitability in cortical neuronal cultures as indicated by an increase of calcium spike amplitudes and neuronal synchronization (Murphy *et al.*, 1992).

My primary measure was the percentage of “active cells” for both conditions during baseline and after application of PTX. I considered “active cells” as those cells that have fluorescence transients >20% of the baseline fluorescence intensity. Interestingly, the cells active during baseline in control conditions were 43% compared to the 58.5% of the

cells treated with LV-shRNA-LGI1 (LV-scramble mean = 43.08 ± 3.87 %; LV-shRNA-LGI1 mean = 58.46 ± 5.16 %; p= 0.02 two-way ANOVA followed by Bonferroni correction for comparisons) (**Figure 4.3 D**). Conversely, this difference disappeared when I applied PTX-aCSF (LV-scramble mean = 76.25 ± 3.49 %; LV-shRNA-LGI1 mean = 76.51 ± 4.383 %; p > 0.9 two-way ANOVA with Bonferroni correction for comparisons F (1,33) = 2.607). In conclusion, the relative increase for the two groups before-after application of PTX is respectively 33.18 ± 5.69% and 18.05 ± 4.1% for LV-scramble and LV-shRNA-LGI1 (p = 0.04, two tailed Student's t test, LV-scramble n = 18, LV-shRNA-LGI1 n= 17 from 4 independent preparations).

I then investigated two other measures of general excitability.

1) the coastline, which reflects the combined effect of frequency and amplitude (Wykes *et al.*, 2012; Shekh-Ahmad *et al.*, 2018). Coastline measures were not different between groups, neither before or after application of PTX in the bath (LV-scramble mean = 0.071 ± 0.006; LV-shRNA-LGI1 mean = 0.085 ± 0.006; PTX-LV-scramble mean = 0.142 ± 0.014 %; PTX-LV-shRNA-LGI1 mean = 0.14 ± 0.011%; p >0.05 two-way ANOVA with Bonferroni correction for comparisons F (1,33) = 0.2328). In conclusion, the relative increase for the two groups before-after application of PTX is respectively 33.18 ± 5.688% and 18.05 ± 4.101% for LV-scramble and LV-shRNA-LGI1 (p > 0.05, two tailed Student's t test, LV-scramble n = 18, LV-shRNA-LGI1 n= 17 from 4 independent preparations) (**Figure 4.3 E**).

2) I measured the spike frequency in both LV-scramble and LV-shRNA-LGI1 conditions. The difference in spike number/second is not significantly different between groups in basal condition. Also, application of PTX in both datasets, causes a comparable increase in spikes activity (before PTX LV-scramble mean = 0.08037 ± 0.009; before PTX LV-shRNA-LGI1 mean = 0.1 ± 0.01; After PTX-LV-scramble mean = 0.12 ± 0.01; after PTX-LV-shRNA-LGI1 mean = 0.13 ± 0.01. p >0.05 two-way ANOVA with Bonferroni correction for comparisons. F(1,33) = 1.88) Relative increase for the two groups before-after

application of PTX is respectively 4.26 ± 1.18 % and 3.01 ± 1.87 % for LV-scramble and shRNA-LGI1, p > 0.05 two tailed Student's t test LV-scramble n = 18, LV-shRNA-LGI1 n= 17) (**Figure 4.3 F**).

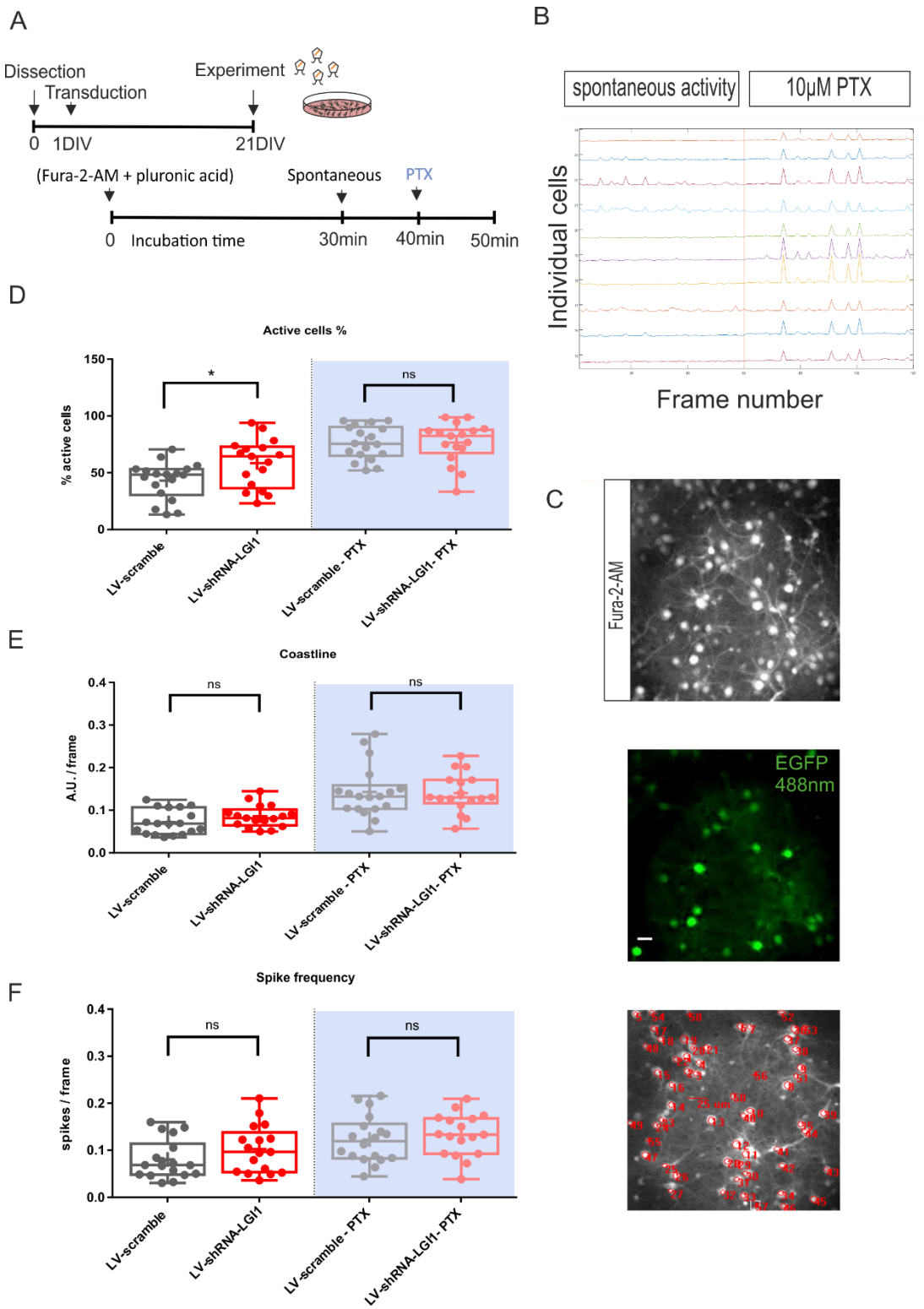

Figure 4.3: LV-shRNA-LGI1 affects basal calcium concentration in primary

cultures. ***A)*** *Timeline of incubation time and imaging experiment.* ***B)*** *Representative image plot showing 340/380nm mean intensity fluctuations in single cells.* ***C)*** *Representative 20X field of view of neuronal cultures treated with Fura-2-AM and pluronic acid (510 nm emission filter). The second picture shows the 488nm EGFP^{+} cells (scale bar = 25µm). Bottom picture is a representative snapshot of cells capturing Fura-2-AM within their cellular membrane. Red circles are manually selected ROI of their soma (scale bar = 25µm).* ***D)*** *Percentage of active cells before (left graph) and after (right) application of the GABA-A receptor blocker PTX (10µM) ($p<0.05$ Two-way ANOVA, Bonferroni correction for comparisons).* ***E)*** *Coastline estimation for spontaneous (left panel) and PTX treatment (right) in LV-scramble and LV-shRNA-LGI1 (A.U. = arbitrary units/frame) ($p>0.05$ Two-way ANOVA Bonferroni correction for comparisons).* ***F)*** *spike frequency for LV-scramble and LV-shRNA-LGI1 treatment in basal activity and after application of PTX(10µM) ($p>0.05$ Two-way ANOVA Bonferroni correction for comparisons).*

4.5.5 The mortality rate in LV-shRNA-LGI1 and LV-scramble transduced coverslips are not different

Neuronal death in cultures and brain slices is an important mechanism of homeostasis, which if uncontrolled, can lead to neurodegeneration (Fricker *et al.*, 2018). To check the hypothesis whether removal of LGI1 in cultures affects cell viability which could lead to the difference in calcium signalling reported in the previous section, I performed a mortality cell assay with the propidium iodide staining (PI). This staining cannot permeate the intact membranes of alive neurons, but it is permeable just to those cellular membranes which are damaged and/or disrupted (Ayşit-Altuncu *et al.*, 2018).

My results show that mortality rate between LV-shRNA-LGI1 virus and LV-scramble virus are comparable (LV-scramble mortality rate median = 51.38%, Range = 44.9% (38 to 82.9%), IQR = 10.68 %, LV-shRNA-LGI1 mortality rate median = 48.25%, Range = 25.3% (42.1 to 6.4%), IQR = 12.38%, Mann-Whitney test two tailed) at 21DIV (LV-

scramble n = 9 coverslips, LV-shRNA-LGI1 n= 9 coverslips from three independent preparations) (**Figure 4.5A** right panel).

4.5.6 LV-shRNA-LGI1 transduced neurons display higher bursting rate and decreased intra-burst frequency

LGI1 is a secreted neuronal protein which has been shown to have a pivotal role in excitatory neuronal signalling (Boillot *et al.*, 2014). Nevertheless, there is no absolute certainty whether LGI1 interacts either with inhibitory GABAergic neurons or with astrocytes and whether these subcellular types help produce LGI1 as well. For this reason, I choose a system in which I could measure the entire *in vitro* neuronal network activity at the same time.

Neuronal cultures were recorded at DIV21, (**Figure 4.4 A, B**). The wells which did not have consistent neuronal density were excluded prior to transduction with the use of a bright field microscope. The experiments were performed in triplicates for a total of 15 wells in 5 different preparations and I was blinded to the treatment group. Multielectrode arrays with less than 4 active electrodes were excluded from the analysis prior to un-blinding procedures. This was done to assure that the distribution of the neurons over the recording surface was as homogeneous as possible. Alternatively, in some cases I found that the neurons plated and transduced ad DIV1, died over the 3 weeks in the incubator.

Ten standard deviations threshold was chosen in order to assure that the spike detection process was not contaminated by noise (**Figure 4.4 C**). After conversion and filtering, the 6 wells were individually split in order to calibrate the appropriate noise threshold for each well. Then spike and burst detection was computed off-line with SpyCode program. According to the sink and source paradigm, an extracellular spike is a negative fluctuation of the local field potential in response to inward and outward currents flowing through the extracellular space in the surroundings neurons and nearby recording

electrodes. A burst is generally defined as a collection of spikes occurring simultaneously in many channels and in a determined time window, separated by quiescent periods (Mary M. Heinricher, 2004; Colombi *et al.*, 2013). Spikes were automatically detected and sorted (threshold 0.02 spikes/second). This value was used to compute the mean firing rate and the mean bursting rate showed here (burst parameters: minimum number of intra burst spikes n = 5, max intra burst ISI (inter spike interval) = 1 ms, bursting rate threshold = 0.4 burst/min).

My primary measure was the mean bursting rate (MBR), which was significantly different between groups (LV-scramble MBR mean = 5.61 ± 0.68 burst/minute, LV-shRNA-LGI1 MBD mean = 8.92 ± 1.18 burst/minute, p = 0.04 two tailed Student's t test) (**Figure 4.4D**).

I then investigated two other measures related to bursts:

1) the first was the Mean Frequency Intra-Burst (MFIB). The increase in excitability was also detectable from this measurement (LV-scramble MFR median = 91.3 spikes/second, Rank = 115.15 spikes/second, IQR = 19.42 spikes/second, LV-shRNA-LGI1 MFR median = 107.1 spikes/second, Rank = 93.08 spikes/second, IQR = 32.41 spikes/second, p = 0.034 two tailed Mann-Whitney test) (**Figure 4.4 E**)

2) the second feature was the duration of the burst (MBD: mean burst duration) which remained constant between treatments (LV-scramble MBD mean = 135.4 ± 7.12 ms, LV-shRNA-LGI1 MBD mean = 132 ± 6.5 ms, p = 0.73 two tailed Student's t- test) (**Figure 4.4 F**).

Further analysis showed that there was a tendency for the average MFR (mean firing rate) of LV-scramble to be less than that of LV-shRNA-LGI1 transduced neurons during the whole 10 minutes of recordings, although this did not reach significance (LV-scramble MFR median = 1.06 spikes/second, Rank = 3.86 spikes/second, IQR = 1.05, LV-shRNA-LGI1 MFR median = 1.79 spikes/second, Rank =6.23 spikes/second, IQR = 2.01, p = 0.07 two tailed Mann-Whitney test) (Mean firing rate LV-scramble n= 18 wells, LV-shRNA-LGI1 = 22 wells, p = 0.069 Mann-Whitney test).

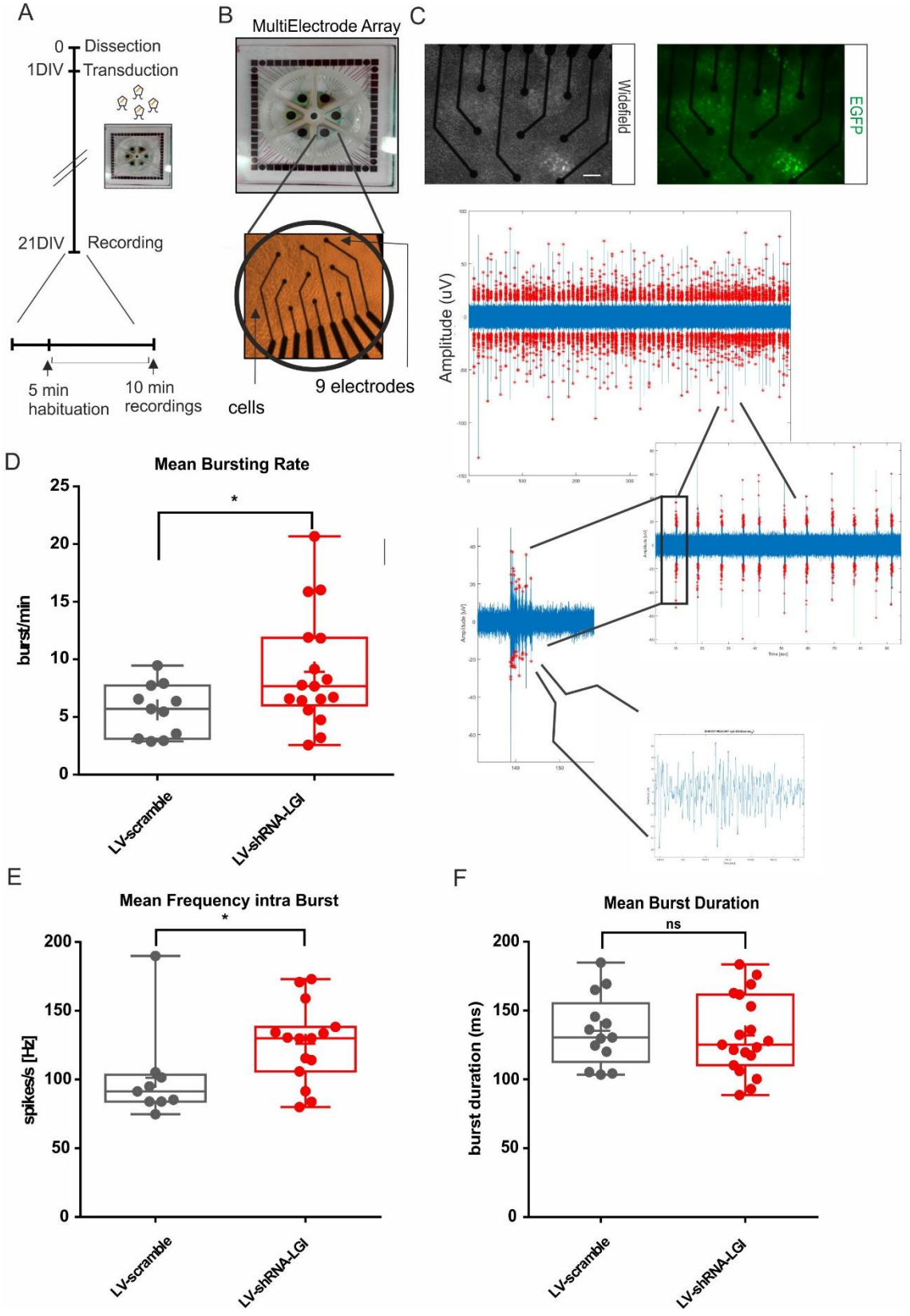

Figure 4.4: LV-shRNA-LGI1 affects network burst activity. A) *timeline of the experiments* ***B)*** *Representative picture of a 6 well multielectrode arrays with zoomed picture of one of the wells. The 9 recording electrodes are in black, over a field of*

neuronal networks. Each electrode is 30µm diameter. ***C)*** *representative pictures of 21 DIV MEAs (left: widefield, right in green: expression of EGFP in transduced cultures, bottom: merged picture. Scale bar = 60µm) and close up of the neuronal activity detected by a single electrode. Zoomed image represents a burst formed by several single extracellular spikes.* ***D)*** *Mean bursting rate (LV-scramble n= 11 wells, LV-shRNA-LGI1 = 17 wells, p = 0.04 Student's t test)* ***E)*** *Mean firing intra burst (LV-scramble n= 11 wells, LV-shRNA-LGI1 = 17 wells, p= 0.03 Mann-Whitney test).* ***F)*** *Mean bursting duration (LV-scramble n= 11 wells, LV-shRNA-LGI1 = 17 wells, p = 0.73 Student's t-test).*

4.5.7 In vitro downregulation of LGI1 protein does not affect the number of active excitatory synapses

The over excitation observed in MEAs and calcium imaging experiments after acute downregulation of LGI1 protein may depend upon a series of factors: increase of neurotransmitter release from the presynapse (Lalic *et al.*, 2011), over excitation of the post synapse cells and either higher number of excitatory synapses or downregulation of inhibitory ones. Since LGI1 has been reported to be important for glutamatergic synapses I investigated the number of active excitatory synapses of *in vitro* hippocampal neurons ad DIV21. Counting of co-localization of vGLUT1 (Vesicular Glutamate Transporter 1), a presynaptic marker of excitatory synapses, and Homer1, a post synaptic marker of active excitatory synapses, did not reveal any significant difference between groups (Mander's coefficient LV-scramble = 0.60 ± 0.037; LV-shRNA-LGI1 = 0.62 ± 0.029, p = 0.584 two tailed t-test, LV-scramble n = 11, LV-shRNA-LGI1 n = 12) (**Figure 4.5 B**).

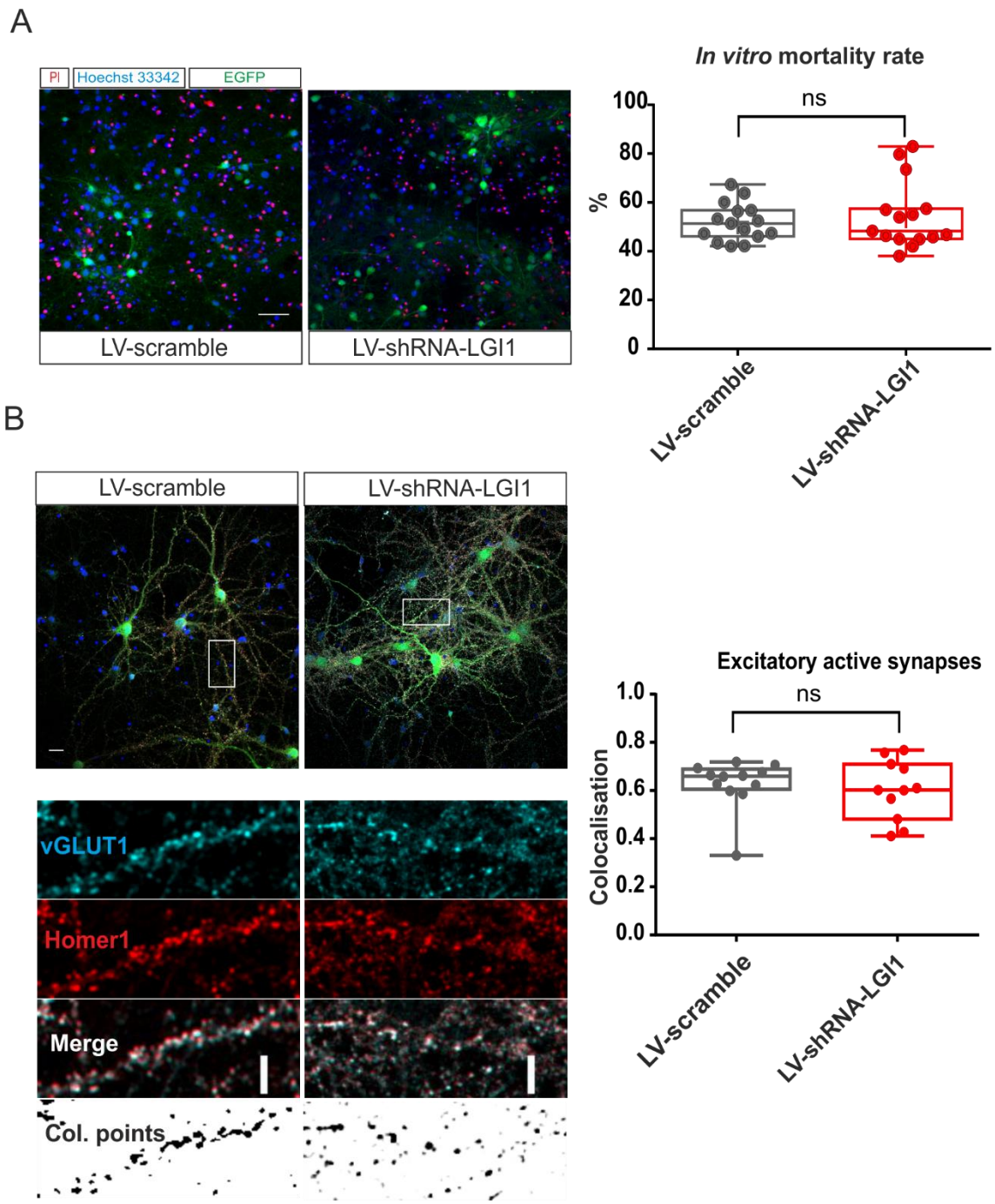

Figure 4.5: Acute knock down of LGI1 does not affect either cellular viability nor number of active excitatory synapses in primary cultures. A) *(left) representative image of propidium iodide staining in primary cultures. Red particles are the nuclei of dead cells with damaged cellular membrane, blue represents the nuclei of all the cell in the coverslips and green neurons are those transduced either by LV-scramble or LV-shRNA-LGI1 virus (scale bar = 50 µm). Quantitative plot of mortality rate (red cells / blue cells) between LV-scramble and LV-shRNA-LGI1 treated cultures at DIV21 (p>0.05, two tailed Mann-Whitney test).* ***B)*** *representative image of neuronal cultures and zoom of a*

dendrite stained for excitatory synapses. Green = LV-shRNA-LGI1 or LV-scramble transduced positive neurons, blue = Hoechst 33342 nucleus staining; cyan = vGLUT1 presynaptic excitatory marker, red = Homer1 post synaptic marker active excitatory synapses. Scale bar is 20 µm.

4.6 Discussion

In this chapter I investigated the hypothesis whether acute reduction of LGI1 protein increases neuronal excitability. I first used auto-antibodies from patients affected by LGI1 encephalitis to determine that in neuronal preparations LGI1 protein was expressed. Then, I used a silencing RNA method with which I achieved a ~40% downregulation of LGI1 in primary cultures. This downregulation did not disrupt cellular viability. I observed that a greater number of neurons had basal calcium transients in cultures in which LGI1 had been knocked down. This difference in basal excitability was confirmed and investigated further with the use of a complementary electrophysiological technique that allowed me to detect higher number of bursts in LV-shRNA-LGI1 cultures.

Previous work has indicated that: LGI1 is highly conserved across species (rat-human 97% similarity) (Ohkawa et al., 2013) and autoantibodies can be reliably used to stain LGI1 proteins in neuronal cultures, instead of commercial antibodies which generally lack specificity for immunohistochemistry experiments (Lai *et al.*, 2010; Boillot *et al.*, 2014).

Therefore, I decided to use autoantibodies coming from patients with limbic encephalitis specific for LGI1 (kindly donated by Prof. S. Irani, Oxford University, UK) to visualise and confirm the existence of this protein in my neuronal preparations. Despite that, my data corroborate previous findings from other groups. The incubation on ice helped to minimise the internalisation of the IgGs and the aspecificity. Further experiments with different antibody concentration and incubation timing, different fixatives alongside concomitant staining with commercial LGI1 antibodies, will be required to confirm these initial data and to evaluate co-localisation.

LGI1 protein has been mainly investigated for its developmental role in the brain and how this influences neuronal circuits (Chabrol *et al.*, 2010; Fukata *et al.*, 2010; Yu *et al.*, 2010). Nevertheless, the upsurge of well-reported cases of patients with acute limbic encephalopathies raises the possibility that LGI1 might also play pivotal roles in regulating cortical excitability (Crisp, Kullmann and Vincent, 2016). The decision to use a silencing RNA to achieve my goal was determined by the fact that with this system I can achieve downregulation of LGI1 concentrations in well-determined circuits and in a selected and restricted time window (Reynolds *et al.*, 2004; Chris B. Moore *et al.*, 2010). A LGI1 conditional inducible KO rat model for glutamatergic neurons (CAMKIIα) was made by Dr. Baulac's group, but the totality of LGI1 ablation in all brain regions, excludes the possibility to study the precise role of LGI1 protein in selected circuits. CAMKIIα-KO rats displayed higher chances to have seizures in adult animals, but with reduced life expectancy (Boillot *et al.*, 2014). A study with LGI1 knock down achieved by antisense morpholino (MO) in fish was also previously published (Teng *et al.*, 2010). The findings correlate mostly to lack of LGI1 during early embryonic development and concomitant behavioural abnormalities were also observed.

The original plasmid was made into an adeno-associated viral backbone. Lentivirus though, offers a quicker expression of the gene of interest and this was an advantage since allowed a more dynamic time window for my investigation. Moreover, LVs are generally less toxic that AAV in non-dividing cells such as neurons (Chris B. Moore *et al.*, 2010). Last, LVs expression is very localised due to the size of the viral particle (100nm) which do not allow them to spread very far away from the infection site (Osten *et al.*, 2007). This peculiarity was very useful for the next step of my work in which I dissect a local and well-confined *ex vivo* circuit in the hippocampus (see Chapter 5).

The shRNA that I used consists of a typical mU6 promoter able to trigger broad production of shRNA in all cell types. This represents an advantage, since it is yet not clear whether glial cells and interneurons contribute to LGI1 production or not (Fukata *et al.*, 2016). In the future, it would be interesting to restrict the downregulation of LV-

shRNA-LGI1 to specific cellular populations and to discern more precisely their role in acute disruption of sub-localised LGI1. The plasmids I obtained from external collaborators were previously tested in Prof. A. Dityatev's lab by Dr. Rahul Kaushik. Dr. Kaushik's personal communication reported that 3 different LV-shRNA-LGI1 (Dharmacon) were initially tested for KD efficiency in HEK293 cells treated with a LGI1 overexpression plasmid. The overall efficiency, also performed by western blot technique with the same antibody for LGI1, was 75% *(not shown)*. These data helped evaluate possible shRNA-LGI1 off-target effects, since it is unlikely that different shRNAs will bind to similar erroneous targets (Chris B. Moore *et al.*, 2010). In the preliminary evaluation for knockdown activity I performed with western blot, I did not include off-target controls for other *LGI* isoforms. *LGI* gene has four isoforms. All are expressed in the brain despite displaying different tropism and molecular weight than LGI1 (Pakozdy *et al.*, 2015). Future experiments will be necessary to understand whether there is also an indirect alteration of other *LGI* isoforms. There were no differences in cell viability between LV-scramble and LV-shRNA-LGI1 treated cultures, confirming the initial suggestion from Dr. Kaushik of the non-toxicity mediated by shRNA-LGI1. Works from other groups with auto-antibodies for LGI1 confirm that acute application of IgG in neuronal cultures does not affect cellular viability, whilst long term chronic application (48-72 hours) significantly increase cellular death (Ayşit-Altuncu *et al.*, 2018).

The downregulation achieved with the selected LV-shRNA-LGI1 was about 40%, when measured with western blot technique. Future experiments with PCR and/or ELISA kit for estimation of LGI1 downregulation could be employed to confirm the KD rate. Possible caveats are the non-specific antibodies so far commercially available for use in the ELISA assay for LGI1.

Interestingly, 40% downregulation can be physiologically correlated to many clinical features related to ADTLE. In fact, the majority of mutations found in these families are a range of heterozygous mutations, such as missense, point mutations, frameshift and missense (Nobile *et al.*, 2009). Striano et al. in 2008, for instance, described an Italian

family with heterozygous mutations for 3 generations in position c.365T>A. This caused reduction in the secreted form of LGI1, but increased chances to experience epileptic insults when patients were sleep deprived and in stressful situations alongside auditory hallucinations and déjà-vu (Kalachikov *et al.*, 2002; Morante-Redolat *et al.*, 2002; Striano *et al.*, 2008; Nobile *et al.*, 2009). This phenotype is also very similar to the heterozygous mice for LGI1 (+/-) for which acute distress increases the chances of seizures (Chabrol *et al.*, 2010). Moreover, the downregulation of LGI1 in acquired model of chronic epilepsy showed in chapter 1 exhibited a ~50% reduction in LGI1 too. Interestingly, patients with encephalitis exhibited a reduced LGI1-ADAM22 interaction due to a loss of ADAM22 in the postsynaptic side (van Sonderen *et al.*, 2016). It would be interesting to investigate further whether this effect is due to reduced concentrations of synaptic LGI1 in the encephalitic brain.

In my experiments I used E18 mouse cortical and hippocampal neurons. Both of these areas express LGI1 protein, and the hippocampus is extremely enriched (Ribeiro *et al.*, 2008). This might explain why there was only a subtle effect of down regulation on cortical neurons on excitability with a reduced % of neurons with calcium increases but the coastline and frequency of calcium signals were unchanged, whilst there was a more robust effect using hippocampal cultures on MEA. Generally, it is recommended to use high density cultures for calcium imaging experiments which provide a more complex and active neuronal networks (Pacico and Meur, 2014). This cellular density was very difficult to achieve with hippocampal cultures, due to the number of triplicates and conditions of each independent experiments, hence the decision to use cortical cultures.

The experiments were performed at DIV21. This age is considered a “mature” stage for neuronal cultures, in which neurons express the final panoply of channels and receptors, calcium waves rate reached a stable plateau and passive and active properties of action potential are established (McCormick and Prince, 1987; Pacico and Meur, 2014). Moreover, *in vivo* evidence indicates that LGI1 is not present at high concentrations at

the embryonic or early post-natal ages, but increases within the first 3 weeks after birth (Chabrol *et al.*, 2010).

The studies of CAMKIIα conditional KO animals, unfortunately, lacked broad electrophysiological and cellular investigations (Boillot et al., 2014). Consequently, the experiments I designed aimed to determine the network consequences from acute LGI1 reduction.

Calcium imaging in LGI1 KO or mutants has never been investigated before. Calcium signals were recorded with Fura-2-AM ratiometric dye. This dye is particularly advantageous to prevent problems with absolute estimates of the fluorescence, avoiding problems of uneven probe loading, photobleaching, illumination intensity and signal-to-noise ratio (Grienberger and Konnerth, 2012). The only work which examines calcium waves using IgG from patients with limbic encephalitis reported decreased calcium signalling when cultures were incubated for 48 and 72 hours with IgG-LGI1. This might be more a reflection of concomitant cell death, rather than a physiological effect of IgGs on neurotransmission (Ayşit-Altuncu *et al.*, 2018). My experiments reported an increase in spontaneous activity in cortical cultures in LV-shRNA-LGI1 cultures compared to control. This difference disappeared when treated with the pro-convulsive agents PTX, probably due to a saturation of activity for both treatments and an occlusion of the effect of LGI1 knockdown. Further experiments could aim to understand whether the effects of LGI1 knockdown are apparent with a lower concentration of PTX and also other pro-convulsive agents such as zero Mg^{2+} ACSF, or low doses of kainic acid. Coastline and frequency were not significantly different from control. This could be due to insensitivity of these measures to a changes in excitability or to poor time resolution (1 frame = 10 seconds) in the acquisition of the images.

For this reason, I used an electrophysiological technique that allows a more direct measure of network activity patterns (spikes and bursts) of *in vitro* cultures chronically treated. The data collected show that cultures treated with LV-shRNA-LGI1 exhibited a significant increase in burst activity and consequent decrease of inter-spike-interval. A

possible interpretation can be that despite the number of spikes being similar between conditions (although there is an evident trend of LV-shRNA-LGI1 cultures to have higher number of spikes/time exists), those spikes were clustered in a higher number of bursts, rather than spread across the whole recording. These results are in line with the data from calcium imaging experiments. In future experiments, short term stimulation (1Hz-10Hz) paradigms through MEA electrodes and different types of pro-epileptic drugs may be tested.

One possible mechanism that could cause hyperexcitation is an increase of the number of excitatory synapses or a reduction of inhibitory ones. Since LGI1 was reported to be mainly involved in excitatory transmission I decided to look at the active glutamatergic synapses using primary cultures. My data revealed no significant difference between phenotypes, corroborating previous findings done by counting of asymmetric synapses with electron microscopy (Lovero *et al.*, 2015; Boillot *et al.*, 2016). Alteration in synapse number has been reported along with developmental problems in LGI1 KO animals (Zhou *et al.*, 2009), and recent work suggests that acute application of exogenous LGI1 in mid-mature cultures can increase excitatory synapses *in vitro.* The same research found that LGI1-/- have fewer mushroom type spines and weaker synapses, with AMPA mEPSC reduced (Thomas *et al.*, 2018).

In conclusion, the results reported in this chapter support my initial hypothesis that an acute reduction of LGI1 *in vitro* increases neuronal and network excitability. These data are of critical value since they support previous findings of acute alteration of LGI1 levels in animal brains, (Teng *et al.*, 2010; Boillot *et al.*, 2014). Importantly, these results also indicate that direct interference with LGI1 by auto-antibodies might be a principal cause of seizure generation in patients with autoimmune encephalitis, and further support that the reduction in LGI1 expression found in chapter 3 could play a part in epileptogenesis.

Chapter 5

5 *Ex vivo* and *in vivo* investigation of LGI1 downregulation in mouse brain

5.1 Summary

In this chapter I investigated *ex vivo* and *in vivo* physiological consequences of the downregulation of LGI1 protein in a specific circuit of the mouse brain. I initially checked the expression profile and downregulation of LGI1 protein in the mossy fibre-CA3 circuit of hippocampi locally injected with LV-shRNA-LGI1 and control virus. The mossy fibres and dentate granule cells are enriched in LGI1 protein (Schulte *et al.*, 2006). ShRNA-LGI1 and scrambled RNA were successfully expressed in DG and CA3 areas of the hippocampus. I determined LGI1 downregulation by western blot of whole lysates of the injected hippocampi; LGI1 was downregulated by about ~20% by LV-shRNA-LGI1.

Subsequently, I examined short term plasticity of mossy fibres-CA3 connections in *ex vivo* tissue using LFP experiments. I found that frequency dependent facilitation of the fEPSP was higher in LV-shRNA-LGI1 than in control, despite no difference in fEPSP amplitude or paired pulse ratio. To determine the mechanisms behind the increased facilitation, I used a specific blocker of Kv1 potassium channels α-DTX (α-dendrotoxin) and found that their loss was responsible for the over-facilitation detected in circuits knocked down of LGI1 protein. Whole patch clamp experiments of DG cells in LV-shRNA-LGI1 injected mice, also indicated that granule cell intrinsic excitability was increased as they had a lower AP threshold and shorter delay between APs with repetitive current injection.

In order to investigate whether this over-facilitation was sufficient to lower seizure threshold *in vivo*, I administered kainic acid in mice previously injected with LV-shRNA-LGI1 in both hippocampi. The results indicate that the local downregulation of LGI1 in DG-CA3 circuit, was not sufficient to increase the probability of observing a stage 5 (Racine scale) behavioural seizure.

5.2 Introduction

Experiments with LGI1 mutations and LGI1 KO in slices and in cell cultures, showed that there are marked pre- and postsynaptic alterations according to the circuit investigated. The effect magnitude and whether pre and/or post-synaptic side is affected differs between transgenic animals and it is probably dependent on the genetic strategy to eliminate *LGI1* from the animal's brain (Fukata *et al.*, 2016). Nevertheless, it is clear that presynaptic effects such as alterations in glutamate release probability are highly affected, especially in hippocampal circuits (Boillot *et al.*, 2016). Postsynaptically, debated AMPARs alterations have been detected by other groups, although such an effect may be restricted mainly to inhibitory neuron populations (Fukata *et al.*, 2010). Recently, IgGs against LGI1 from patients with limbic encephalitis have been reported to have similar effects (Ohkawa *et al.*, 2013; Petit-pedrol *et al.*, 2018). Nevertheless, such studies cannot exclude that the pathogenic impact of autoantibodies is through an immune/inflammatory effect rather than a direct effect on receptors/channels.

The great majority of families with LGI1 mutations affected by ADLTE and patients with LGI1-IgGs suffering from limbic encephalitis display temporal lobe seizures. Abnormal structure and function of granule cells and mossy fibres are a hallmark of epileptogenesis, and it has been suggested that changes in DG and CA3 excitability are of critical importance in the generation of temporal lobe seizures (Devinsky *et al.*, 2018).

Hence, my aim in this chapter was to determine whether specific downregulation of LGI1 in mossy fibres – CA3 pathway affects neuronal neurotransmission and if this is sufficient

to decrease seizure thresholds *in vivo*. Lastly, I aimed to determine the molecular mechanisms responsible for this effect.

5.3 Hypothesis

The hypotheses I aimed to test in this chapter are:

- Downregulation of LGI1 protein is sufficient to increase facilitation of neurotransmission in mossy fibres-CA3 circuits ex-vivo
- This increased facilitation is due to loss of/decreased function of Kv1 channels
- Downregulation of LGI1 protein in the dentate gyrus is sufficient to lower the threshold for seizure generation in-vivo

5.4 Experimental paradigm

Immunohistochemistry: staining for synapse counting (coverslips):

E18 mice hippocampal cultures were plated at 110K cells/coverslip and transduced at DIV1. Coverslips were fixed as previously described in general method section. Blocking solution was made of 5%BSA in PBS. Primary antibodies used were guinea pig vGLUT1 1:1000 (Millipore #ab5905) and rabbit Homer1 1:500 (SynapticSystem #160 033). Secondary antibodies were goat-anti-guinea pig AlexFluor® 647 (1:1000 in PBS, ThermoFisher # A-21450) and donkey-anti-rabbit AlexaFluor ® 568 (1:1000 in PBS, ThermoFisher # A10042). All the images were acquired at Zeiss confocal microscope, with same laser power for all the samples and blinded to the treatment group.

Immunohistochemistry: staining of 400µm thick floating slices:

Slices were cut and prepared as described in the general methods. After LFP experiments slices were fixed in 500µl PFA o/n at 4°C and stored in PBS at 4°C until used. Slices were permeabilised in 0.01% tritonX-100 for 1 hour, blocked in 5% BSA in

PBS for 30 minutes and incubated o/n at 4°C on a shaker with 1:1000 GFP (Abcam #ab6556) in blocking solution antibody as previously described. The next morning after 3x10 minutes PBS washes, anti-rabbit secondary antibody (1:1000 in PBS, ThermoFisher, AlexaFluro® 488 # R37118) was incubated at RT for 1hr. Slices were then mounted, left to dry o/n at 4°C on a flat surface and imaged as previously described.

LFP short term plasticity protocol:

Slices were transferred to a submerged setup chamber perfused with aCSF (with 95% O_2 5% CO_2). They were left to equilibrate for 1 hour. Stimulating bipolar electrodes were placed on the granule cell layer of the DG, meanwhile a recording field electrode filled with aCSF was placed in CA3 stratum lucidum ~100µm below the surface. Paired pulses were delivered with 50µs stimulus interval and the ratio was computed as slope of the second pulse divided by slope of the first pulse. The position of the stimulation electrode was adjusted until maximum fEPSP amplitude was detected and stimulation intensity was adjusted to elicit fEPSPs that were 1/3 of the maximum amplitude. Slices were discarded if it was not possible to elicit a fEPSP, probably due to the slicing plane of the hippocampus resulting in few/no mossy fibres running from dentate gyrus to CA3. The short term plasticity protocol chosen for assessing the MF-CA3 circuit, consisted of 10 repeated stimuli at 0.05 Hz (referred from now on as “baseline”), followed by a 40 stimuli at 1Hz which, in mossy fibres, results in progressive facilitation of the excitatory potential, termed wind-up (Chandler *et al.*, 2003). This wind-up stimulation paradigm was elicited twice in a row and signals were averaged during off-line analysis. Wind-up ratio was obtained by normalizing the facilitation by the average baseline amplitude. After the wind-up protocol, the pathway was confirmed as the mossy fibre pathway through application of the group II metabotropic glutamate receptor agonist, 1µM DGC-IV ((2S,2'R,3'R)-2-(2',3'-Dicarboxycyclopropyl glycine, Tocris Bioscience #0975/1). This was then followed by application of the AMPA/kainite receptor antagonist 50µM NBQX (2,3-Dioxo-6-nitro-1,2,3,4-tetrahydrobenzo [f] quinoxaline-7-sulfonamide disodium salt, Tocris Bioscience

#1044) (Chandler *et al.*, 2003) in order to isolate the fiber volley signal which was then subtracted off-line from fEPSP recordings with a custom script in Python 3.0 and slopes were analysed off-line. 1µM α-Dendrotoxin (Alomone Lab #D-350) was dissolved in 0.1% BSA and acutely applied to the slice.

Whole cell patch clamp protocol:

Details are contained in general methods. In brief, slices were transferred to a submerged setup chamber with bubbling recording solution aCSF (95% O_2 5% CO_2). After initial compensations and stabilization of the access (AR ≤ 20 MΩ), neurons were tested in current clamp by injection of increasing current steps (100ms initial delay, 1000ms pulse with 10pA step increase from -10pA up to 100pA).

5.5 Results

5.5.1 Immunofluorescence pattern expression of LV-shRNA-LGI1 and ex vivo knocking down activity

I initially injected LV-shRNA-LGI1 and LV-scramble viruses in the central part of the hippocampi in adult mice. To check the viruses' expression, I performed immunofluorescence on 400 µm thick slices. Several slices coming from the same cerebral hemisphere were cut, stained and imaged as previously described. **Figure 5.1B** shows transverse fluorescent images of the hippocampus 10 days after injection. Injection of 1µl of each virus into the hippocampus leads to strong, but localised (~400µm) EGFP expression of the fluorescent reporter protein for each of the two injection sites. EGFP expression was typically detectable in 2-3 slices for each hippocampus along the central part of the structure, suggesting an approximate spreading distance of ~1000 µm.

Thereafter, in order to confirm the results already obtained from the *in vitro* experiments, I quantified LGI1 downregulation *ex vivo* by western blot. Each brain was removed, as described for LFP experiments, and transverse slices were made as previously described. Slices were then visualised in an electrophysiology setup submerged chamber, and selected by their expression of EGFP in the DG/CA3 area. Slices were then snap frozen and treated as described in chapter 3 and general methods. The absolute intensity of the LGI1 protein is reduced by about 21% in the ex-vivo slice preparations (**Figure 5.1C**). Experiments were done in duplicate, blinded to the treatment group (LV-scramble mean = 1.109 ± 0.24; LV-shRNA-LGI1 mean = 0.889 ± 0.166. LV-shRNA-LGI1 slice n = 12 from 2 animals, LV-scramble slice n = 11 from 2 animals). HEK293 cells and LGI1 overexpression (LV-EF1α-LGI1-ires-dscGFP) were used as negative and positive control for rabbit-anti-LGI1 antibody used (Abcam #EPR9084, 0.5ug/ml).

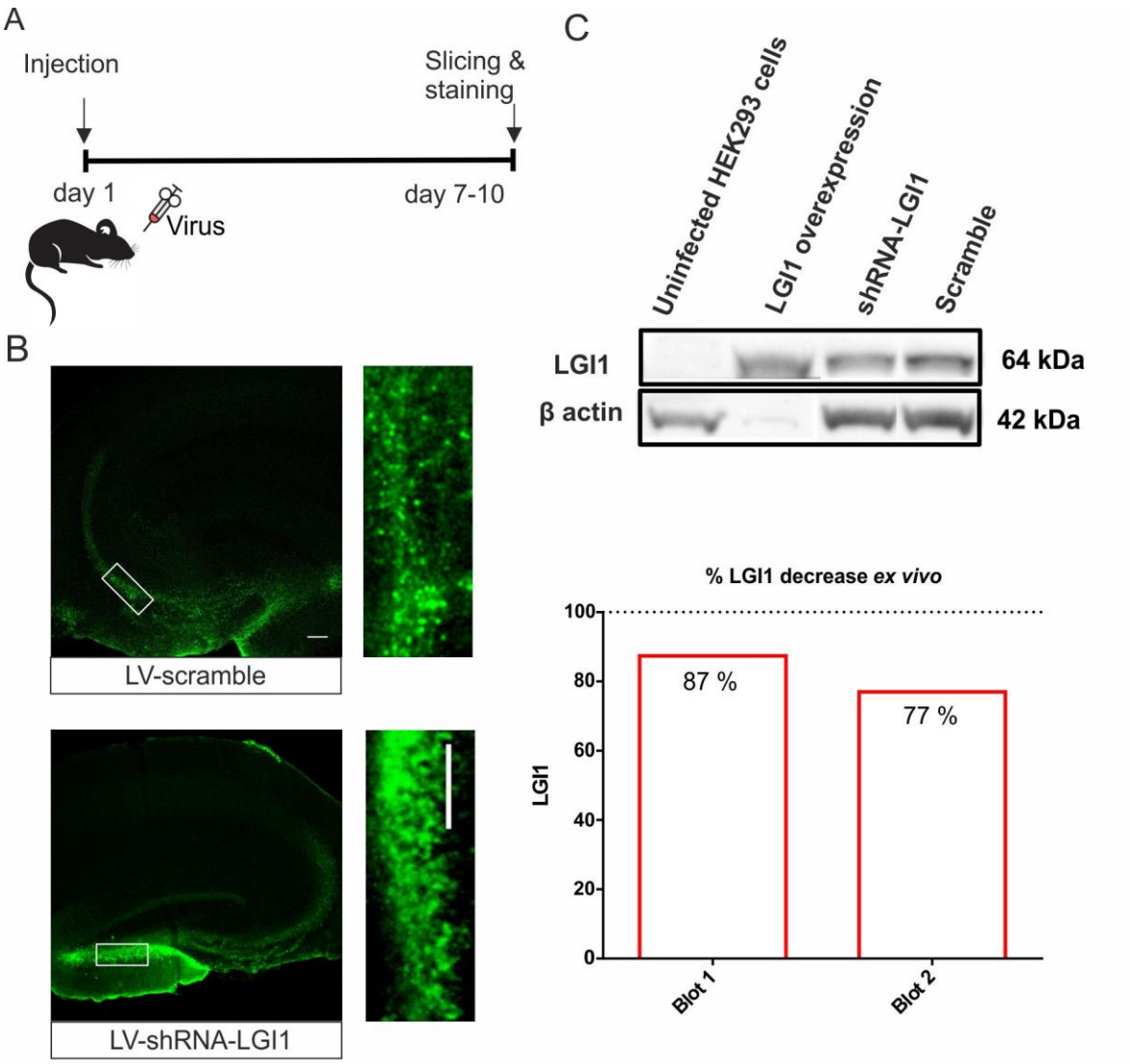

Figure 5.1: LV-shRNA-LGI1 expression in the hippocampus and effects of shRNA. ***A)*** *experimental time line and paradigm* ***B)*** *representative images for ventral and dorsal part of the hippocampus injected with LV-scramble and LV-shRNA-LGI1 (scale bar = 100µm). green = EGFP reporter expression.* ***C)*** *upper panel shows a representative blot for brain lysates of LGI1 protein. Bottom graph shows the absolute quantification of LGI1 protein in scramble vs shRNA-LGI1 treated brain slices.*

5.5.2 Ex vivo LFP experiments revealed an increase in the facilitation of mossy fibres in hippocampi expressing LV-shRNA-LGI1

It has been suggested that the LGI1 protein plays an important role in synaptic transmission in the brain. In particular, MF boutons and CA3 brain region display strong expression for LGI1 protein, suggesting a key function in those circuits (Schulte *et al.*, 2006). Hippocampal circuits are involved in focal epilepsy when the equilibrium between excitation and inhibition is lost (McNamara, 1999).

In experiments with LV-scramble injected hippocampi, the amplitude of mossy fibre wind-up was 3.27 fold baseline levels (3.27 ± 0.37, n=27 slices from 8 animals), in accordance with what other groups already showed (Henze, Urban and Barrionuevo, 2000; Chandler *et al.*, 2003). Interestingly, in LV-shRNA-LGI1 slices, this increment in the amplitude reached up to 3.90 (3.89 ± 0.56, n = 20 slices from 9 animals) (**Figure 5.B** right panel). Normalised amplitude comparison of the last 10 wind-up stimuli between LV-scramble and LV-shRNA-LGI1 revealed a significant difference between treatments (LV-scramble mean = 3.132 ± 0.049; LV-shRNA-LGI1 = 3.707 ± 0.068, $p < 0.0001$ two tailed Student's t test).

Nevertheless, the measurement of the amplitude can be prone to errors in determining the peak since it can be contaminated by several other factors: population spike, commissural fiber potentials from the second pathway present in the DG and recurrent over-excitation from CA3 area (Bortolotto *et al.*, 2001). All these signals can appear during the first part of the decay slope of the amplitude, masking the true value of the maximum amplitude detected. Additionally, the variance of the analysis of the slope was less variable than that one of the amplitude. For these reasons, the first part of the fEPSP decay slope was also measured and it was used as the primary measure of fEPSP amplitude. Evaluation of the slope with a custom python script (see general methods), confirmed that mossy fibres in LV-shRNA-LGI1 injected hippocampi facilitated to a

significantly greater degree than did LV-scramble (**Figure 5.2 B**) (LV-scramble mean = 1.89 ± 0.04; LV-shRNA-LGI1 = 3.17 ± 0.04, $p < 0.0001$ two tailed Student's t test)

At the end of every stimulation, the specific agonist of mGlur receptors II (Metabotropic glutamate receptor 2) DCG-IV was applied to check that the potential recorded was mediated by mossy fibres (Kamiya, Shinozaki and Yamamoto, 1996; Chandler et al., 2003). After a few minutes of perfusion, it was able to block up to 88% of the slope fEPSP recorded, and generally the threshold chosen as a criterion for a mossy fibre signal was >70% reduction of the detected potential. (Figure 5.2 D). As further control we assessed that there was not difference in baselines slopes before and after the windup in control conditions (LV-scramble baseline#1: 0.032 ± 0.008, LV-scramble baseline#2: 0.039 ± 0.015, $p>0.5$two tailed Wilcoxon test).

Last, short term plasticity was also assessed by paired pulse stimulation. This form of rapid homeostatic plasticity in the DG is generally reported as facilitating and it is dependent upon presynaptic mechanisms such as calcium entry, but also potassium channels activity (Meneses *et al.*, 2016). During the first pulse (p1) of the stimulation, the calcium which has not been entirely cleared from the presynaptic terminal can contribute to the neurotransmitter release of the second pulse (p2), especially when the interval between p1 and p2 is within 50 ms (Bortolotto *et al.*, 2001). These results in a larger peak amplitude of the second fEPSP, here also expressed as measure of the downward slope. Moreover, Kv1 channels are a major player of presynaptic modulation (Bialowas *et al.*, 2015; Rama *et al.*, 2015; Meneses *et al.*, 2016). The results show that there is no significant difference in paired pulse ratio in LV-shRNA-LGI1 and LV-scramble at 50 ms delay (LV-scramble median = 1.99, range = (0.86 to 8.33) 7.47, IQR = 2.33; LV-shRNA-LGI1 median = 2.00, range = (0.85 to 4.66) 3.81, IQR = 1.46, $p > 0.5$ Mann-Whitney test. LV-scramble n = 15 from 5 mice and LV-shRNA-LGI1 n= 17 from 8 mice) (**Figure 5.2 C**).

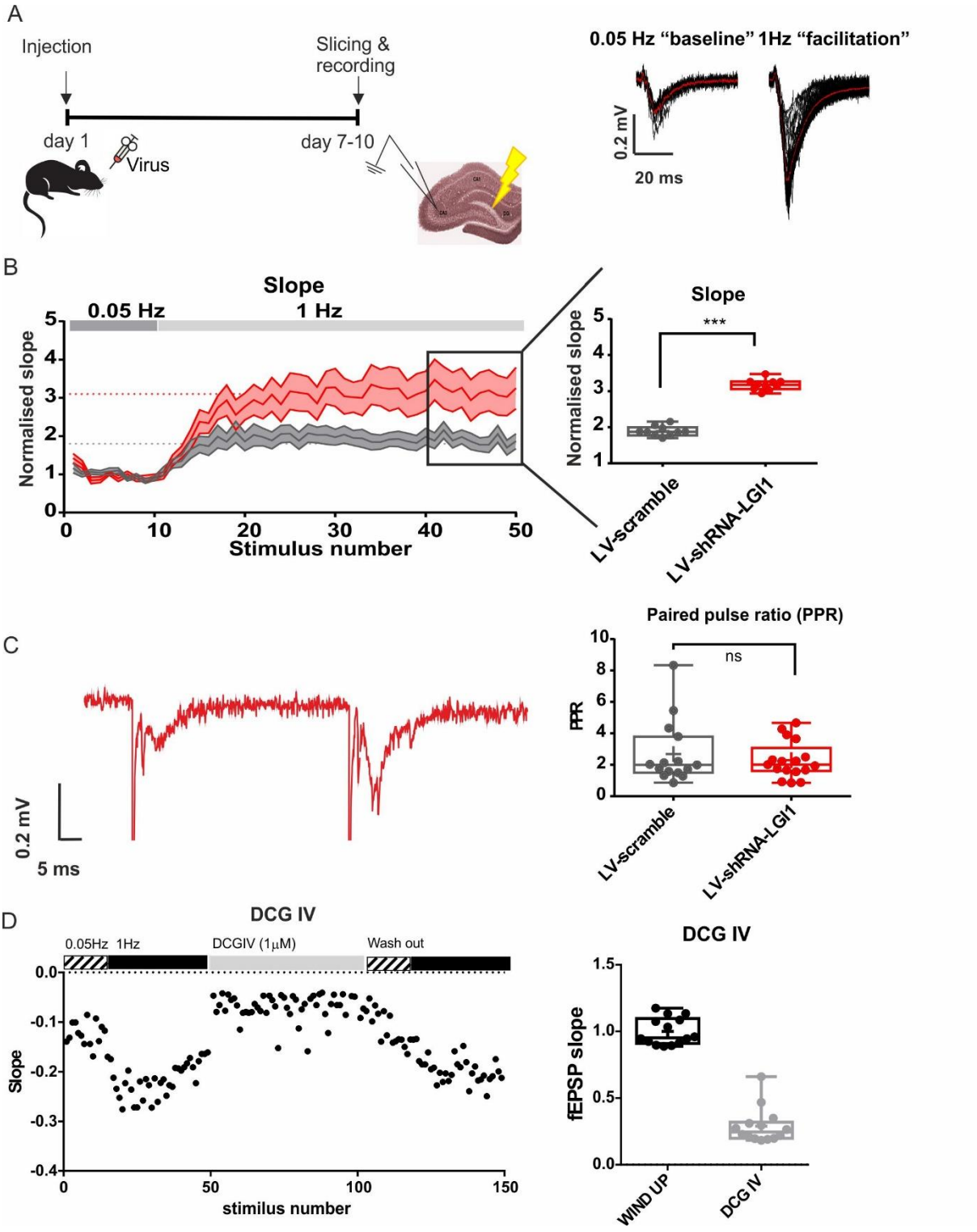

Figure 5.2: MF to CA3 local field potential is increased in animals knocked down by shRNA-LGI1. A) *experimental timeline and paradigm. On the right side are shown original representative trace of baseline and wind-up stimulation of MF-CA3 circuit. Red trace represents the averaged signal between 10 baselines traces and 40 facilitation traces. Black lines represent single recordings.* ***B)*** *pooled time-line data showing the increase in slope following different stimulation frequency. In 1Hz stimulation, the*

amplitude in LGI1 conditions is 30% greater than in the scramble. The bar graph represents the averaged last 10 traces of each recording. ***C)*** *representative traces with bar graph illustrating no difference in paired pulse ratio between groups* ***D)*** *representative trace showing the effect of 1 µM DCG IV in reducing fEPSP slope; bar graph quantifies the effects of 1Hz facilitation in control condition and of 1 µM DCG.*

5.5.3 Blocking presynaptic Kv1.1 potassium channels occludes the increase in facilitation observed in MF to CA3 circuit in hippocampi injected with LV-shRNA-LGI1

It has been reported that LGI1 protein affects post synaptic AMPA receptors and presynaptic KV1.1 ion channels through direct contact with anchor proteins ADAM22 and ADAM23 respectively (Fukata *et al.*, 2016). Recent work demonstrated that LGI1 has the ability to set the amount of Kv1 channels at the synapse and AIS, and that heterozygous mice for LGI1 (+/-) expressed 40% less membrane Kv1.1 compared to control mice (Seagar *et al.*, 2017). Previous work has reported that non-secreted LGI1 proteins are also able to change Kv1.1 kinetics through direct blockage of Kvβ1 regulatory subunit (Schulte *et al.*, 2006). Kv1 family and LGI1 protein largely overlap in their expression in the medial perforant path, granule cell molecular layer and axons and terminals of DG mossy fibres (Trimmer and Rhodes, 2004; Schulte *et al.*, 2006; Trimmer, 2015).

To test if the increased facilitation was due to changes in the activity of Kv1.1 channel, I repeated the aforementioned wind-up experiments applying a broad blocker of Kv1 family, α-Dendrotoxin (1µM/0.01%BSA), in the perfusion system (Geiger and Jonas, 2000). In LV-scramble condition, application of DTX increased the wind-up facilitation, while, in LV-shRNA-LGI1 condition, DTX application decreased the facilitation **(Figure 5.3 B, C**) (LV-scramble α-DTX mean = 32.8± 5.3% larger than with aCSF; LV-shRNA-

LGI1 α-DTX mean = 67.76 ± 6.25% smaller than with aCSF; $p < 0.0001$ paired Student's t test. LV-scramble n = 14 from 6 mice, LV-shRNA-LGI1 n= 11 from 6 mice). As a control, 0.1% BSA alone had no effect on the rate of facilitation observed in two slices. (Wt + 0.1% BSA = 7.85 ± 0.08%, n=2 slices from 1 mouse).

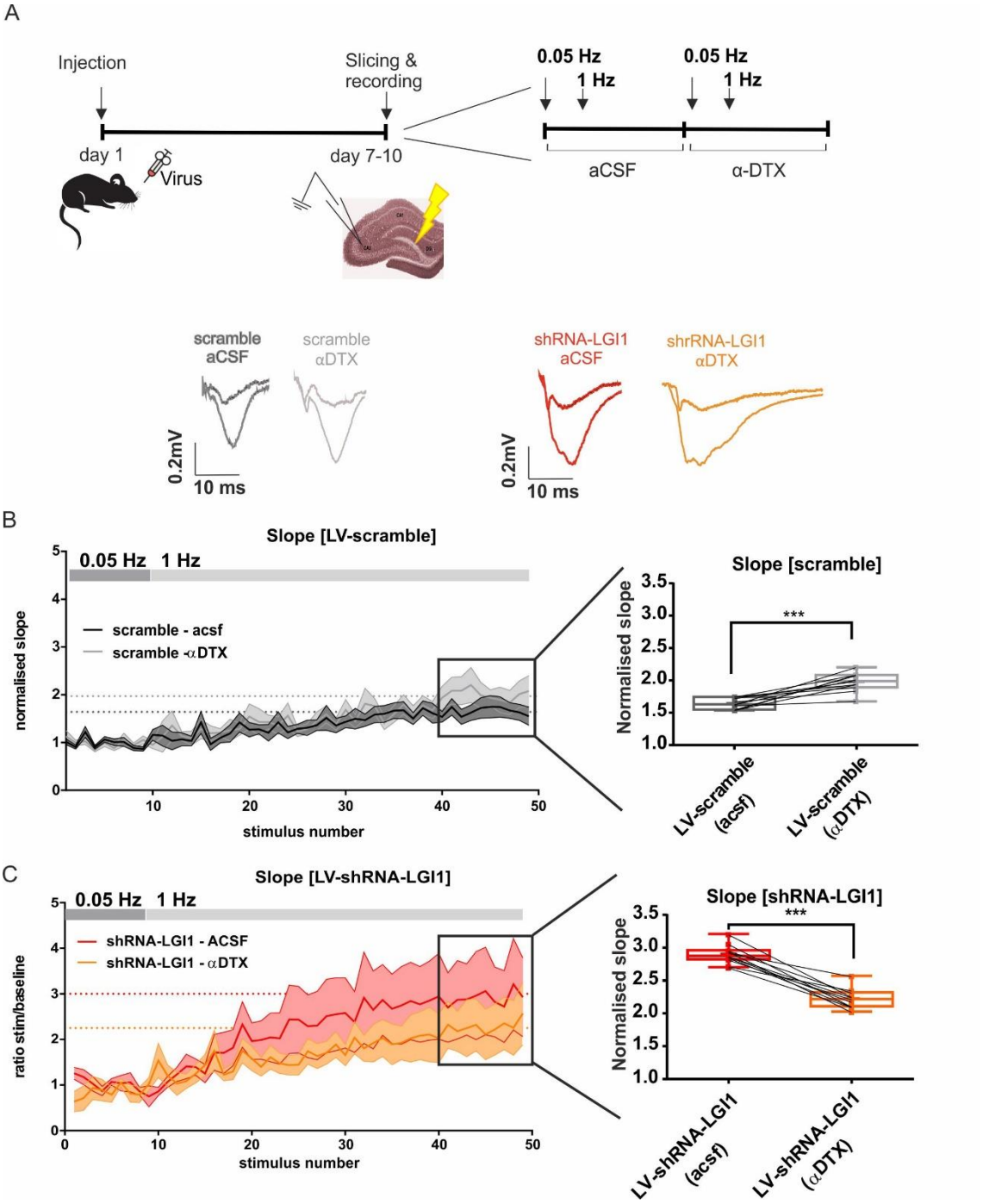

Figure 5.3: the over facilitation observed in animals with acute reduction of LGI1 in MF to CA3 circuits is due to early inactivation of Kv1.1 channels. A) *experimental*

timeline and paradigm. ***B)*** *representative trace and pooled time line data of wind-up stimulation of MF-CA3 circuit before and after application of α-DTX in scramble conditions and* ***C)*** *in shRNA-LGI1 injected slices. Bar graphs on the right hand side show the quantification of the slope of the last 10 wind-up stimuli normalised over baseline stimulation.*

Analysis of the effects of α-DTX on baseline fEPSP was performed using a repeat measure Two-way ANOVA with the factors as presence of α-DTX, scrambled or shRNA and the interaction. This revealed that both phenotypes had a small increase in the fEPSP slope (LV-scramble α-DTX increased 2.9 % of the baseline slope for LV-scramble, LV-shRNA-LGI1 α-DTX increased 1.8% of the baseline slope for LV-shRNA-LGI1), but overall there was no significant difference between before and after α-DTX application (baseline slope ACSF vs. α-DTX, Repeated measure Two-way ANOVA, $p = 0.1$, $F(1, 20) = 1.8$). Nevertheless, LV-shRNA-LGI1 shows a trend in having smaller baseline compared to control (LV-scramble n= 13 from 6 mice, LV-shRNA n= 9 from 6 mice) (**Figure 5.4 A**).

I then analysed the fiber volley as a measure of the number of presynaptic fibre recruited using also a repeat measure Two-way ANOVA with the factors as addition of α-DTX, scrambled or shRNA and the interaction. The analysis revealed that the absolute value for fiber volley slope during baseline was not significantly different before and after application of α-DTX between groups (fiber volley slope ACSF vs. α-DTX, Repeated measure Two-way ANOVA, $p = 0.18$, $F(1, 17) = 1.9$). Nevertheless, for both phenotypes, after application of α-DTX the slope of the fiber volley was reduced of 12.7 % of the baseline for LV-scramble and 12.6 % for LV-shRNA-LGI1 (LV-scramble n= 12 from 5 mice, LV-shRNA n= 7 from 5 mice) (**Figure 5.4 B**).

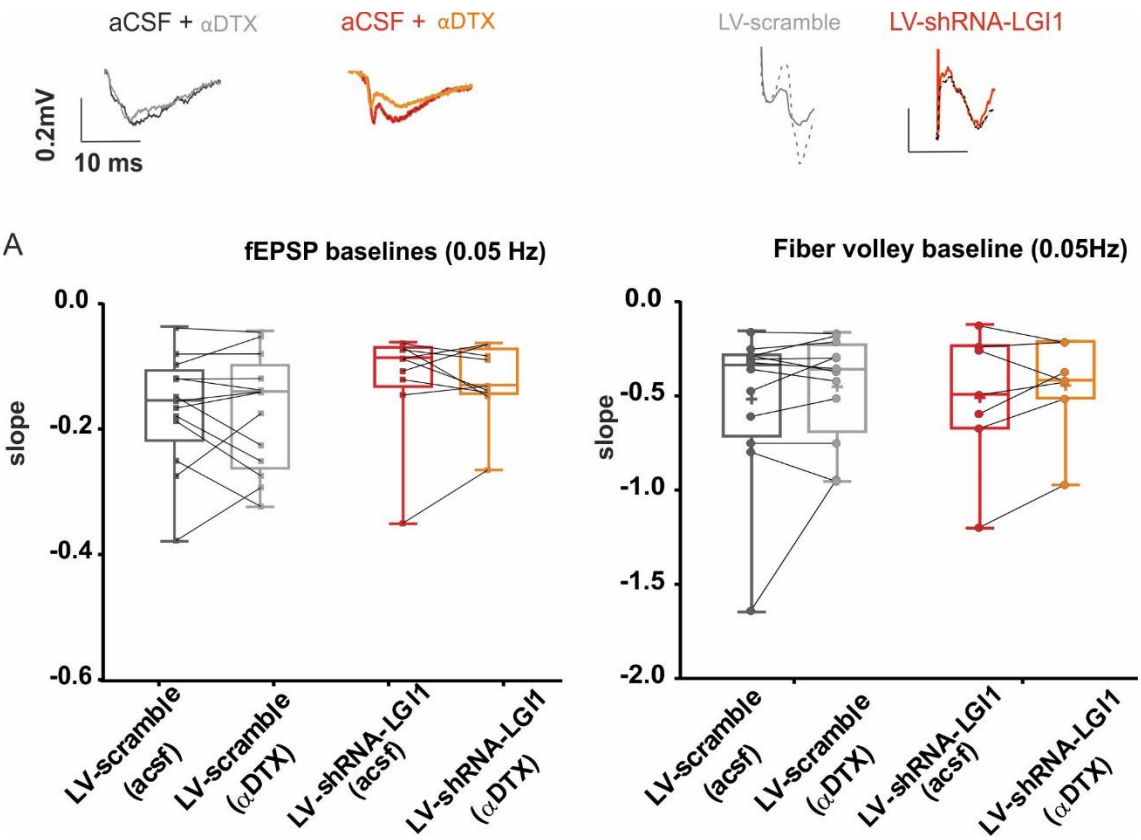

Figure 5.4: Baseline and fiber volley are not significantly different before and after application of alpha dtx. ***A)*** *scatter plot illustrating the slope of the amplitude relative to the baseline stimuli across groups.* ***B)*** *scatter plot illustrating the fiber volley slope during baseline stimulations (0.05Hz) across groups.*

5.5.4 Paracrine effects of acute LGI1 downregulation in granule cells of the hippocampus on intrinsic excitability

Previous works have demonstrated that LGI1 is a secreted protein, probably released from the dendritic and axonal compartment of neurons (Lovero *et al.*, 2015). Total deprivation of LGI1 from early embryonic stage has many different effects on neuronal physiological properties, spanning both pre- and post-synaptic features: lower excitability threshold, reduced D-type current, altered amplitude of mEPSC and of AMPA/NMDA ratio of EPSC (Boillot et al., 2016; Y. Fukata et al., 2010; Zhou et al., 2009). Interestingly, Lovero and colleagues found that when LGI1 was reintroduced onto LGI1 KO neurons,

the AMPA/NMDA ratio was rescued on both transfected positive neurons and on nearby cells as well (Lovero *et al.*, 2015).

In my experiments I aimed to test whether acute removal of LGI1 in granule cells, had a paracrine effect on active and passive electrophysiological neuronal properties. For this reason, I patched cells which were in close proximity to EGFP positive neurons and measured spike threshold and cellular passive properties. Threshold excitability was assessed by progressive injection of current steps in current clamp configuration. The number of action potentials were counted and plotted against the current injected as shown in **Figure 5.5 B, C.** Neighbouring LV-shRNA-LGI1 positive neurons displayed a lower threshold to elicit the first AP, compared to neighbouring LV-scramble neurons (LV-scramble vs. LV-shRNA-LGI1 $p = 0.001$ Repeated measure Two-way ANOVA with Bonferroni correction for comparisons $F(1, 25) = 12.62$). Since the average firing frequency was never above 70 Hz (as for previously reported (Vida and Frotscher, 2000)) in both for LV-scramble and LV-shRNA-LGI1, I could conclude that the population of neurons patched is likely to be from glutamatergic neurons (LV-scramble = 18 Hz, Range = 5 to 36.9 Hz; LV-shRNA-LGI1 = 21.6 Hz, Range = 17.6 to 42 Hz).

Meanwhile the half width of the action potential measured at rheobase was not significantly different within the two groups (LV-scramble mean = 1.645 ± 0.58 ms; LV-shRNA-LGI1 = 1.675 ± 0.66 ms; $p = 0.739$ two tailed Student's t test) (**Figure 5.5 D**), the latency to the first spike between the first 4 spikes over 90pA injected current was shorter for LV-shRNA-LGI1 neighbouring neurons (LV-scramble vs. LV-shRNA-LGI1 $p < 0.0001$ Repeated measure Two-way ANOVA with Bonferroni correction for comparisons $F(3, 57) = 25.88$) (**Figure 5.5 E**). 90pA was chosen as current step in which all the neurons had at least 4 AP.

Importantly, analysis of passive properties of patched neurons highlighted a significant difference in the input resistance (LV-scramble vs.LV-shRNA-LGI1 $p = 0.001$ two tailed Student's t test), leaving the membrane capacitance unaffected (LV-scramble mean = 1.158 ± 0.028 pF; LV-shRNA-LGI1 = 1.244 ± 0.03 pF; $p = 0.06$ two tailed Student's t test)

(**Figure 5.5 F, G**). Resting membrane potential was not different between treatments (LV-scramble = -66.4 ± 2.4 mV, LV-shRNA-LGI1 = -70.6 ± 2.5 mV; p = 0.25 two tailed Student's t test). All the experiments were performed and analysed blinded to the experimental group (LV-scramble n = 12, LV-shRNA-LGI1 n= 13 in 3 mice for each group).

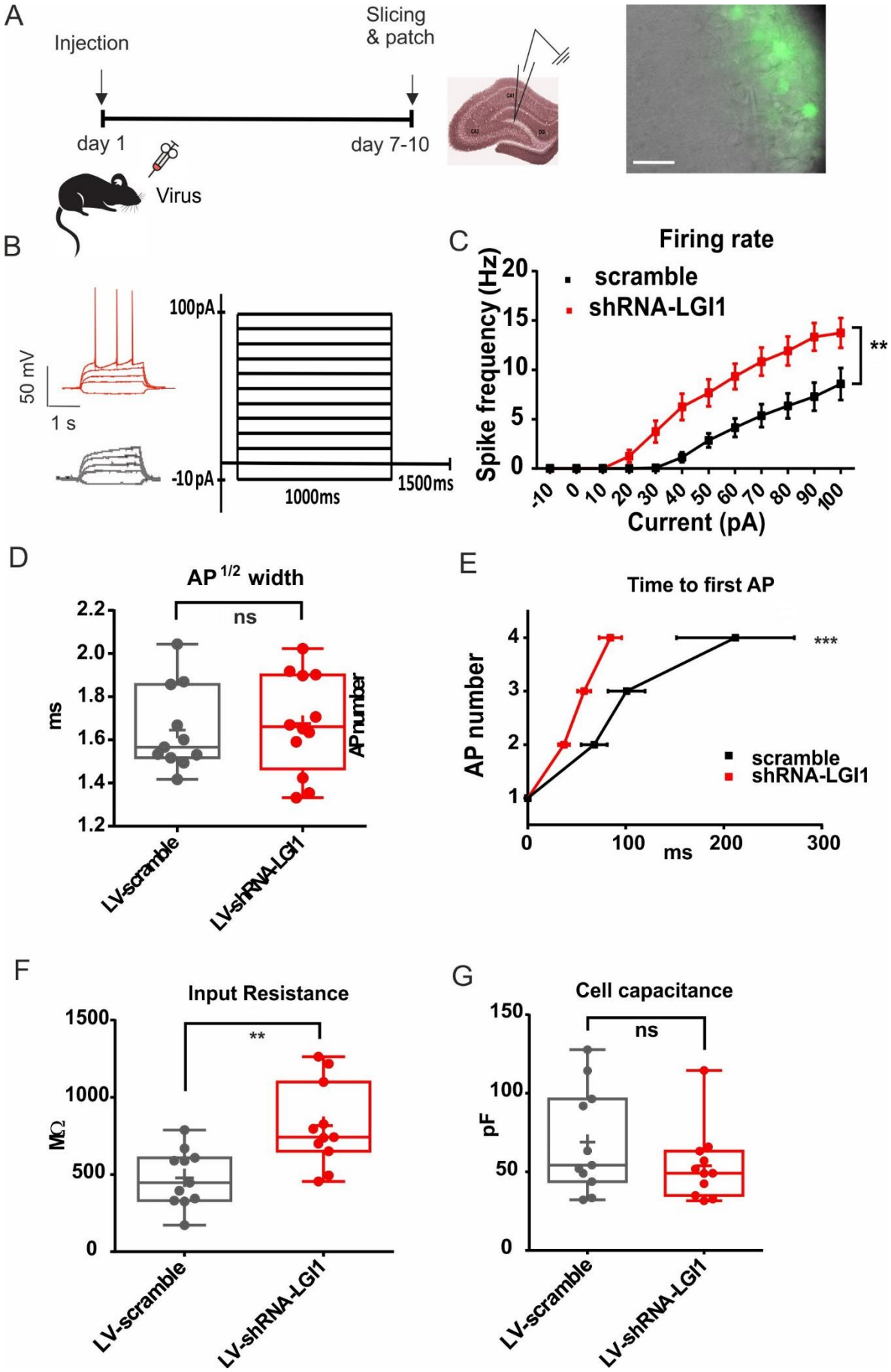
A
Injection
Slicing
& patch
day 1
day 7-10
Virus
B
100pA
-10pA
50 mV
1 s
1000ms
1500ms
C
Firing rate
scramble
shRNA-LGI1
Spike frequency (Hz)
Current (pA)
**
D
AP 1/2 width
ns
ms
APnumber
LV-scramble
LV-shRNA-LGI1
E
Time to first AP
AP number
ms
***
scramble
shRNA-LGI1
F
Input Resistance
**
MΩ
LV-scramble
LV-shRNA-LGI1
G
Cell capacitance
ns
pF
LV-scramble
LV-shRNA-LGI1

Figure 5.5: Acute knock down of LGI1 increases intrinsic neuronal excitation A) *experimental timeline and paradigm. The image shows granule cells in acute slicing. The pipette is patching a neuron nearby neurons positive for LV-shRNA-LGI1 (Scale bar = 50 µm).* ***B)*** *Current injection protocol and AP shape* ***C)*** *Excitability thresholds of neurons close to cells positive for LV-shRNA-LGI1 infection. Representative traces show the current injection from -10pA to 40pA for shRNA-LGI1 and scramble treatment.* ***D)*** *Bar graph showing the half width of the first action potential at rheobase* ***E)*** *spike latency between the first four APs at 90pA. 90pA was chosen as current step in which all the cells in the data base where spiking at least 4 times.* ***E)*** *Bar graph showing membrane cell capacitance and F) input resistance in of neurons close to cells positive for LV-shRNA-LGI1and LV-scramble.*

5.5.5 Acute reduction of LGI1 protein in MF to CA3 circuit is not sufficient to lower seizure susceptibility

Heterozygous mice for LGI1, rats with acute whole reduction of LGI1 in the late adulthood and zebrafish with downregulation of LGI1 protein all have lower threshold for seizures occurrence compared to WT animals (Chabrol *et al.*, 2010; Teng *et al.*, 2010; Boillot *et al.*, 2014).

I therefore asked whether the changes I observed above following acute and localised downregulation of LGI1 in specific circuits of the hippocampus were sufficient to lower the threshold to trigger tonic clonic seizures following administration of KA. For these experiments I chose to inject repeated subthreshold amount of KA (5mg/kg) every 30 minutes (Tse *et al.*, 2014), which has been described to cause recurrent excitability of hippocampal network, neuronal damage and loss in CA3 cells, mossy fibres sprouting in DG and progressive seizures (Hellier *et al.*, 1998).

My results indicate that, there was no significant difference between LV-shRNA-LGI1 animals and LV-scramble animals ($p>0.99$ One-way ANOVA) (**Figure 5.6 A, B**). Analysis

of the latency to stage 3 did not reveal significant alteration in the score between LV-scramble and LV-shRNA-LGI1 ($p>0.99$ One-way ANOVA) (**Figure 5.6 C**). Interestingly, both LV-shRNA-LGI1 and LV-scramble were very different from littermate WT ($p = 0.006$ One-way ANOVA $F(2,31) = 6.067$). Injection, score evaluation and analysis were performed double blinded to the treatment group (LV-shRNA-LGI1 n = 12, LV-scramble n = 11, WT n = 11 from three independent data set).

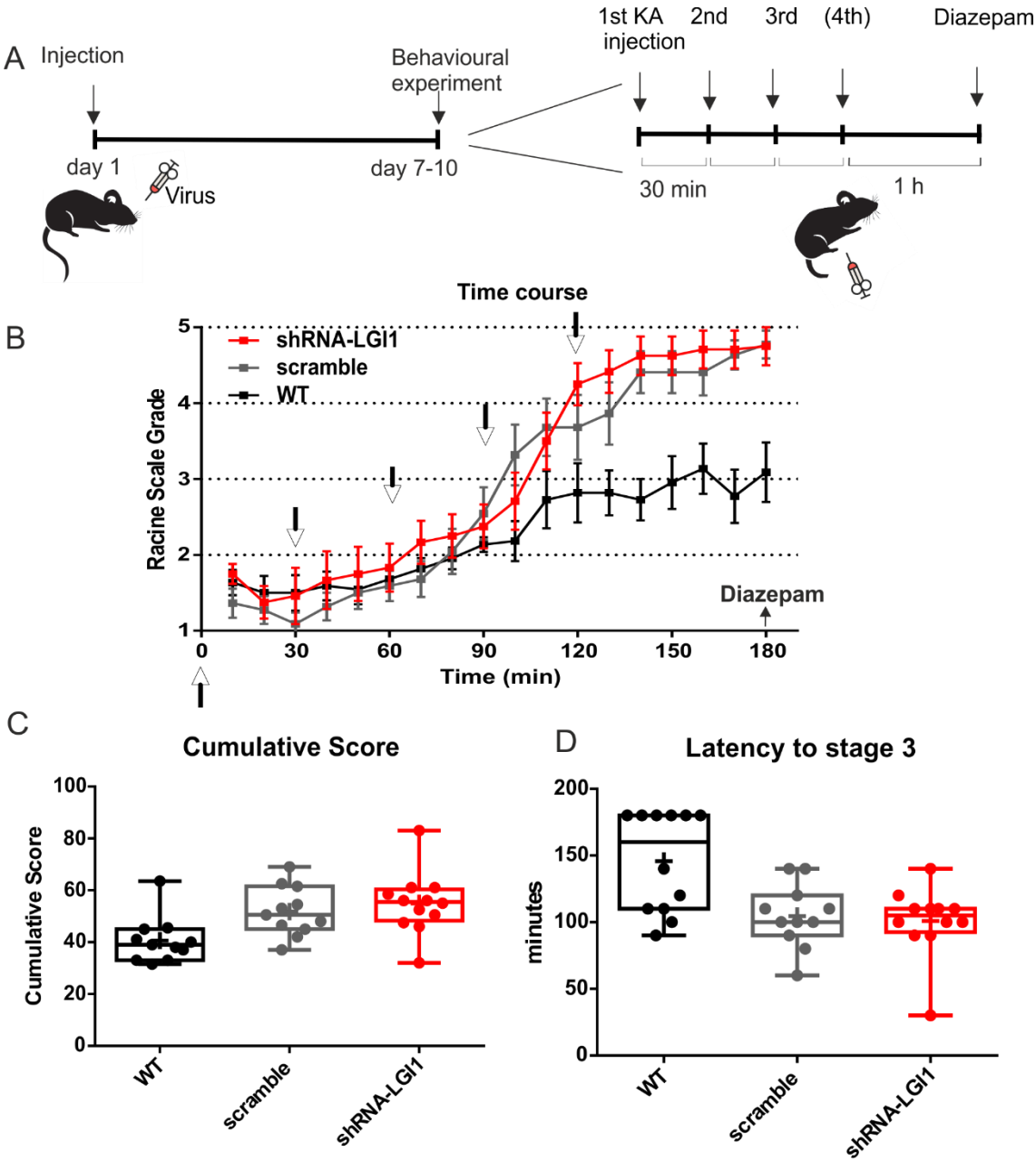

Figure 5.6: Acute reduction of LGI1 in MF to CA3 circuits are not sufficient to lower seizure threshold in vivo. A) *Pooled data from the three phenotype: LV-shRNA, LV-scramble and WT mice. Cumulative seizures severity over time. White arrows indicate injections time.* ***B)*** *averaged cumulative seizure severity until stage 5 and* ***C)*** *time to arrive to stage 3 (Rearing, forelimb clonus and upstretched tail).*

5.6 Discussion

In this chapter I tested the effects of *in vivo* acute reduction of LGI1, using *ex vivo* hippocampal preparations first and then adult mice injected with a pro convulsant agent. Initially, I injected LV-shRNA-LGI1 into the DG/CA3 area of 3 weeks old mice, showing that 1-2 weeks later it was able to reduce LGI1 protein to about ~20% *in situ*. Then I explored the changes in short term plasticity in the MF to CA3 circuit using extracellular field recordings and showing that tissue positive for shRNA-LGI1 was able to facilitate more compared to control. This over-facilitation was investigated further by the use of α-DTX, a broad blocker of the Kv1 family. Blocking Kv1 channels occluded the increased facilitation, indicating that they are contributing to the increased facilitation. Acute reduction of LGI1 in slices, had also a paracrine effect on neurons proximal to positive cells for LV-shRNA-LGI1. I was, however, unable to demonstrate that these changes lowered seizure threshold.

I focussed on the mossy fibre pathway and CA3 neurons because LGI1 protein is highly expressed in these areas, so it is likely that LGI1 exerts crucial role at these synapses, (Head *et al.*, 2007) and the hippocampus plays an important role in the generation of seizures in ADLTE and in LGI1 KO mice (Winawer *et al.*, 2000; Chabrol *et al.*, 2010). The delivery of the virus by stereotaxic injection could not constrain it to just one or the other pathway, preventing the opportunity to study precise a pre or post synaptic effect of acute LGI1 downregulation. Estimation of the downregulation achieved *in vivo* by use of lentivirus was less than that achieved with *in vitro* systems. This may be due to the method of slice selection positive to viral EGFP expression: whole CA1, CA3 and DG lysates might mask the real effect exerted over granule cells and CA3 area. Microdissection of the tissue might be required to have a more precise estimate of the localised downregulation. Another reason may be due to the limited amount of virus (1µl) injected per hemisphere and its restricted spreading. This amount was chosen in order to reduce the damage induced by the injection and to avoid local inflammation.

Nevertheless, stereotaxic injection itself seemed to have quite an important impact, as all the WT animals IP-injected with kainate demonstrate a significantly larger delay to stage 5 compared to LV-scramble and LV-shRNA-LGI1 injected littermates. These, in turn, had similar susceptibility to the pro epileptic agent, showing comparable behaviour over time and dose given in respect the evolution of the epileptic phenotype. To check for possible local inflammation, control experiments would aim to stain for markers of neuronal inflammation such as microglia and astrocytic activation. Investigation of mossy fibre to CA3 transmission nevertheless revealed a marked increase of fEPSP facilitation during short term plasticity protocols in slices injected with LV-shRNA-LGI1. Similar experiments were carried out following infusion of VGKC-abs from patients with limbic encephalitis on acute hippocampal slices. Stimulation of MF and recording of CA3 revealed increased epileptiform activity by measurement of the population spike coastal burst index. Minimal stimulation protocol from the MF to the CA3 area, also revealed an increase in the synaptic transmission in cells treated with VGKC-IgG (Lalic *et al.*, 2011). Field potential recordings from granule cells of mutant LGI1 mice (835delC), also revealed an increase in the number and amplitude of population spikes and after spike discharges after picrotoxin application (Zhou *et al.*, 2009). Whole cell recordings and field potentials data from CA1 area also suggested that LGI1 KO mice exhibited higher interictal events and glutamatergic release from pyramidal cells, which could indeed explain the higher facilitations of mossy fibres observed in my wind-up experiments in LV-shRNA-LGI1 tissue (Boillot *et al.*, 2016).

The above mentioned effect could be replicated by application of Kv1 family blocker α-DTX (Schulte *et al.*, 2006; Lalic *et al.*, 2011). Also in my experiments, application of α-DTX in scramble injected hippocampi, resulted in a higher facilitation rate compared to previous paired recordings. Interestingly, the shRNA-LGI1 injected slices when treated with the same concentration of α-DTX had an opposite effect, reducing the amount of facilitation evoked during the 1Hz stimulation frequency. This seems counterintuitive, but would suggest that a decrease in LGI1 increases Kv1.1's contribution to wind-up. Schulte and colleagues reported that LGI1 serves also as a presynaptic modulatory protein for

Kvβ1, Kv1.1 “ball and chain” regulatory subunit. When LGI1 is present at the synapse, it can block Kvβ1 action, prolonging the opening of Kv1.1 ion channel in order to dampen down neuronal excitation. Hence, the faster closure of Kvβ1 gate causes a quicker membrane depolarization (Schulte *et al.*, 2006). Seagar et al (2017), also suggested that the absence of LGI1 would increase the stoichiometric ratio of Kv1 and Kvβ1, increasing the probability of binding (Seagar *et al.*, 2017). Previous works reported that whole Kv1.1 inactivation require just one Kvβ1 subunit, but that multiple LGI1 proteins are needed to prevent a single Kvβ1 to act (Schulte *et al.*, 2006). Indeed, MF and CA3 areas of the hippocampus, happen to be highly positive to labelling for Kv1.1 channels, Kvβ1subunits and other subclasses of Kv1 family such as Kv1.1, Kv1.2 and Kv1.6 (Veh *et al.*, 1995; Trimmer, 2015), all channels with which Kv1.1 forms heterodimers.

Geiger and Jonas, pointed out that the half width of the action potential at the mossy fiber boutons varies according to frequencies of the presynaptic stimulation and it is mainly dependent upon potassium channels inactivation. Slow stimuli do not affect so much AP shape, but higher frequencies causes broadening of the AP up to three fold. This mechanism, in turn, helps the increase of presynaptic calcium at the bouton, leading to higher neurotransmitter release. In both cases, Kv1.1 channel exhibits a very long period of recovery (in seconds) (Geiger and Jonas, 2000). Without LGI1 the inactivation kinetics of Kv1.1 were reported to be even faster and significantly enhanced (4 fold) (Schulte *et al.*, 2006), which fits and confirms the results reported here.

Hence, I propose that Kv1.1 is normally active during the baseline facilitation at MF to CA3 synapse. However, when LGI1 is reduced such as in my system, the kinetics of Kv1.1 change and the channel inactivates faster and recovers from inactivation even more slowly. This would result in an accumulation of inactive Kv1.1 during the wind-up hence enhancing facilitation (**Figure 5.7**). Noticeably, when α-DTX was applied, this caused a delayed increase of the facilitations in LV-scramble condition probably due to a small accumulation of inactivated Kv1.1 channels, while in LV-shRNA-LGI1 slices there was a complete occlusion of Kv1.1 channels, which mimics the LV-scramble situation.

Remarkably, fibre volley analysis, which is a measure of the number of fibres recruited as well as presynaptic excitability (Bortolotto *et al.*, 2001), showed a trend to a decrease in the response (in slope) during baseline stimulations in LV-shRNA-LGI1, and during application of α-DTX . This could be due to several factors. Fiber volley could decrease because of a general run down of the quality of the slice after the two hours of average experiment and therefore having less neurons which are alive and responsive. Alternatively, since the use of α-DTX blocks Kv1.1 channels, the total membrane resistance would increase, causing the axons to be more resilient to excitation due to the slower rate of rise of the voltage (Tau = R * C, tau: time constant to change the membrane voltage (ms), R: resistance (Ω), C: capacitance (μF)). This would require more time for the sodium channels to open and to cause depolarisation. Lastly, the sodium channel may go to depolarisation block due to depolarisation of the membrane potential, causing a block of axonal recruitment. In general, this run down is not consistent with the increased frequency-dependent facilitation, but these mechanisms are difficult to discriminate.

Baselines analysis (0.05Hz) during the short term plasticity protocol, revealed a slightly smaller fEPSP slope for LV-shRNA-LGI1 compared to LV-scramble, but surprisingly this was not significantly affected by application of α-DTX. Being LGI1 a trans-synaptic protein important also for AMPAR mediated current, this might be due to a post synaptic effect of LGI1 acute downregulation, and particularly due to a decrease of total AMPAR number. Recent studies support in fact that LGI1 is part of Kv1 and ADAM22 complex at juxtaparanodes and AIS of myelinated axons (Ogawa *et al.*, 2010). ADAM22 has been found fundamental for the post-synaptic macrostructure formed by PSD-95 and AMPAR. LGI1 may hence help to bring together pre and post synaptic partners in the right conformation and its dislocation may cause alteration of AMPA receptor synaptic transmission (Fukata *et al.*, 2016). To address this question, experiments may be

repeated with the specific low affinity AMPA blocker γ-DGG (γ -D-glutamylglycine) (Boillot *et al.*, 2016).

Application of α-DTX in both LV-scramble and LV-shRNA, caused a small increase in the amplitude of the response (in slope). At the same time, I measured also a decrease in the fiber volley slope, implying fewer axons recruited by the stimulation. Together these results indicate that the release probability for any single fiber may be increased, suggesting that Kv1.1 could be contributing to the initial release probability. My findings can therefore be explained by the fact that the reduction of LGI1 promotes inactivation of Kv1.1 during the wind-up resulting in a greater release probability.

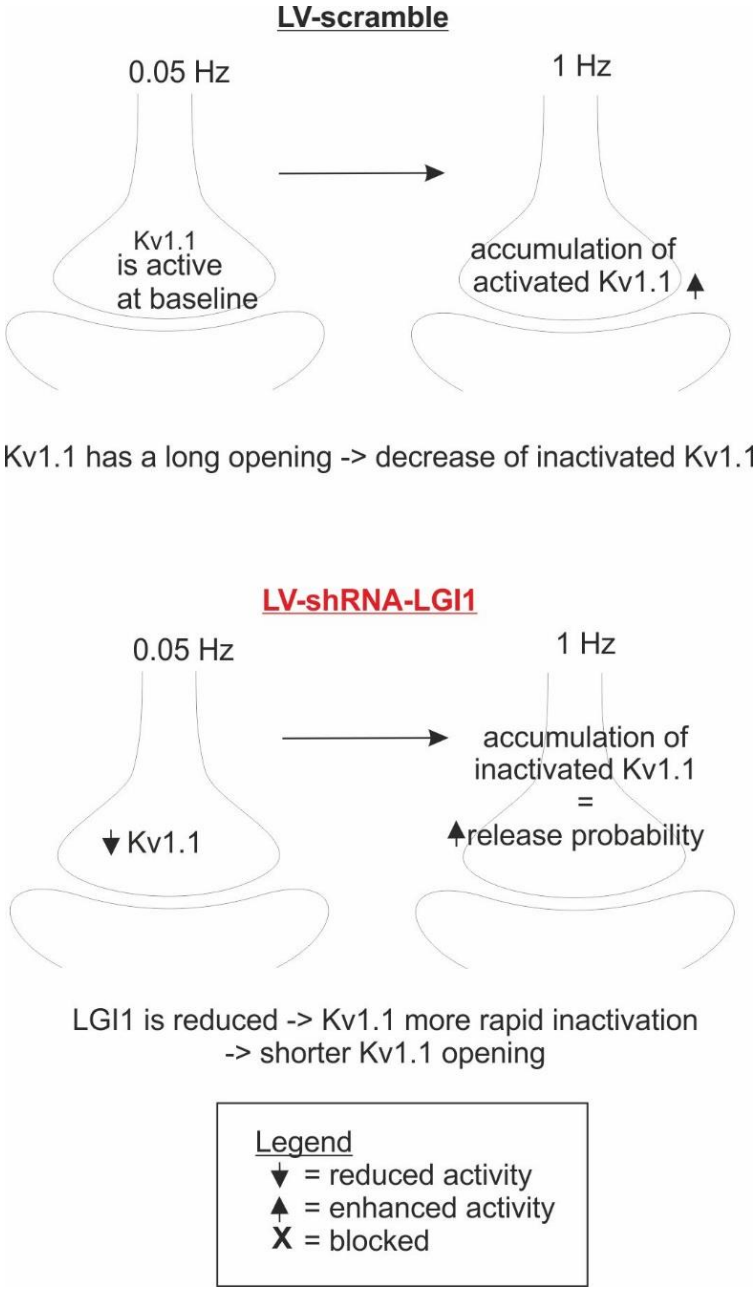

Figure 5.7: Kv1.1 role during baseline and windup in LV-scramble and LV-shRNA-LGI1 synapses. *Kv1.1 kinetics and cellular excitability change according to the amount of LGI1 at the synapse.*

There are contrasting findings concerning LGI1 effects on the passive properties of neurons (Zhou *et al.*, 2009; Boillot *et al.*, 2016). Nonetheless, my data indicate that reducing LGI1 increased input resistance, similar to other studies of the acute application of sera from patients with limbic encephalitis (Lalic *et al.*, 2011).

Patch clamp experiments of cells near to EGFP+ neurons in LV-shRNA-LGI1 slices, revealed that reduction of LGI1 affects the physiological properties of neurons close by transduced LV-shRNA-LGI1 positive cells. This is supposedly a paracrine mediated effect of the downregulation of LGI1 in neighbouring neurons, but, since LGI1 does not have specific blocking agents or its method of release is still unknown, I could not have a mechanistic demonstration of the mentioned effect. Rescue experiments support that LGI1 may have paracrine effects onto neighbouring neurons, hence local and circumscribed reduction may affect other neurons too (Lovero *et al.*, 2015). My data shows that acute reduction of LGI1 reduce AP threshold (Seagar *et al.*, 2017). This was also observed with acute incubation of VGKC-IgG (Lalic *et al.*, 2011). LGI1 acute reduction in my experiments decreases the inter spike interval but does not affect the AP half width. This is probably due to the expression pattern of Kv1.1, which is more abundant at the AIS and axons. Future experiments with α-DTX will clarify if this effect is also mediated by alteration of Kv1 ion channel kinetics.

Paired pulse LFP experiments revealed that there was no difference in paired pulse ratio between groups. This might be explained by the fact that presynaptic impairments might be due to a decrease of density of Kv1.1 potassium channels, but not for a change in the kinetics, as proposed in my results. This result contrasts with the effect on wind-up but at short interstimulus intervals the effects of LGI1 on inactivation would not be evident. In the future, we could use alternative methodologies to investigate presynaptic release such as application of MK801 use-dependent-NMDA blocker during LFP experiments (Scimemi *et al.*, 2004), or analysis of the coefficient of variation by measuring several successive EPSCs by patch clamp technique (Faber and Korn, 1991; Choi and Lovinger, 1997).

Increase of facilitation observed in wind-up experiments might be indeed caused by an additional factor of the number of active synapses in the circuit. Previous experiments

showed in chapter 4 revealed that LV-scramble and LV-shRNA-LGI1 have similar number of excitatory active synapses *in vitro*. In the future, this experiment could be repeated in slices to confirm the effect.

The *in vivo* data alone demonstrate that a 20% sparse reduction in LGI1 was not sufficient to lower the threshold for seizure induction but any effect may have been masked by the effect of the injection itself. In a future, mice could be implanted with wireless recording electrodes in order to record EcoG during the days prior to injection of kainic acid and during kainic acid administration, in order to monitor for possible interictal events.

In conclusion, in this chapter I showed that acute removal of LGI1 in *ex vivo* hippocampal areas affects network excitability and that this effect is largely mediated by changes in kinetics of presynaptic Kv1.1 channels, without affecting the number of active synapses. Nevertheless, an effect on post synaptic AMPAR cannot be completely excluded. My results corroborate and extend previous data from acute application of VGKC antibodies in slices (Lalic *et al.*, 2011). Localised and acute reduction of LGI1 *in* vivo was never been achieved or investigated before. Hence these data could potentially shed light on epileptogenic mechanisms of seizure occurrence in patents with mutations for LGI1, people with LGI1 specific limbic encephalitis and, from the results of chapter 3, may be relevant to acquired epilepsy.

Chapter 6

6 General Discussion

6.1 Summary

Extracellular matrix proteins have recently emerged as key contributors in the maintaining and regulation of physiological processes. This thesis aimed to investigate the acute role of LGI1, a trans-synaptic secreted protein part of the ECM, in neuronal networks.

In the chapter 3, I examined if acquired epilepsy resulted in alteration of hippocampal LGI1 concentrations and whether this resulted in modified properties of hippocampal circuits. To do so, I utilised an electrical model of acquired TLE in adult rats and showed that LGI1 protein levels are reduced three weeks after the establishment of self-sustained status epilepticus. This reduction is accompanied by alteration of presynaptic properties in the DG circuits.

In the chapter 4 I established a silencing RNA method to downregulate LGI1 in an acute way and validated its efficiency with biochemical, electrophysiological and imaging methods. These experiments indicated that 40% downregulation of LGI1 in primary neuronal cultures was sufficient to alter the basal calcium levels and network bursts, without affecting neurons survival.

In the chapter 5 I extended my investigation to a more complex biological system and demonstrated that acute removal of LGI1 in MF-CA3 hippocampal circuits was able to alter the local network excitability, but it was not sufficient to lower seizures threshold *in vivo.* Pharmacological experiments with blocker of Kv1 ion channels, indicated that modification of Kv1 kinetics was the likely basis of the observed increased facilitation observed in MF-CA3 circuits.

6.2 LGI1 is downregulated following acquired epilepsy

LGI1 has been greatly investigated for the last two decades, initially because of the involvement of heterozygous mutations in familial form of epilepsy associated with auditory auras. More recently, patients with limbic forms of acquired epilepsy caused by autoimmune diseases against specific antigens of LGI1 were also reported. The former LGI1 epilepsy disorder is associated with developmental abnormalities, while the latter was initially described as secondary symptom due to brain inflammation, from autoantibodies generated in response to underlying tumour or, possibly, acute viral infections. Use of early or preventive immunotherapy revealed that decreasing the levels of LGI1 auto-antibodies in the patient's plasma, ameliorate the seizure phenotype and recovered cognitive impairments. Therefore, it opened up the possibility that the disruption of LGI1 protein in the brain was the major reason of the manifestation of the epilepsy and not the undergoing inflammation.

To investigate the role of LGI1 in epilepsy, I initially addressed the question whether acute forms of epilepsy alter the concentrations of LGI1 in the brain. To do so, I used a well-established model of acquired epilepsy in rats, the perforant path model, avoiding the use of any chemical pro-convulsants. For the first time, it emerged that LGI1 is downregulated in the hippocampus of animals with acquired forms of epilepsy and that the severity of the epilepsy may correlate with the levels of LGI1 downregulation. Previous work suggest that LGI1 decrease is not likely due to hippocampal neuronal death since cellular loss happens predominantly right after the SSSE and terminate a few hours later (Sloviter, 1983).

Secondly we investigated whether acute LGI1 downregulation was at the basis for physiological impairments in the hippocampus of PPS animals. *Ex vivo* electrophysiological evaluations pointed out that the paired pulse ratio was overall

comparable between sham and epileptic animals in standard conditions. This ratio was not conserved when a broad Kv1 antagonist, α-DTX, was applied over the slices, since the proportion of % change in PPR before and after the drug was greater for epileptic animals than in sham animals. The lack of a baseline change might be due to homeostatic plasticity changes occurring at the AIS and at the presynaptic synaptic bouton since Kv1 is enriched in those compartments. LGI1 has been shown to regulate the density and/or the kinetics of Kv1 channels, and hence to indirectly influence neuronal excitability (Fukata *et al.*, 2006; Schulte *et al.*, 2006; Seagar *et al.*, 2017). Indeed, previously (*not shown*) data in the laboratory reported that, in the same epileptic model, Kv1.1 is downregulated alongside LGI1. These findings seem to support an activity-dependent release and elimination of LGI1 and Kv1.1 as suggested previously (Lee *et al.*, 2015). It would be interesting to explore how LGI1 and Kv1.1 protein levels change at different time points after the establishment of the SSSE. It would be especially important for future studies to understand whether the initial increase in the mRNAs correlates with a protein increase and whether this would be protective for the development of epilepsy.

6.3 Acute reduction of LGI1 on neuronal circuits

So far, investigation of LGI1 in the physiology of the neuronal circuits have been explored with the use of transgenic animals or with acute applications of auto-antibodies against LGI1 in primary cultures and slices (Fukata *et al.*, 2016). With these models it was possible to understand that LGI1 displays crucial roles during the embryonic development and that LGI1 modulates both pre and post synaptic transmission. Several discrepancies in the effects described from multiple groups could be ascribed to the different genetic background of the animal models used, the differing ages of the brain samples examined and the diverse anatomical zones investigated. Moreover, some LGI1 mutations cause a loss of functional monomer, while others have a dominant

negative effects, hence triggering epilepsy probably via two different mechanisms of action. Finally, experiments with auto-antibodies from patients with LGI1 limbic encephalitis seem to indicate that acute interference with LGI1 is sufficient to have alteration of neuronal circuits and synaptic transmission, without a significant immune/inflammatory component.

In order to separate the contribution of developmental issues and of the inflammatory response from the removal of LGI1 protein in neuronal circuits, I designed and validated an acute method based on small silencing RNA for downregulation of LGI1 avoiding the use of mutants or of polyclonal IgGs encephalitic patients. This approach has not been used before in the investigation of the role of LGI1 but it can establish the effects of acute LGI1 downregulation. In my experiments, I achieved ~40% knockdown of the endogenous LGI1 protein, avoiding the use of any overexpression construct (such as FLAG-LGI1, GFP-LGI1 or myc-LGI1, as previously used) (Fukata *et al.*, 2006; Kunapuli *et al.*, 2009; Zhou *et al.*, 2018). These over-expressions tagged approaches have been historically employed to facilitate the detection of LGI1 protein, but they may misestimate the real effect and produce misfolded and mislocalised LGI1 monomers. The knock down detected is also close to a heterozygous state, helping to dissect realistic physiological consequences of LGI1 molecular alterations on neuronal circuits.

In this thesis, the term “acute effect” applies to a knock down period of a few days compared to developmental depletion of the protein (from weeks to month), and it is not an immediate effect of the reduction of LGI1 (hours or minutes). This time course is in accordance with the onset of symptoms in patients affected by limbic encephalitis and with *ex vivo* experiments (Irani *et al.*, 2013).

6.4 Acute reduction of LGI1 is sufficient to alter *in vitro* and *ex vitro* neuronal excitability

LGI1 is a secreted protein. Still many doubts exist related to the production, secretion and role of LGI1, hence it is difficult to restrict its effects to a well-defined neuronal population. Single cell studies revealed that LGI1 is likely to regulate mainly excitatory glutamatergic transmission (Boillot *et al.*, 2014, 2016), whilst the other half of the literature available claims that LGI1 may provoke epilepsy by affecting AMPAR conductance in interneurons only (Yamagata *et al.*, 2018). Glial cells also express and/or produce LGI1, although a functional role has yet to be assigned to them (Head *et al.*, 2007). In excitatory cortical and hippocampal cells, LGI1 helps translocate Kv1.1 to the membrane and the quantity of LGI1 protein at the synapse affects the kinetics of presynaptic Kv1.1 channels. This, in turn, may highly influence the amount of presynaptic calcium in the bouton and glutamate neurotransmitter released. Developmentally, LGI1 is important for axonal growth and dendritic formation through its interactions with the presynaptic ADAM23 TM protein and the postsynaptic NgR1, since LGI1 KO, ADAM23 KO and NgR1 KO mice exhibit mild anatomical brain abnormalities. At the postsynaptic side of asymmetric synapses, LGI1 has been pointed out to influence interneuronal activity by decreasing the amplitude of events AMPAR-mediated, therefore leading to unbalance of inhibition over the excitation. In my study, I consequently decided to use a broad promoter (PGK) able to induce a constant production of the shRNA in any cell type.

This thesis also includes investigations using techniques that permit network studies of acute LGI1 downregulation, such as *in vitro* calcium imaging of whole coverslips and extracellular field potential of primary neuronal cultures by MEA devices. Calcium measurements and MEAs devices were successfully employed in this thesis to show for the first time that acute LGI1 results in alteration in neuronal network excitability. The measurement of calcium waves is of critical importance since they are strongly correlated with epileptic-like burst and action potentials *in vitro* (Kovac *et al.*, 2014). These initial studies indicated that broad heterozygous-like LGI1 downregulation was sufficient to

alter basal calcium levels and burst activities of *in vitro* neuronal networks. These results corroborate previous findings from studies of LGI1 mutants in cell lines (Nobile *et al.*, 2009; Pakozdy *et al.*, 2014) and extend the present knowledge about LGI1-IgGs. Interestingly, only one previous work investigated calcium waves in neuronal cultures showing opposite effect to what I showed here. This might be attributable to long term (24 -72 hours) IgGs incubations leading to neuronal toxicity (Ayşit-Altuncu *et al.*, 2018).

Measurements of short-term plasticity investigated in chapter 5 using *ex vivo* hippocampal slices previously injected with LV-shRNA-LGI1, showed a greater facilitation of MF to CA3 transmission. This result is crucial to attribute functional alterations of excitatory transmission to acute downregulation of LGI1, without the contribution of developmental circuits abnormalities or temporal lobe inflammation. These results are in line with previous works which measured higher spontaneous burst activity and interictal-like depolarisation by extracellular field recordings in CA1 of LGI-KO (Yu *et al.*, 2010; Boillot *et al.*, 2016). Also acute application of VGKC-IgGs in the DG-CA3 pathway confirmed that acute interference with LGI1 provoked higher neurotransmitter release from the granule cells and increased postsynaptic excitability (Lalic *et al.*, 2011). This increased facilitation is likely due to the higher release of glutamate from the presynapse, from an increase in Kv1.1 inactivation during repetitive stimulation. This could act as an initiator of seizures and could facilitate propagation in the hippocampus, as previously hypothesised (Seagar *et al.*, 2017).

To test this hypothesis, I used repeated subthreshold injection of kainate, a well-established pro-convulsive drug, but found no difference in behavioural seizure threshold and latencies between treatments. Hence, despite a consistent difference in excitation measured at DG-CA3 synapses in animals with local reduction of LGI1, this element alone is not sufficient to have a global lowering of the seizure threshold. Whole brain heterozygous mice for LGI1 have instead early seizure onset when tested for audiogenic

seizures. This might be related to the decrease in LGI1 also in the auditory brain stem, an important gateway for sound volume and timing, which is enriched in LGI1 and Kv1.1 proteins (Robbins and Tempel, 2012).

6.5 Dissection of the mechanisms behind LGI1 network hyperexcitability

The fact that an extracellular structural protein influences network excitability and glutamate release has been debated for many years. The first evidence that LGI1 indirectly may have a role in cellular excitability arrived when it was first co-purified in the macromolecular structure formed by Kv1.1 presynaptic potassium channel and postsynaptic AMPAR. Since then, it has been suggested that LGI1 influences Kv1.1 channel by two mechanisms: a prolongation of its opening state by interference with the Kvβ1 regulatory subunit, and an influence on the number of Kv1.1 recruited at the presynapse.

In the experiments described in chapter 3 I found that acquired, but long lasting induced SSSE, is correlated with LGI1 and Kv1.1 downregulation. Examination of paired pulse ratios indicate that epileptic animals lose their response to application of α-DTX. These are the first data showing that acquired epilepsy diseases are associated with alteration of LGI1 and Kv1.1 proteins; however, it is not possible to attribute this effect as causative or a consequence of the acquired disorder. Further investigation will be required to determine if this alteration is limited to the presynaptic partners or there is a contribution of AMPARs and ADAM22 components as well. These results are in line with previous studies showing brain LGI1 alterations in patients affected by limbic encephalitis and from LGI1 *null* mice which exhibit fewer Kv1.1 channels (Seagar *et al.*, 2017; Petit-pedrol *et al.*, 2018).

But LGI1 seems to act also *via* a second and well described route. Inside-out patches in oocytes showed that mutations or removal of LGI1 proteins lead to shortening of the opening time of Kv1.1 channels. This has been attributed to the ability of a single kvβ1

unit to block the whole Kv1.1 tetramer. Instead, multiple LGI1 are required to interfere with kvβ1, so that a small decrease in LGI1 relative to kvβ1 causes a much greater effect than expected (Schulte *et al.*, 2006).

In chapter 4 and 5 I used a silencing RNA method to downregulate LGI1 in primary cultures and mouse hippocampus. Just ~20% LGI1 reduction affected short-term plasticity of MF to CA3 synapses, resulting in a significant over facilitation during repetitive stimulation. This is probably caused by early inactivation of Kv1.1 channels, since blockage with α-DTX occluded this effect. Therefore, it is also possible that acute reduction of LGI1 proteins causes alteration of neurotransmission by functional modification of Kv1.1 kinetics.

I cannot exclude a post-synaptic contribution from LGI1 reduction. Slow (0.05Hz) stimulations of MF and recordings from CA3 dendritic layer, showed that fEPSC slope of LV-shRNA-LGI1 slices show a trend to be smaller than that those in controls. This effect is not mediated by Kv1 since application of α-DTX did not change the results. Impairments in LTP formation in CA1 have been recently attributed to lack of recruitment of postsynaptic AMPAR after chronic application of LGI1 auto-antibodies. This opens the possibility that acute removal of LGI1 affects also postsynaptic transmission.

6.6 Future directions

The results reported so far showed that the acute decrease of LGI1 can result in *in vitro* network hyperexcitability and in *ex vivo* alteration of the DG-CA3 pathway. Nevertheless, additional experiments could explore in more details certain aspects which have not been addressed so far or to verify the results from a different perspective.

In the first chapter, I showed that LGI1 is decreased three weeks after acquisition of SSSE, together with Kv1.1 potassium channel. It would be important to see at which

point this decrease starts and if it undergoes changes in the period before 21 days. Also, the extent to which LGI1 affects other potassium channels important for glutamate release at mossy fibers, such as Kv3 that important for the high frequency neuronal activity, has not been investigated so far (Kaczmarek and Zhang, 2017). Since LGI1 interacts with different pre and post synaptic partners, I would like to see whether ADAM22, ADAM23 and AMPAR are also altered during this time. Such knowledge would give supplementary information about mechanisms of epileptogenesis in acquired epileptic disorders.

In the second result chapter of this thesis I showed that acute LGI1 knock down increased network bursting rate when measured by MEAs. Mean Cross-correlation peaks levels could be also extrapolated from the data and this would offer a further link between neuronal activation and epilepsy-like activity *in vitro*, since high neuronal synchronisation is observed in seizures generation and spreading.

In the third result session I showed that local injection of LV-shRNA-LGI1 in the MF-CA3 circuit, causes increase of mossy fibres facilitation. This is likely due to early blocking of Kv1.1 channels using α-DTX. Nevertheless, the results shown so far would need a higher number of recordings and testing whether this effect is dependent upon different concentrations of α-DTX employed. α-DTX applied in control slices should also mimic the effects seen in neurons patched in LV-shRNA-LGI1 slices, confirming that the lowering of the excitability threshold is due to Kv1.1 shut down. In collaboration with Chris Norman and Dr. Yulia Timofeeva at Warwick University (UK), I also aim to investigate if the over facilitation seen in MF to CA3 could be explained by an early inactivation of Kv1.1 channel using activation dynamic modelling based on Markov model (Rama *et al.*, 2015).

A drawback of the broad PGK promoter used to deliver the shRNA-LGI1 was the difficulty to target and to restrain the hippocampal injections to a certain hippocampal subzone. Creation of a modified shRNA-LGI1 plasmid with promoter Prox-1 could permit specific

shRNA-LGI1 expression in granule cells of the DG, allowing to study with great precision the presynaptic impairments of acute LGI1 downregulation (Lovero *et al.*, 2015). Specific promoters (such as parvalbumin or somatostatin interneurons) could also help in dissect the effects seen in inhibitory neurons regarding the alterations of AMPA signalling (Fukata *et al.*, 2016).

ShRNA is a great approach for acute and controlled downregulation of a protein, but recently other methods have been employed to study protein disruption. CRISPR-Cas9 (clustered regularly interspaced short palindromic repeats) technique has been recently developed and it emerges as convenient biotechnological tool able to alter DNA in a fast and precise way. CRISPR-Cas9 Is based on small sequences of synthetic RNA targeting a specific sequence of the host DNA. The modifications are mediated by RNA-DNA interaction by a nuclease (Richner and Krook-Magnuson, 2018). This approach could be used in either decrease or augmentation of LGI1 *in vivo*. Alternatively, specific peptide interference could be designed to target either the presynaptic link with ADAM22 or the post synaptic connection with ADAM23. This is now possible from the recent crystal structure elucidated in a recent work (Yamagata *et al.*, 2018) and would corroborate previous findings showed using LGI1 mutants (Nobile *et al.*, 2009).

Nevertheless, the current shRNA for LGI1 could be employed to study LGI1 function also in other circuits, such as the medial superior olive, part of the brain stem. This is one of the major centres for sound processing and their neurons are enriched of LGI1 proteins and Kv1.1 channels. It would be interesting to discover whether localised downregulation of LGI1 would be sufficient to have seizures caused by high noises, as previously showed in mice heterozygous for LGI1 (Chabrol *et al.*, 2010).

LGI1 is a fairly recent protein and an extracellular secreted protein which is difficult to study with standard techniques (Chernova, Somerville and Cowell, 1998). Still many

features are unknown such as LGI1 secretion pathway and the location from where it is released. Previous works pointed out that acute application of pro-convulsant to primary cultures increase the levels of released LGI1-mRNA, suggesting a possible activity dependent mechanism of release. If so, after an epileptic insult LGI1 could be initially released in order to try to decrease neuronal excitability, increasing the number and the opening state of Kv1.1 at AIS and synapses. After the prolonged activity tough, mRNA-LGI1 decrease, and this could explain the decrease found in animals affected by SSSE (Lee *et al.*, 2015).

All the results described here are showing that acute reduction of LGI1 alters neuronal excitability. Rescue experiments should be also included in order to confirm if the aforementioned effects disappear when LGI1 is reintroduced in the system or when an anti-convulsive agent is applied. Use of AEDs, such as carbamazepine, in either multielectrodearrays or LFP experiments on LV-shRNA-LGI1 positive cultures would permit me to interrogate if AED treatment allows a decrease of the hyperexcitability to wild type levels. Moreover, an overexpression plasmid has already been employed in this thesis (see chapter 4) as positive control for biochemical experiments. Production of a lentiviral overexpression system co-transduced with the shRNA described in this thesis would corroborate previous results showing that only the addition of LGI1 rescues the phenotype but not any other LGI1 isoforms (Fukata *et al.*, 2010). The reintroduction of LGI1 proteins might be beneficial for patients affected by focal epilepsy and hence could also be employed as an innovative gene therapy approach.

Bibliography

Abramovici, S. and Bagić, A. (2016) *Epidemiology of epilepsy*. 1st edn, *Handbook of Clinical Neurology*. 1st edn. Elsevier B.V. doi: 10.1016/B978-0-12-802973-2.00010-0.

Amaral, D. G., Scharfman, H. E. and Lavenex, P. (2007) 'The dentate gyrus: fundamental neuroanatomical organization (dentate gyrus for dummies)', *Progress in Brain Research*, 163, pp. 3–22. doi: 10.1016/S0079-6123(07)63001-5.

Andersen, P. *et al.* (2007a) 'Hippocampal Neuroanatomy', in *The Hippocampus Book*. 6th edn. Oxford University Press., pp. 1–177. doi: 10.1093/acprof.

Andersen, P. *et al.* (2007b) 'Structural Plasticity', in *The Hippocampus Book*. 6th edn. Oxford University Press, pp. 1–63. doi: 10.1093/acprof.

Androsova, G. *et al.* (2017) 'Comparative effectiveness of antiepileptic drugs in patients with mesial temporal lobe epilepsy with hippocampal sclerosis', pp. 1734–1741. doi: 10.1111/epi.13871.

Aurangzeb, S. *et al.* (2017) 'LGI1-antibody encephalitis is characterised by frequent , multifocal clinical and subclinical seizures', *Seizure: European Journal of Epilepsy*. BEA Trading Ltd, 50, pp. 14–17. doi: 10.1016/j.seizure.2017.05.017.

Ayşit-Altuncu, N. *et al.* (2018) 'Effect of LGI1 antibody-positive IgG on hippocampal neuron survival: A preliminary study', *NeuroReport*, 29(11), pp. 932–938. doi: 10.1097/WNR.0000000000001055.

Ben-Ari, Y. (2002) 'Excitatory actions of gaba during development: the nature of the nurture', *Nature Reviews Neuroscience*. Nature Publishing Group, 3, p. 728. Available at: https://doi.org/10.1038/nrn920.

Berretta, S. (2012) 'Extracellular matrix abnormalities in schizophrenia', *Neuropharmacology*. Elsevier Ltd, 62(3), pp. 1584–1597. doi: 10.1016/j.neuropharm.2011.08.010.

Bialowas, A. *et al.* (2015) 'Analog modulation of spike-evoked transmission in CA3 circuits is determined by axonal Kv1.1 channels in a time-dependent manner', *European Journal of Neuroscience*, 41(3), pp. 293–304. doi: 10.1111/ejn.12787.

Blau, A. *et al.* (2009) 'Replica-moulded polydimethylsiloxane culture vessel lids attenuate osmotic drift in long-term cell cultures', *Journal of Biosciences*, 34(1), pp. 59–69. doi: 10.1007/s12038-009-0009-3.

Blumcke, I. *et al.* (2017) 'Histopathological Findings in Brain Tissue Obtained during Epilepsy Surgery', *New England Journal of Medicine*. Massachusetts Medical Society, 377(17), pp. 1648–1656. doi: 10.1056/NEJMoa1703784.

Boillot, M. *et al.* (2014) 'Glutamatergic neuron-targeted loss of LGI1 epilepsy gene

results in seizures', *Brain*, 137(11), pp. 2984–2996. doi: 10.1093/brain/awu259.

Boillot, M. *et al.* (2016) 'LGI1 acts presynaptically to regulate excitatory synaptic transmission during early postnatal development', *Scientific Reports*. Nature Publishing Group, 6(February), pp. 1–9. doi: 10.1038/srep21769.

Bologna, L. L. *et al.* (2010) 'Investigating neuronal activity by SPYCODE multi-channel data analyzer', *Neural Networks*. Elsevier Ltd, 23(6), pp. 685–697. doi: 10.1016/j.neunet.2010.05.002.

Bortolotto, Z. A. *et al.* (2001) 'Synaptic plasticity in the hippocampal slice preparation.', *Current protocols in neuroscience*, Chapter 6, p. Unit 6.13. doi: 10.1002/0471142301.ns0613s16.

Bragin, A. *et al.* (1995) 'Gamma (40-100 Hz) oscillation in the hippocampus of the behaving rat', *The Journal of Neuroscience*, 15(1), p. 47 LP-60. doi: 10.1523/JNEUROSCI.15-01-00047.1995.

Bromfield, E., Cavazos, J. and Sirven, J. (2006) 'Clinical Epilepsy', in *An introduction to epilepsy*. West Hartford (CT): American Epilepsy Society; 2006., pp. 1–98. Available at: http://www.ncbi.nlm.nih.gov/books/NBK2511/.

Bumanglag, A. V. and Sloviter, R. S. (2008) 'Minimal latency to hippocampal epileptogenesis and clinical epilepsy after perforant pathway stimulation-induced status epilepticus in awake rats', *Journal of Comparative Neurology*, 510(6), pp. 561–580. doi: 10.1002/cne.21801.

Carmignoto, G. and Haydon, P. G. (2012) 'Astrocyte calcium signaling and epilepsy', *Glia*, 60(8), pp. 1227–1233. doi: 10.1002/glia.22318.

Chabrol, E. *et al.* (2007) 'Two novel epilepsy-linked mutations leading to a loss of function of LGI1', *Archives of Neurology*, 64(2), pp. 217–222. doi: 10.1001/archneur.64.2.217.

Chabrol, E. *et al.* (2010) 'Electroclinical characterization of epileptic seizures in leucine-rich, glioma-inactivated 1-deficient mice', *Brain*, 133(9), pp. 2749–2762. doi: 10.1093/brain/awq171.

Chandler, K. E. *et al.* (2003) 'Plasticity of GABA(B) receptor-mediated heterosynaptic interactions at mossy fibers after status epilepticus.', *The Journal of Neuroscience*, 23(36), pp. 11382–11391. Available at: http://www.jneurosci.org/content/23/36/11382.

Chernova, O. B., Somerville, R. P. T. and Cowell, J. K. (1998) 'A novel gene, LGI1, from 10q24 is rearranged and downregulated in malignant brain tumors', *Oncogene*, 17(22), pp. 2873–2881. doi: 10.1038/sj.onc.1202481.

Cho, K. *et al.* (2015) 'epilepsy and associated cognitive decline', *Nature Communications*. Nature Publishing Group, 6, pp. 1–13. doi:

10.1038/ncomms7606.

Choi, S. and Lovinger, D. M. (1997) ‘Decreased Frequency But Not Amplitude of Quantal Synaptic Responses Associated with Expression of Corticostriatal Long-Term Depression’, *The Journal of Neuroscience*, 17(21), p. 8613 LP-8620. doi: 10.1523/JNEUROSCI.17-21-08613.1997.

Cohen, I. *et al.* (2002) ‘On the Origin of Interictal Activity in Human Temporal Lobe Epilepsy in Vitro’, *Science*, 298(5597), p. 1418 LP-1421. doi: 10.1126/science.1076510.

Colombi, I. *et al.* (2013) ‘Effects of antiepileptic drugs on hippocampal neurons coupled to micro-electrode arrays’, *Frontiers in Neuroengineering*, 6(November), pp. 1–11. doi: 10.3389/fneng.2013.00010.

Counsell, J. R. *et al.* (2018) ‘Foamy Virus Vectors Transduce Visceral Organs and Hippocampal Structures following In Vivo Delivery to Neonatal Nice’, *Molecular Therapy - Nucleic Acids*. Elsevier Ltd., 12(September), pp. 626–634. doi: 10.1016/j.omtn.2018.07.006.

Crisp, S. J., Kullmann, D. M. and Vincent, A. (2016) ‘Autoimmune synaptopathies’, *Nature Reviews Neuroscience*. Nature Publishing Group, 17(2), pp. 103–117. doi: 10.1038/nrn.2015.27.

Cudmore, R. H. *et al.* (2010) ‘Spike-Time Precision and Network Synchrony Are Controlled by the Homeostatic Regulation of the D-Type Potassium Current’, 30(38), pp. 12885–12895. doi: 10.1523/JNEUROSCI.0740-10.2010.

Curia, G. *et al.* (2008) ‘The pilocarpine model of temporal lobe epilepsy’, *Journal of Neuroscience Methods*. Elsevier/North-Holland Biomedical Press, 172(2–4), pp. 143–157. doi: 10.1016/j.jneumeth.2008.04.019.

de Curtis, M. *et al.* (2018) ‘Potassium dynamics and seizures: Why is potassium ictogenic?’, *Epilepsy Research*, 143, pp. 50–59. doi: https://doi.org/10.1016/j.eplepsyres.2018.04.005.

Dalmau, J., Geis, C. and Graus, F. (2017) ‘Autoantibodies to Synaptic Receptors and Neuronal Cell Surface Proteins in Autoimmune Diseases of the Central Nervous System’, *Physiological Reviews*, 97(2), pp. 839–887. doi: 10.1152/physrev.00010.2016.

Devinsky, O. *et al.* (2018) ‘Epilepsy’, *Nature Reviews Disease Primers*, 4(May). doi: 10.1038/nrdp.2018.24.

Diehl, B. and Duncan, S. J. (2017) ‘EPILEPSY 2017, From Bench to Bedside, A practival guide’, in Rugg-Gunn, F. J. and Stapley, H. B. (eds). International League Against Epilepsy (British Chapter), pp. 179–182.

Dityatev, A., Wehrle-Haller, B. and Pitkänen, A. (2014) ‘Brain Extracellular Matrix in

Health and Disease', in *Progress in Brain Research*. Elsevier, pp. xiii–xvii. doi: 10.1016/B978-0-444-63486-3.09998-9.

Dixon, C. L., Zhang, Y. and Lynch, J. W. (2015) 'Generation of Functional Inhibitory Synapses Incorporating Defined Combinations of GABA(A) or Glycine Receptor Subunits ', *Frontiers in Molecular Neuroscience* , p. 80. Available at: https://www.frontiersin.org/article/10.3389/fnmol.2015.00080.

Dull, T. *et al.* (1998) 'A third-generation lentivirus vector with a conditional packaging system.', *Journal of virology*, 72(11), pp. 8463–71. doi: 98440501.

Einevoll, G. T. *et al.* (2013) 'Modelling and analysis of local field potentials for studying the function of cortical circuits', *Nature Reviews Neuroscience*. Nature Publishing Group, 14(11), pp. 770–785. doi: 10.1038/nrn3599.

Eunson, L. H. *et al.* (2000) 'Clinical, genetic, and expression studies of mutations in the potassium channel gene KCNA1 reveal new phenotypic variability', *Annals of Neurology*, 48(4), pp. 647–656. doi: 10.1002/1531-8249(200010)48:4<647::AID-ANA12>3.0.CO;2-Q.

Faber, D. S. and Korn, H. (1991) 'Applicability of the coefficient of variation method for analyzing synaptic plasticity', *Biophysical journal*, 60(5), pp. 1288–1294. doi: 10.1016/S0006-3495(91)82162-2.

Feyissa, A. M. and López, A. S. (2017) 'Antiepileptic drug therapy in patients with autoimmune epilepsy', 0. doi: 10.1212/NXI.0000000000000353.

Fisher, R. S. *et al.* (2014) 'ILAE Official Report: A practical clinical definition of epilepsy', *Epilepsia*, 55(4), pp. 475–482. doi: 10.1111/epi.12550.

Fricker, M. *et al.* (2018) 'Neuronal Cell Death', *Physiological Reviews*, 98(2), pp. 813–880. doi: 10.1152/physrev.00011.2017.

Fukata, Y. *et al.* (2006) 'Epilepsy-Related Ligand/Receptor Complex LGI1 and ADAM22 Regulate Synaptic Transmission', *Science*, 313(5794), p. 1792 LP-1795. Available at: http://science.sciencemag.org/content/313/5794/1792.abstract.

Fukata, Y. *et al.* (2010) 'Disruption of LGI1-linked synaptic complex causes abnormal synaptic transmission and epilepsy', *Proceedings of the National Academy of Sciences*, 107(8), pp. 3799–3804. doi: 10.1073/pnas.0914537107.

Fukata, Y. *et al.* (2016) 'The LGI1–ADAM22 protein complex in synaptic transmission and synaptic disorders', *Neuroscience Research*. Elsevier Ireland Ltd and Japan Neuroscience Society, 116, pp. 39–45. doi: 10.1016/j.neures.2016.09.011.

Furlan, S. *et al.* (2006) 'The LGI1/Epitempin gene encodes two protein isoforms differentially expressed in human brain', *Journal of Neurochemistry*, 98(3), pp. 985–991. doi: 10.1111/j.1471-4159.2006.03939.x.

Geiger, J. R. P. and Jonas, P. (2000) 'Dynamic Control of Presynaptic Ca2+ Inflow by

Fast-Inactivating K+ Channels in Hippocampal Mossy Fiber Boutons', *Neuron*, 28(3), pp. 927–939. doi: 10.1016/S0896-6273(00)00164-1.

Grauert, A., Engel, D. and Ruiz, A. J. (2014) 'Endogenous zinc depresses GABAergic transmission via T-type Ca 2 + channels and broadens the time window for integration of glutamatergic inputs in dentate granule cells', 1, pp. 67–86. doi: 10.1113/jphysiol.2013.261420.

Grienberger, C. and Konnerth, A. (2012) 'Imaging Calcium in Neurons', *Neuron*. Elsevier Inc., 73(5), pp. 862–885. doi: 10.1016/j.neuron.2012.02.011.

Gu, W., Brodtkorb, E. and Steinlein, O. K. (2002) 'LGI1 is mutated in familial temporal lobe epilepsy characterized by aphasic seizures', *Annals of Neurology*, 52(3), pp. 364–367. doi: 10.1002/ana.10280.

Gunn, B. G. and Baram, T. Z. (2017) 'Stress and Seizures : Space , Time and Hippocampal Circuits', 40(11), pp. 667–679.

Harvey, A. and Robertson, B. (2004) 'Dendrotoxins: Structure-Activity Relationships and Effects on Potassium Ion Channels', *Current Medicinal Chemistry*, 11(23), pp. 3065–3072. doi: 10.2174/0929867043363820.

Head, K. *et al.* (2007) 'Defining the expression pattern of the LGI1 gene in BAC transgenic mice', *Mammalian Genome*, 18(5), pp. 328–337. doi: 10.1007/s00335-007-9024-6.

Hellier, J. L. *et al.* (1998) 'Recurrent spontaneous motor seizures after repeated low-dose systemic treatment with kainate: Assessment of a rat model of temporal lobe epilepsy', *Epilepsy Research*, 31(1), pp. 73–84. doi: 10.1016/S0920-1211(98)00017-5.

Henze, D. A., Urban, N. N. and Barrionuevo, G. (2000) 'The multifarious hippocampal mossy fiber pathway: A review', *Neuroscience*, 98(3), pp. 407–427. doi: 10.1016/S0306-4522(00)00146-9.

Herranz-Pérez, V. *et al.* (2010) 'Regional distribution of the leucine-rich glioma inactivated (LGI) gene family transcripts in the adult mouse brain', *Brain Research*. Elsevier B.V., 1307, pp. 177–194. doi: 10.1016/j.brainres.2009.10.013.

Herring, A. *et al.* (2012) 'Reelin depletion is an early phenomenon of alzheimer's pathology', *Journal of Alzheimer's Disease*, 30(4), pp. 963–979. doi: 10.3233/JAD-2012-112069.

Hiragi, T., Ikegaya, Y. and Koyama, R. (2018) 'Microglia after Seizures and in Epilepsy', *Cells*. MDPI, 7(4), p. 26. doi: 10.3390/cells7040026.

Hoffman, D. A. *et al.* (1997) 'channel regulation of signal propagation in dendrites of hippocampal pyramidal neurons Neuronal dendrites contain a variety of voltage-gated Na þ and Ca', *Nature*, 387(26). doi: 10.1038/43119.

Instruments, A. (2010) ‘The Axon Guide’, *The British journal of ophthalmology*, 94(2500), pp. 1078–82. doi: 10.1136/bjo.2009.169052.

Irani, S. R. *et al.* (2010) ‘Antibodies to Kv1 potassium channel-complex proteins leucine-rich, glioma inactivated 1 protein and contactin-associated protein-2 in limbic encephalitis, Morvan’s syndrome and acquired neuromyotonia’, *Brain*, 133(9), pp. 2734–2748. doi: 10.1093/brain/awq213.

Irani, S. R. *et al.* (2012) ‘Morvan syndrome: Clinical and serological observations in 29 cases’, *Annals of Neurology*, 72(2), pp. 241–255. doi: 10.1002/ana.23577.

Irani, S. R. *et al.* (2013) ‘Faciobrachial dystonic seizures: The influence of immunotherapy on seizure control and prevention of cognitive impairment in a broadening phenotype’, *Brain*, 136(10), pp. 3151–3162. doi: 10.1093/brain/awt212.

Jan, M. M., Sadler, M. and Rahey, S. R. (2018) ‘Electroencephalographic Features of Temporal Lobe Epilepsy’, pp. 439–448.

Jang, Y. *et al.* (2018) ‘LGI1 expression and human brain asymmetry : insights from patients with LGI1-antibody encephalitis’. Journal of Neuroinflammation, pp. 1–7. doi: 10.1186/S12974-018-1314-2.

Jimenez-pacheco, A. *et al.* (2016) ‘Transient P2X7 Receptor Antagonism Produces Lasting Reductions in Spontaneous Seizures and Gliosis in Experimental Temporal Lobe Epilepsy’, 36(22), pp. 5920–5932. doi: 10.1523/JNEUROSCI.4009-15.2016.

Kaczmarek, L. K. and Zhang, Y. (2017) ‘Kv3 Channels: Enablers of Rapid Firing, Neurotransmitter Release, and Neuronal Endurance’, *Physiological Reviews*. American Physiological Society, 97(4), pp. 1431–1468. doi: 10.1152/physrev.00002.2017.

Kalachikov, S. *et al.* (2002) ‘Auditory Features’, *American Journal of Human Genetics, The*, 30(3), pp. 335–341. doi: 10.1038/ng832.Mutations.

Kamiya, H., Shinozaki, H. and Yamamoto, C. (1996) ‘Activation of metabotropic glutamate receptor type 2/3 suppresses transmission at rat hippocampal mossy fibre synapses’, *Journal of Physiology*, 493(2), pp. 447–455. doi: 10.1113/jphysiol.1996.sp021395.

Kandel, E. R., Schwartz, J. H. and Jessell, T. M. (2000) ‘Principles of neural science’, in. New York: McGraw-Hill, Health Professions Division.

Kegel, L. *et al.* (2013) ‘LGI Proteins in the Nervous System’, *ASN Neuro*, 5(3), p. AN20120095. doi: 10.1042/AN20120095.

Kelly, M. E. and McIntyre, D. C. (1994) ‘Hippocampal kindling protects several structures from the neuronal damage resulting from kainic acid-induced status epilepticus’, *Brain Research*, 634(2), pp. 245–256. doi: 10.1016/0006-

8993(94)91927-5.

Khalil, A. *et al.* (2017) 'Carvacrol after status epilepticus (SE) prevents recurrent SE, early seizures, cell death, and cognitive decline', *Epilepsia*, 58(2), pp. 263–273. doi: 10.1111/epi.13645.

Knierim, J. J. (2015) 'The hippocampus'. doi: 10.1016/j.cub.2015.10.049.

Kobe, B. and Kajava, A. V (2001) 'The leucine-rich repeat as a protein recognition motif.', *Current Opinion in Structural Biology*, 11(6), pp. 725–32. doi: 10.1016/S0959-440X(01)00266-4.

Kovac, S. *et al.* (2014) 'Seizure activity results in calcium- and mitochondriaindependent ros production via nadph and xanthine oxidase activation', *Cell Death and Disease*. Nature Publishing Group, 5(10), pp. e1442-12. doi: 10.1038/cddis.2014.390.

Kovac, S. *et al.* (2017) 'Metabolic and Homeostatic Changes in Seizures and Acquired Epilepsy — Mitochondria , Calcium Dynamics and Reactive Oxygen Species'. doi: 10.3390/ijms18091935.

Kunapuli, P. *et al.* (2004) 'LGI1, a putative tumor metastasis suppressor gene, controls in Vitro invasiveness and expression of matrix metalloproteinases in glioma cells through the ERK1/2 pathway', *Journal of Biological Chemistry*, 279(22), pp. 23151–23157. doi: 10.1074/jbc.M314192200.

Kunapuli, P. *et al.* (2009) 'Mass spectrometry identifies LGI1-interacting proteins that are involved in synaptic vesicle function in the human brain', *Journal of Molecular Neuroscience*, 39(1–2), pp. 137–143. doi: 10.1007/s12031-009-9202-y.

Kunapuli, P., Chitta, K. S. and Cowell, J. K. (2003) 'Suppression of the cell proliferation and invasion phenotypes in glioma cells by the LGI1 gene', *Oncogene*, 22(26), pp. 3985–3991. doi: 10.1038/sj.onc.1206584.

Kwan, P. and Brodie, M. J. (2000) 'Early Identification of Refractory Epilepsy', *New England Journal of Medicine*. Massachusetts Medical Society, 342(5), pp. 314–319. doi: 10.1056/NEJM200002033420503.

Ladino, L. D., Moien-Afshari, F. and Tellez-Zenteno, J. F. (2014) 'A comprehensive review of temporal lobe epilepsy', *Iconceptpress.Com*, (November), pp. 1–35. Available at: http://iconceptpress.com/download/paper/13060312133760.pdf%5Cnhttp://www.researchgate.net/publication/263965704_A_Comprehensive_Review_of_Temporal_Lobe_Epilepsy.

Lai, M. *et al.* (2010) 'Investigation of LGI1 as the antigen in limbic encephalitis previously attributed to potassium channels: A case series', *The Lancet Neurology*. Elsevier Ltd, 9(8), pp. 776–785. doi: 10.1016/S1474-4422(10)70137-X.

Lalic, T. *et al.* (2011) 'Human limbic encephalitis serum enhances hippocampal mossy fiber-CA3 pyramidal cell synaptic transmission', *Epilepsia*, 52(1), pp. 121–131. doi: 10.1111/j.1528-1167.2010.02756.x.

Lee, K. Y. *et al.* (2015) 'N-methyl-D-aspartate receptors mediate activity-dependent down-regulation of potassium channel genes during the expression of homeostatic intrinsic plasticity', *Molecular Brain*, 8(1), pp. 1–16. doi: 10.1186/s13041-015-0094-1.

Leonardi, E. *et al.* (2011) 'A computational model of the LGI1 protein suggests a common binding site for ADAM proteins', *PLoS ONE*, 6(3). doi: 10.1371/journal.pone.0018142.

López González, F. J. *et al.* (2015) 'Drug-resistant epilepsy: Definition and treatment alternatives', *Neurología (English Edition)*, 30(7), pp. 439–446. doi: https://doi.org/10.1016/j.nrleng.2014.04.002.

Lovero, K. L. *et al.* (2015) 'The LGI1–ADAM22 protein complex directs synapse maturation through regulation of PSD-95 function', *Proceedings of the National Academy of Sciences*, 112(30), pp. E4129–E4137. doi: 10.1073/pnas.1511910112.

Magloire, V. *et al.* (2019) 'KCC2 overexpression prevents the paradoxical seizure-promoting action of somatic inhibition', *Nature Communications*, 10(1), p. 1225. doi: 10.1038/s41467-019-08933-4.

Marchi, N. *et al.* (2012) 'Blood-brain barrier dysfunction and epilepsy: pathophysiologic role and therapeutic approaches', *Epilepsia*. 2012/08/20, 53(11), pp. 1877–1886. doi: 10.1111/j.1528-1167.2012.03637.x.

Mary M. Heinricher (2004) 'Principles of Extracellular Single-Unit Recording', in Israel, Z. and Burchiel, K. J. (eds) *Microelectrode Recording in Movement Disorder Surgery*. Stuttgart: Georg Thieme Verlag, pp. 8–13. doi: 10.1055/b-0034-56092.

Mathews, G. C. (2007) 'The dual roles of GABA in seizures and epilepsy generate more excitement', *Epilepsy currents*. Blackwell Science Inc, 7(1), pp. 28–30. doi: 10.1111/j.1535-7511.2007.00159.x.

Mazarati, A. M. *et al.* (1998) 'Time-dependent decrease in the effectiveness of antiepileptic drugs during the course of self-sustaining status epilepticus', *Brain Research*, 814(1–2), pp. 179–185. doi: 10.1016/S0006-8993(98)01080-4.

McCormick, D. A. and Prince, D. A. (1987) 'Postnatal development of electrophysiological properties of rat cerebral cortical pyramidal neurones.', *The Journal of Physiology*, 393(1), pp. 743–762. doi: 10.1113/jphysiol.1987.sp016851.

Mcnamara, J. O. (1999) 'Emerging insights into the genesis of epilepsy', pp. 15–22.

McNamara, J. O. *et al.* (1980) 'The kindling model of epilepsy: A review', *Progress in*

Neurobiology, 15(2), pp. 139–159. doi: 10.1016/0301-0082(80)90006-4.

Meneses, D. *et al.* (2016) 'KV1 and KV3 Potassium Channels Identified at Presynaptic Terminals of the Corticostriatal Synapses in Rat', *Neural Plasticity*. Hindawi Publishing Corporation, 2016. doi: 10.1155/2016/8782518.

Michelucci, R. *et al.* (2007) 'A De Novo Lgi1 mutation Causing Idiopathic Partial Epilepsy with Telephone-Induced Seizures', *Neurology*, 68(24), p. 2150 LP-2151. Available at: http://n.neurology.org/content/68/24/2150.abstract.

Mitchell, K. J. *et al.* (2001) 'Functional analysis of secreted and transmembrane proteins critical to mouse development', *Nature Genetics*, 28(3), pp. 241–249. doi: 10.1038/90074.

Moore, C. B. *et al.* (2010) 'RNA Therapeutics', 629(2), pp. 1–15. doi: 10.1007/978-1-60761-657-3.

Moore, C. B. *et al.* (2010) 'Short hairpin RNA (shRNA): design, delivery, and assessment of gene knockdown.', *Methods in molecular biology (Clifton, N.J.)*, 629, pp. 141–158. doi: 10.1007/978-1-60761-657-3_10.

Morante-Redolat, J. M. *et al.* (2002) 'Mutations in the LGI1/Epitempin gene on 10q24 cause autosomal dominant lateral temporal epilepsy', *Human Molecular Genetics*, 11(9), pp. 1119–1128. doi: 10.1093/hmg/11.9.1119.

Murphy, T. H. *et al.* (1992) 'Spontaneous synchronous synaptic calcium transients in cultured cortical neurons.', *The Journal of neuroscience : the official journal of the Society for Neuroscience*, 12(December), pp. 4834–4845. doi: 1361198.

Naba, A., Clauser, K. R. and Hynes, R. O. (2015) 'Enrichment of Extracellular Matrix Proteins from Tissues and Digestion into Peptides for Mass Spectrometry Analysis', *Journal of Visualized Experiments*, (101), pp. 1–9. doi: 10.3791/53057.

Neves, G., Cooke, S. F. and Bliss, T. V. P. (2008) 'Synaptic plasticity, memory and the hippocampus: a neural network approach to causality', *Nature Reviews Neuroscience*. Nature Publishing Group, 9, p. 65. Available at: https://doi.org/10.1038/nrn2303.

Nirwan, N., Vyas, P. and Vohora, D. (2018) 'Animal models of status epilepticus and temporal lobe epilepsy: A narrative review', *Reviews in the Neurosciences*, 29(7), pp. 757–770. doi: 10.1515/revneuro-2017-0086.

Nobile, C. *et al.* (2009) 'LGI1 mutations in autosomal dominant and sporadic lateral temporal epilepsy', *Human Mutation*, 30(4), pp. 530–536. doi: 10.1002/humu.20925.

Norman, G. R. and Streiner, D. L. (2000) *Biostatitics: The bare essential*. Mosby Year Book.

Ogawa, Y. *et al.* (2010) 'ADAM22, A Kv1 Channel-Interacting Protein, Recruits

Membrane-Associated Guanylate Kinases to Juxtaparanodes of Myelinated Axons', *Journal of Neuroscience*, 30(3), pp. 1038–1048. doi: 10.1523/JNEUROSCI.4661-09.2010.

Ohkawa, T. *et al.* (2013) 'Autoantibodies to Epilepsy-Related LGI1 in Limbic Encephalitis Neutralize LGI1-ADAM22 Interaction and Reduce Synaptic AMPA Receptors', *Journal of Neuroscience*, 33(46), pp. 18161–18174. doi: 10.1523/JNEUROSCI.3506-13.2013.

Osten, P. *et al.* (2007) 'Stereotaxic gene delivery in the rodent brain', *Nature Protocols*, 1(6), pp. 3166–3173. doi: 10.1038/nprot.2006.450.

Ottman, R. *et al.* (2004) 'LGI1 mutations in autosomal dominant partial epilepsy with auditory features.', *Neurology*, 62(7), pp. 1120–6. Available at: http://www.ncbi.nlm.nih.gov/pubmed/15079011.

Owuor, K. *et al.* (2009) 'LGI1-associated epilepsy through altered ADAM23-dependent neuronal morphology', *Molecular and cellular neurosciences*, 42(4), pp. 448–457. doi: 10.1016/j.mcn.2009.09.008.LGI1-associated.

Pacico, N. and Meur, A. M. Le (2014) 'New in vitro phenotypic assay for epilepsy: Fluorescent measurement of synchronized neuronal calcium oscillations', *PLoS ONE*, 9(1). doi: 10.1371/journal.pone.0084755.

Pacifici, M. and Peruzzi, F. (2012) 'Isolation and Culture of Rat Embryonic Neural Cells: A Quick Protocol', *Journal of Visualized Experiments*. MyJoVE Corp, (63), p. e3965. doi: 10.3791/3965.

Pakozdy, A. *et al.* (2014) 'EEG-confirmed epileptic activity in a cat with VGKC-complex / LGI1 limbic encephalitis', *Epileptic Disorders*, 16(1), pp. 116–120. doi: 10.1684/epd.2014.0635.

Pakozdy, A. *et al.* (2015) 'LGI proteins and epilepsy in human and animals', *Journal of Veterinary Internal Medicine*, 29(4), pp. 997–1005. doi: 10.1111/jvim.12610.

Palma, B. M. D. E. and Naldini, L. (2002) 'Transduction of a Gene Expression Cassette Using Advanced Generation Lentiviral Vectors', 346(1996), pp. 514–529.

Pasquale, V., Martinoia, S. and Chiappalone, M. (2010) 'A self-adapting approach for the detection of bursts and network bursts in neuronal cultures', *Journal of Computational Neuroscience*, 29(1–2), pp. 213–229. doi: 10.1007/s10827-009-0175-1.

Pelliccia, V. *et al.* (2013) 'Ictal EEG modifications in temporal lobe epilepsy', 15(4), pp. 392–399.

Penn, A. C. *et al.* (2017) 'Hippocampal LTP and contextual learning require surface diffusion of AMPA receptors', *Nature Publishing Group*. Nature Publishing Group, 549(7672), pp. 384–388. doi: 10.1038/nature23658.

Petit-pedrol, M. *et al.* (2018) 'LGI1 antibodies alter Kv1.1 and AMPA receptors changing synaptic excitability, plasticity and memory.', *Brain*, pp. 1–16. doi: 10.1093/brain/awy253.

Piepoli, T. *et al.* (2006) 'Expression studies in gliomas and glial cells do not support a tumor suppressor role for LGI11', *Neuro-Oncology*, 8(2), pp. 96–108. doi: 10.1215/15228517-2005-006.

Pitkänen, A. *et al.* (2014) 'Chapter 11 - Neural ECM and epilepsy', in Dityatev, A., Wehrle-Haller, B., and Pitkänen, A. B. T.-P. in B. R. (eds) *Brain Extracellular Matrix in Health and Disease*. Elsevier, pp. 229–262. doi: https://doi.org/10.1016/B978-0-444-63486-3.00011-6.

Pitkänen, A. and Bolkvadze, T. (2012) 'Head Trauma and Epilepsy', in Noebels JL, Avoli M, Rogawski MA, et al. (ed.) *Basic Mechanisms of the Epilepsies*. 4th editio, pp. 1–18.

Pitkänen, A. and Lukasiuk, K. (2009) 'Molecular and cellular basis of epileptogenesis in symptomatic epilepsy', *Epilepsy and Behavior*. Elsevier Inc., 14(1 SUPPL. 1), pp. 16–25. doi: 10.1016/j.yebeh.2008.09.023.

Plantone, D. *et al.* (2013) 'Teaching NeuroImages: Basal ganglia involvement in facio-brachial dystonic seizures associated with LGI1 antibodies', *Neurology*, 80(17). doi: 10.1212/WNL.0b013e31828f17fa.

van den Pol, A. N., Obrietan, K. and Chen, G. (1996) 'Excitatory Actions of GABA after Neuronal Trauma', *The Journal of Neuroscience*, 16(13), p. 4283 LP-4292. doi: 10.1523/JNEUROSCI.16-13-04283.1996.

Pugliatti, M. *et al.* (2007) 'Estimating the cost of epilepsy in Europe: A review with economic modeling', *Epilepsia*, 48(12), pp. 2224–2233. doi: 10.1111/j.1528-1167.2007.01251.x.

Racine, R. J. (1972) 'Modification of seizure activity by electrical stimulation: II. Motor seizure', *Electroencephalography and Clinical Neurophysiology*, 32(3), pp. 281–294. doi: 10.1016/0013-4694(72)90177-0.

Rama, S. *et al.* (2015) 'Presynaptic hyperpolarization induces a fast analogue modulation of spike-evoked transmission mediated by axonal sodium channels', *Nature Communications*, 6. doi: 10.1038/ncomms10163.

Rama, S. *et al.* (2017) 'The role of axonal Kv1 channels in CA3 pyramidal cell excitability', *Scientific Reports*, 7(1), pp. 1–12. doi: 10.1038/s41598-017-00388-1.

Reynolds, A. *et al.* (2004) 'Rational siRNA design for RNA interference', *Nature Biotechnology*, 22(3), pp. 326–330. doi: 10.1038/nbt936.

Ribeiro, P. A. O. *et al.* (2008) 'Expression profile of Lgi1 gene in mouse brain during development', *Journal of Molecular Neuroscience*, 35(3), pp. 323–329. doi:

10.1007/s12031-008-9096-0.

Richner, T. J. and Krook-Magnuson, E. (2018) ‘Progress toward precise genetic repair in neurons’, *Epilepsy Currents*, 18(2), pp. 121–122. doi: 10.5698/1535-7597.18.2.121.

Rigon, L. *et al.* (2011) ‘ADAM23, a Gene Related to LGI1, Is Not Linked to Autosomal Dominant Lateral Temporal Epilepsy.’, *Epilepsy research and treatment*, 2011, p. 258365. doi: 10.1155/2011/258365.

Robbins, C. A. and Tempel, B. L. (2012) ‘Kv1.1 and Kv1.2: Similar channels, different seizure models’, *Epilepsia*, 53(SUPPL. 1), pp. 134–141. doi: 10.1111/j.1528-1167.2012.03484.x.

Rojas, A. *et al.* (2014) ‘Cyclooxygenase-2 in epilepsy’, *Epilepsia*, 55(1), pp. 17–25. doi: 10.1111/epi.12461.

Ruiz, A. J. and Kullmann, D. M. (2013) ‘Ionotropic receptors at hippocampal mossy fibers : roles in axonal excitability , synaptic transmission , and plasticity’, 6(January), pp. 1–12. doi: 10.3389/fncir.2012.00112.

Sagane, K., Ishihama, Y. and Sugimoto, H. (2008) ‘LGI1 and LGI4 bind to ADAM22, ADAM23 and ADAM11’, *International Journal of Biological Sciences*, 4(6), pp. 387–396. doi: 10.7150/ijbs.4.387.

Sakai, A. *et al.* (2018) ‘Ectopic neurogenesis induced by prenatal antiepileptic drug exposure augments seizure susceptibility in adult mice’, pp. 1–6. doi: 10.1073/pnas.1716479115.

Sandy, P., Ventura, A. and Jacks, T. (2005) ‘Mammalian RNAi: A practical guide’, *BioTechniques*, 39(2), pp. 215–224. doi: 10.2144/05392RV01.

Scheel, H., Tomiuk, S. and Hofmann, K. (2002) ‘A common protein interaction domain links two recently identified epilepsy genes.’, *Human molecular genetics*, 11(15), pp. 1757–62. doi: 12095917.

Scheffer, I. E. *et al.* (2017) ‘ILAE classification of the epilepsies: Position paper of the ILAE Commission for Classification and Terminology’, *Epilepsia*, 58(4), pp. 512–521. doi: 10.1111/epi.13709.

Schulte, J. T., Wierenga, C. J. and Bruining, H. (2018) ‘Chloride transporters and GABA polarity in developmental, neurological and psychiatric conditions’, *Neuroscience & Biobehavioral Reviews*, 90, pp. 260–271. doi: https://doi.org/10.1016/j.neubiorev.2018.05.001.

Schulte, U. *et al.* (2006) ‘The epilepsy-linked Lgi1 protein assembles into presynaptic Kv1 channels and inhibits inactivation by Kvβ1’, *Neuron*, 49(5), pp. 697–706. doi: 10.1016/j.neuron.2006.01.033.

Scimemi, A. *et al.* (2004) ‘NR2B-Containing Receptors Mediate Cross Talk among

Hippocampal Synapses', 24(20), pp. 4767–4777. doi: 10.1523/JNEUROSCI.0364-04.2004.

Seagar, M. *et al.* (2017) 'LGI1 tunes intrinsic excitability by regulating the density of axonal Kv1 channels', *Proceedings of the National Academy of Sciences*, 114(29), pp. 7719–7724. doi: 10.1073/pnas.1618656114.

Selinger, J. V. *et al.* (2007) 'Methods for characterizing interspike intervals and identifying bursts in neuronal activity', *Journal of Neuroscience Methods*, 162(1–2), pp. 64–71. doi: 10.1016/j.jneumeth.2006.12.003.

Senechal, K. R., Thaller, C. and Noebels, J. L. (2005) 'ADPEAF mutations reduce levels of secreted LGI1, a putative tumor suppressor protein linked to epilepsy', *Human Molecular Genetics*, 14(12), pp. 1613–1620. doi: 10.1093/hmg/ddi169.

Senkov, O. *et al.* (2014) 'Chapter 3 - Neural ECM molecules in synaptic plasticity, learning, and memory', in Dityatev, A., Wehrle-Haller, B., and Pitkänen, A. B. T.-P. in B. R. (eds) *Brain Extracellular Matrix in Health and Disease*. Elsevier, pp. 53–80. doi: https://doi.org/10.1016/B978-0-444-63486-3.00003-7.

Shekh-Ahmad, T. *et al.* (2018) 'KEAP1 inhibition is neuroprotective and suppresses the development of epilepsy', *Brain*, 141(5), pp. 1390–1403. doi: 10.1093/brain/awy071.

Shorvon, S. D. (1990) 'Epidemiology, classification, natural history, and genetics of epilepsy', *The Lancet*, 336(8707), pp. 93–96. doi: https://doi.org/10.1016/0140-6736(90)91603-8.

Shorvon, S. D. (2011) 'The etiological classification of epilepsy', *The Causes of Epilepsy: Common and Uncommon Causes in Adults and Children*, 9780521114(6), pp. 21–23. doi: 10.1017/CBO9780511921001.004.

Shu, Y. *et al.* (2007) 'Selective control of cortical axonal spikes by a slowly inactivating K⁺ current', *Proceedings of the National Academy of Sciences*, 104(27), p. 11453 LP-11458. doi: 10.1073/pnas.0702041104.

Sirerol-Piquer, M. S. *et al.* (2006) 'The epilepsy gene LGI1 encodes a secreted glycoprotein that binds to the cell surface', *Human Molecular Genetics*, 15(23), pp. 3436–3445. doi: 10.1093/hmg/ddl421.

Sloviter, R. S. (1983) '"Epileptic" brain damage in rats induced by sustained electrical stimulation of the perforant path. I. Acute electrophysiological and light microscopic studies', *Brain Research*, 10, pp. 675–697.

Sloviter, R. S. (1992) 'Possible functional consequences of synaptic reorganization in the dentate gyrus of kainate-treated rats', *Neuroscience Letters*, 137(1), pp. 91–96. doi: https://doi.org/10.1016/0304-3940(92)90306-R.

Sloviter, R. S. (2003) 'Excitatory Dentate Granule Cells Normally Contain GAD and

GABA, but Does That Make Them GABAergic, and Do Seizures Shift Granule Cell Function in the Inhibitory Direction?', *Epilepsy currents*, 3(1), pp. 3–5. doi: 10.1046/j.1535-7597.2003.03101.x.

Smith, S. E. P. *et al.* (2012) 'Mutant LGI1 inhibits seizure-induced trafficking of Kv4.2 potassium channels', *Journal of Neurochemistry*, 120(4), pp. 611–621. doi: 10.1111/j.1471-4159.2011.07605.x.

van Sonderen, A. *et al.* (2016) 'From VGKC to LGI1 and Caspr2 encephalitis: The evolution of a disease entity over time', *Autoimmunity Reviews*. The Authors, 15(10), pp. 970–974. doi: 10.1016/j.autrev.2016.07.018.

Staub, E. *et al.* (2002) 'The novel EPTP repeat defines a superfamily of proteins implicated in epileptic disorders', *Trends in Biochemical Sciences*, 27(9), pp. 441–444. doi: 10.1016/S0968-0004(02)02163-1.

Stödberg, T. *et al.* (2015) 'Mutations in SLC12A5 in epilepsy of infancy with migrating focal seizures', *Nature communications*. Nature Pub. Group, 6, p. 8038. doi: 10.1038/ncomms9038.

Stone, T. J. *et al.* (2018) 'Review: Molecular characteristics of long-term epilepsy-associated tumours (LEATs) and mechanisms for tumour-related epilepsy (TRE)', *Neuropathology and Applied Neurobiology*, 44(1), pp. 56–69. doi: 10.1111/nan.12459.

Striano, P. *et al.* (2008) 'A Novel Loss-of-Function LGI1 Mutation Linked to Autosomal Dominant Lateral Temporal Epilepsy', *Archives of Neurology*, 65(7), pp. 9–12. doi: 10.1001/archneur.65.7.939.

Swanson, L. W., Wyss, J. M. and Cowan, W. M. (1978) 'An autoradiographic study of the organization of intrahippocampal association pathways in the rat', *Journal of Comparative Neurology*, 181(4), pp. 681–715. doi: 10.1002/cne.901810402.

Tagliatti, E. *et al.* (2016) 'Arf6 regulates the cycling and the readily releasable pool of synaptic vesicles at hippocampal synapse', *eLife*. Edited by C. Rosenmund. eLife Sciences Publications, Ltd, 5, p. e10116. doi: 10.7554/eLife.10116.

Teng, Y. *et al.* (2010) 'Knockdown of zebrafish lgi1a results in abnormal development, brain defects and a seizure-like behavioral phenotype', *Human Molecular Genetics*, 19(22), pp. 4409–4420. doi: 10.1093/hmg/ddq364.

Thomas, R. *et al.* (2010) 'LGI1 Is a Nogo Receptor 1 Ligand that Antagonizes Myelin-Based Growth Inhibition', *Journal of Neuroscience*, 30(19), pp. 6607–6612. doi: 10.1523/JNEUROSCI.5147-09.2010.

Thomas, R. A. *et al.* (2018) *The Nogo receptor ligand LGI1 regulates synapse number and synaptic activity in hippocampal and cortical neurons The Nogo receptor ligand LGI1 regulates synapse number and synaptic activity in hippocampal and*

cortical neurons . Short Title : LGI1 regulate. doi: 10.1523/ENEURO.0185-18.2018.

Trimmer, J. S. (2015) 'Subcellular localization of K+channels in mammalian brain neurons: Remarkable precision in the midst of extraordinary complexity', *Neuron*. Elsevier Inc., 85(2), pp. 238–256. doi: 10.1016/j.neuron.2014.12.042.

Trimmer, J. S. and Rhodes, K. J. (2004) 'Localization of Voltage-Gated Ion Channels IN Mammalian Brain', *Annual Review of Physiology*, 66(1), pp. 477–519. doi: 10.1146/annurev.physiol.66.032102.113328.

Tse, K. *et al.* (2014) 'Advantages of repeated low dose against single high dose of kainate in C57BL/6J mouse model of status epilepticus: Behavioral and electroencephalographic studies', *PLoS ONE*, 9(5). doi: 10.1371/journal.pone.0096622.

Veh, R. W. *et al.* (1995) 'Immunohistochemical Localization of Five Members of the KV1 Channel Subunits: Contrasting Subcellular Locations and Neuron-specific Co-localizations in Rat Brain', *European Journal of Neuroscience*, 7(11), pp. 2189–2205. doi: 10.1111/j.1460-9568.1995.tb00641.x.

Vida, I. and Frotscher, M. (2000) 'A hippocampal interneuron associated with the mossy fiber system.', *Proceedings of the National Academy of Sciences of the United States of America*, 97(3), pp. 1275–1280. doi: 10.1073/pnas.97.3.1275.

Walker, M. C. *et al.* (1999) 'Halothane as a neuroprotectant during constant stimulation of the perforant path', *Epilepsia*, 40(3), pp. 359–364. doi: 10.1111/j.1528-1157.1999.tb00718.x.

Walker, M. C., Ruiz, A. and Kullmann, D. M. (2002) 'Do Mossy Fibers Release GABA ?', 43, pp. 196–202.

Winawer, M. R. *et al.* (2000) 'Autosomal dominant partial epilepsy with auditory features: Defining the phenotype', *Neurology*, 54(11), p. 2173 LP-2176. Available at: http://n.neurology.org/content/54/11/2173.abstract.

Witter, M. P. *et al.* (2014) 'Architecture of spatial circuits in the hippocampal region', pp. 11–13.

Wong, R. K., Miles, R. and Traub, R. D. (1984) 'Local circuit interactions in synchronization of cortical neurones.', *The Journal of experimental biology*, 112, pp. 169–178.

Wykes, R. C. *et al.* (2012) 'Epilepsy: Optogenetic and potassium channel gene therapy in a rodent model of focal neocortical epilepsy', *Science Translational Medicine*, 4(161). doi: 10.1126/scitranslmed.3004190.

Xie, Y. J. *et al.* (2015) 'Essential roles of leucine-rich glioma inactivated 1 in the development of embryonic and postnatal cerebellum', *Scientific Reports*, 5, pp. 1–11. doi: 10.1038/srep07827.

Yamagata, A. *et al.* (2018) ‘Structural basis of epilepsy-related ligand-receptor complex LGI1-ADAM22’, *Nature Communications*, 9(1), pp. 1–13. doi: 10.1038/s41467-018-03947-w.

Yang, S., Kwok, J. C. F. and Fawcett, J. W. (2014) ‘Chapter 8 - Neural ECM in regeneration and rehabilitation’, in Dityatev, A., Wehrle-Haller, B., and Pitkänen, A. B. T.-P. in B. R. (eds) *Brain Extracellular Matrix in Health and Disease*. Elsevier, pp. 179–192. doi: https://doi.org/10.1016/B978-0-444-63486-3.00008-6.

Yokoi, N. *et al.* (2015) ‘Chemical corrector treatment ameliorates increased seizure susceptibility in a mouse model of familial epilepsy’, *Nature Medicine*. Nature Publishing Group, 21(1), pp. 19–26. doi: 10.1038/nm.3759.

Yu, Y. E. *et al.* (2010) ‘Lgi1 null mutant mice exhibit myoclonic seizures and CA1 neuronal hyperexcitability’, *Human Molecular Genetics*, 19(9), pp. 1702–1711. doi: 10.1093/hmg/ddq047.

Zhang, W. *et al.* (2019) ‘Seizure characteristics , treatment , and outcome in autoimmune synaptic encephalitis : A long-term study’, *Epilepsy & Behavior*. Elsevier Inc., 94, pp. 198–203. doi: 10.1016/j.yebeh.2018.10.038.

Zhou, L. *et al.* (2018) ‘Celecoxib Ameliorates Seizure Susceptibility in Autosomal Dominant Lateral Temporal Epilepsy.’, *The Journal of neuroscience : the official journal of the Society for Neuroscience*, 38(13), pp. 3346–3357. doi: 10.1523/JNEUROSCI.3245-17.2018.

Zhou, Y. D. *et al.* (2009) ‘Arrested maturation of excitatory synapses in autosomal dominant lateral temporal lobe epilepsy’, *Nature Medicine*, 15(10), pp. 1208–1214. doi: 10.1038/nm.2019.